Detecting Cerebellar Phenotypes with the Erasmus Ladder

Alexander Cupido

Detecting Cerebellar Phenotypes with the Erasmus Ladder

Het detecteren van cerebellaire fenotypes
met de Erasmus Ladder

Proefschrift

ter verkrijging van de graad van doctor aan de
Erasmus Universiteit Rotterdam
op gezag van de rector magnificus
Prof.dr. H.G. Schmidt
en volgens besluit van het College voor Promoties

De openbare verdediging zal plaatsvinden op
woensdag 23 september 2009 om 09.30 uur

door

Alexander Cupido

geboren te Leiden

ERASMUS UNIVERSITEIT ROTTERDAM

PROMOTIECOMMISSIE

Promotor: Prof.dr. C.I. De Zeeuw

Overige leden: Prof.dr. Y. Elgersma
                    Prof.dr. B.A. Oostra
                    Prof.dr. G.T. van der Horst

Copromotor: Dr. S.K.E. Koekkoek

TABLE OF CONTENTS

CHAPTER I

General Introduction

CHAPTER 1   GENERAL INTRODUCTION

Adapting to changes in the environment is essential for every species. Throughout development we learn how to avoid objects and stay away from harmful situations. We do this by changing our motor behavior to cues from the outside world. For example, during driving lessons we learn how to merge into traffic. During the first driving lesson merging into traffic seems like a very difficult task and you depend a lot on your instructor. But after obtaining your driving license, you can merge into traffic while changing the station on your car radio and complain at the same time of the inability of other road users to drive properly. How can something that seemed so difficult and possibly life threatening turn into something that you can do routinely?

Which parts of the brain are involved in learning? How and where is the information stored? Neuroscientist would like to answer these questions. There are two different types of learning: reflexive learning and declarative learning. Kupfermann[1] gives the following definitions. Reflexive learning has an automatic or reflexive quality, and its formation or readout is not dependent on awareness, consciousness, or cognitive processes such as comparison and evaluation. Reflexive learning accumulates slowly through repetition over many trials. This type of memory is expressed primarily by improved performance. This type of learning will be referred to as motor performance in this thesis. Declarative learning depends on conscious reflection for its acquisition and recall, and it relies on cognitive processes such as evaluation, comparison and interference and is often established in a single trial and this type of learning will be referred to as associative motor learning in this thesis. In the same chapter[1], Kupfermann summarizes what is known about learning in four generalizations: (1) learning has stages and its representation is continually changing; (2) long-term learning is represented by plasticity in the brain; (3) the plasticity changes that encode learning are localized in multiple regions throughout the nervous system and (4) reflexive and declarative learning may involve different neuronal circuits.

Although a lot of brain sites are important for learning, this thesis will focus on the role of the cerebellum in motor behavior. Already in the nineteenth century lesion studies in animals showed that the cerebellum plays an important role in motor behavior[2-4]. As opposed to lesions of other motor processing centers, damage or even removal of the cerebellum does not produce paralysis or involuntary movements, but erroneous movements, which can be summarized as a combination of ataxia, a decrease of muscle tone and intention tremor[5].

In neuroscience, a lot of different experimental approaches can be used to increase our knowledge about the cerebellum. The anatomy can be studied, molecular pathways can be elucidated, electric currents of cerebellar neurons can be recorded, models can be made about the functioning of the cerebellum and the behavior in which the cerebellum is involved can be assessed with several behavioral tasks. In the next paragraphs, I will briefly discuss some of the knowledge that is gathered with the abovementioned experimental approaches and explain why we developed a new behavioral task to study cerebellar motor behavior in mice.

1.1   ANATOMY OF THE CEREBELLUM

The cerebellum (**figure 1.1**[6]) is situated in the posterior part of the scull, dorsal to the brainstem. The cerebellum is divided into an anterior lobe and a posterior lobe by the deep primary fissure. Transverse fissures divide the cerebellum further into 10 lobules[7]. From medial to lateral, the cerebellum is divided into a vermis and a laterally positioned hemisphere. The paravermis is located between the vermis and the hemisphere. The cerebellum consists of a superficially located cortex, which, due to the impressive foliations possesses an enormous surface. The cerebellar nuclei (vestibular nuclei and deep cerebellar nuclei) are located in the white matter of the cerebellar cortex and provide the sole output of the cerebellar cortex. The cerebellum is connected to the brainstem by three cerebellar peduncles (superior, medius and inferior). Functionally, the cerebellum is divided into three regions. The vestibulocerebellum is involved in controlling balance and eye movements. The second part anatomically consists of the vermis and paravermis and is referred to as the spinocerebellum due to the fact that it receives abundant somatosensory input from the spinal cord. It is thought to be involved in reflexive executed motor control. The cerebrocerebellum, consisting of most of the hemispheres, is concerned with the planning, coordination and learning of complex movements but has also been implicated in cognitive functions[8,9]. Although the cerebellum only takes up 10% of the brain volume, due to its big surface, the cerebellum contains more neurons than the rest of the brain.

1.1.1   Neurons in the cerebellar cortex

The cerebellar cortical circuit was described in detail more than a century ago by Ramón y Cajal[10]. **Figure 1.2** gives an overview of the neurons in the cerebellar cortex. The cerebellar cortex is divided into three layers. From superficial to deep these are: the molecular layer, the Purkinje cell layer and the granular layer. The molecular layer predominantly consists of parallel fibers. These fibers are distal T-parts of the bifurcation of ascending segments of the axons of granule cells (see **figure 1.3c**), which themselves are located in the granular layer. The other two types of neurons in the molecular layer are the stellate and basket cells. They receive excitatory input from the parallel fibers and inhibit the Purkinje cells (see **figure 1.3a** and **figure 1.3b**). The Purkinje cells are arranged in one single layer. The dendrites of the Purkinje cells are arranged perpendicular to the parallel fibers. A single Purkinje cell is contacted by approximately 175000 parallel fibers[11]. Purkinje cells provide the sole output of the cerebellar cortex and inhibit the deep cerebellar nuclei. The granular layer consists of granule cells, unipolar brush cells and Golgi cells. Granule cells receive excitatory input from mossy fibers and brush cells. Granule cells receive inhibitory input from Golgi cells. Each granule cell can excite via their parallel fibers hundreds of Purkinje cells. The cerebellar cortex receives input from two systems: the climbing fiber system and the mossy fiber system.

Figure 1.1
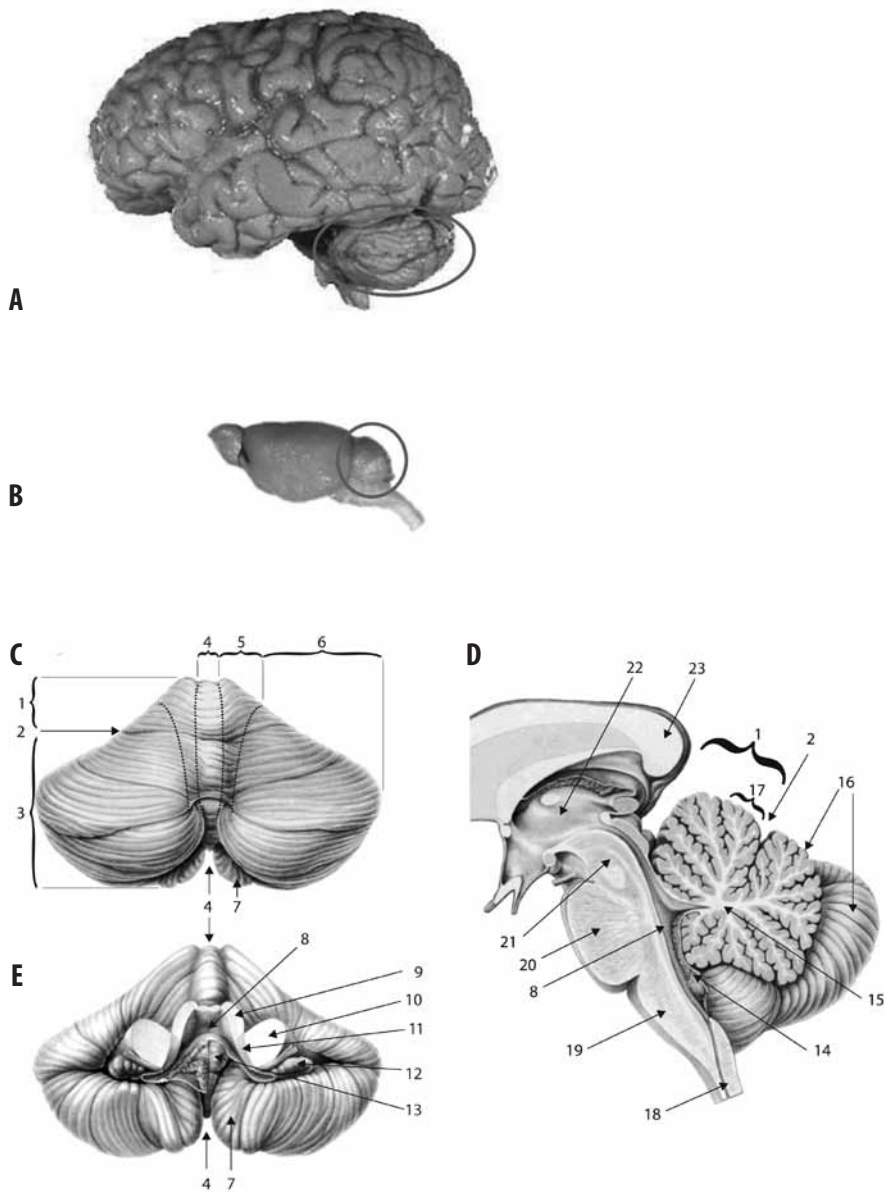
A Human Brain. B Mouse brain. Red circles indicate the cerebellum. The brains are not in the same scale. **CDE** Macroscopic view of the human cerebellum. **C** Dorsal view. **D** Ventral view. **E** Midsagittal View. 1. lobus anterior 2. fissura prima 3. lobus posterior 4. vermis 5. paravermis 6. hemisphere 7. tonsil 8. fourth ventricle 9. penduculus cerebellaris superior 10. pendunculus cerebellaris medius 11. penduclus cerebellaris inferior 12. flocculus 13. nodulus 14. plexus choroideus 15. white matter 16. folia 17. lobuli 18. spinal cord 19. medulla oblongata 20. pons 21. mesencefalon 22. third ventricle 23. corpus callosum

Figure 1.2

PURKINJE CELL
GOLGI CELL
GRANULE CELL AND PARALLEL FIBER
STELLATE CELL
BASKET CELL
CLIMBING FIBER
MOSSY FIBER
UNIPOLAR BRUSH CELL
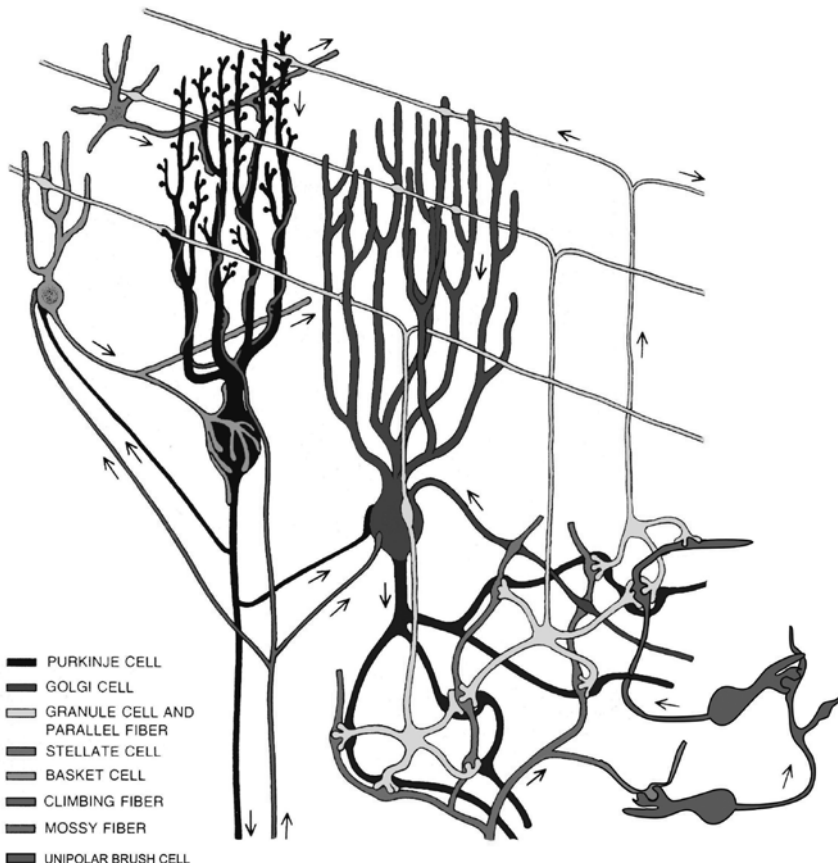
The sole output of the cerebellar cortex comes from the Purkinje cells and inhibits the cerebellar nuclei. The excitatory input comes from the climbing fibers and the mossy fibers. Arrows in the graph indicate the pathway of the neuronal signaling. One Purkinje cell gets excited by ± 175 000 parallel fibers and by one single climbing fiber and inhibited by stellate cells and basket cells. Purkinje cells themselves inhibit the cerebellar nuclei (not shown), Golgi cells and basket cells. Golgi cells get excited by parallel fibers and climbing fibers and inhibited by Purkinje cells and other Golgi cells. Golgi cells themselves inhibit granule cells. Granule cells get excited by mossy fibers and unipolar brush cells and inhibited by Golgi cells. Granule cells themselves excite via their parallel fibers Purkinje cells, Golgi cells, basket cells and stellate cells. Stellate cells get excited by parallel fibers and one stellate cell itself inhibits several Purkinje cells. Basket cells get excited by climbing fibers and parallel fibers and inhibited by Purkinje cells. One basket cell itself inhibits several Purkinje cells. Climbing fibers excite basket cells, Purkinje cells and Golgi cells. Mossy fibers excite granule cells and unipolar brush cell. Unipolar brush cells themselves excite granule cells.

1.1.2   Cerebellar circuitry

Climbing fiber input

All climbing fibers (see **figure 1.3d**) originate in the inferior olive[12]. The inferior olive[13-15] is located in the ventral part of the brainstem. In the inferior olive, sensory information from

Figure 1.3
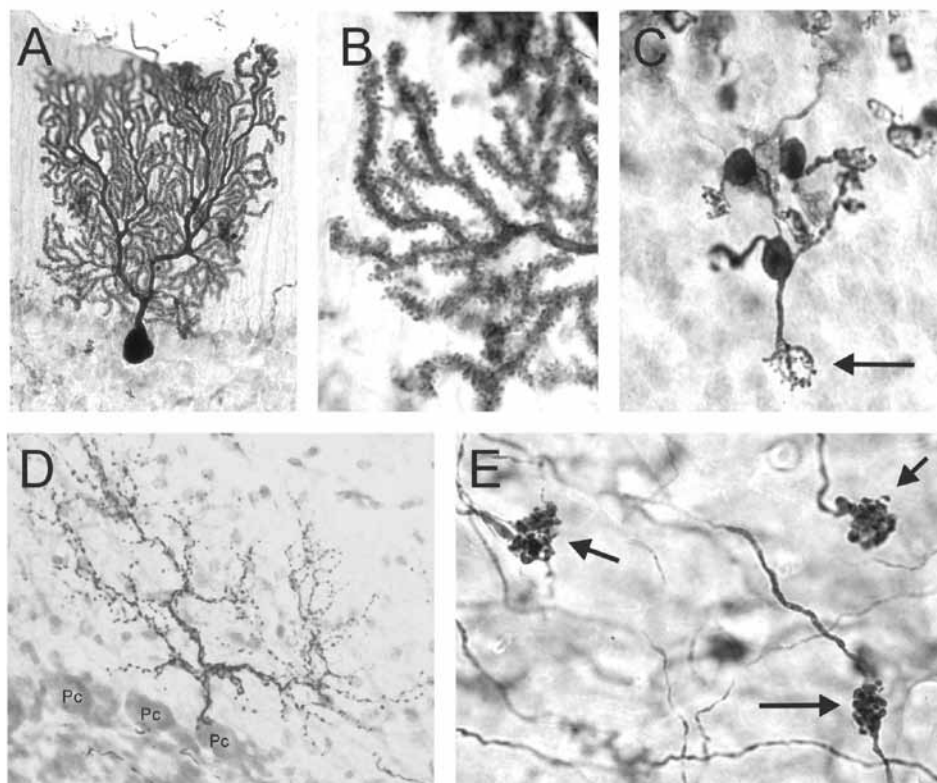
Cells and fibers in the cerebellum are visualized with Biotin Dextran Amine (BDA). **A** Purkinje cell. **B** Spines of the Purkinje cell. Parallel fibers connect with the Purkinje cell here **C** Granule cells. **D** Climbing fibers terminals. Purkinje cells are indicated with Pc. **E** Mossy fiber terminals (indicated with arrows) in the granule cell layer.

different body parts is integrated and relayed through to the cerebellum. All olivary neurons give rise to a single axon. Each olivary axon branches into 8-10 climbing fibers that each 'climb' into a single Purkinje cell[16]. One climbing fiber has approximately 250 contact points (synapses) with one Purkinje cell[17].

Mossy fiber input

Mossy fibers (see **figure 1.3e**) derive their name from the conspicuously shaped terminals that end on granule cells. The organization of the mossy fiber system appears less structured than that of the climbing fiber system. They originate from many parts of the central nervous system such as the pontine nuclei, trigeminal complex, lateral reticular nucleus, dorsal column nuclei and the spinal cord carrying information from the periphery and the cerebral cortex.

Output of the cerebellar cortex

The output of the cerebellar cortex is organized in zones. Purkinje cells of a particular zone project to a specific part of the cerebellar nuclei (deep cerebellar nuclei or vestibular nuclei)[18]. Climbing fibers of a particular olivary nucleus project to a particular Purkinje cell zone and climbing fiber collaterals (see **figure 1.4**) project to the cerebellar nuclei or target cells of that same micro zone. These cerebellar nuclei in turn provide an inhibitory projection (not shown in **figure 1.4**) to the corresponding olivary cells.

Figure 1.4
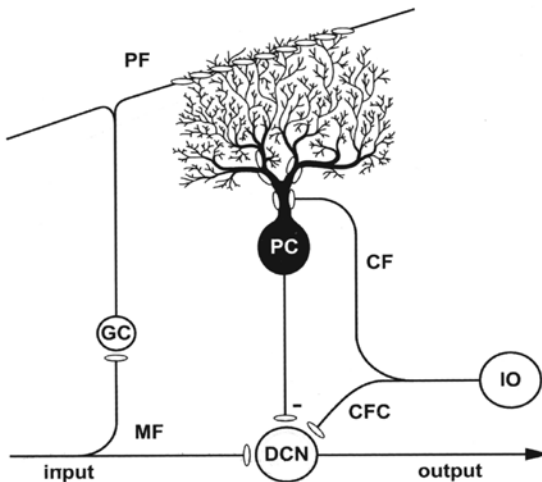
Simplified cerebellar circuitry. Mossy fiber (MF) input from the precerebellar nuclei projects to the deep cerebellar nuclei (DCN). DCN excitatory output targets premotor centers. Synapses are excitatory except when indicated (-). GC=granule cell. PF=parallel fiber. PC=Purkinje cell. IO=inferior Olive. CF=climbing fiber. CFC=climbing fiber collateral.

1.1.3 Models for cerebellar circuitry

Unlike the cerebral cortex, the cerebellar cortex has no regional differences. The organization of the cerebellum has put forward theories that implicated the cerebellum as a pattern-learning machine that could guide the learning of specific motor tasks[19,20]. Marr[19] suggested that the parallel fiber input to Purkinje cells would be potentiated when activated in conjunction with a climbing fiber. Contrary, Albus[20] thought that simultaneous parallel fiber and climbing fiber input would lead to depression, because he thought that the cerebellum would learn to recognize patterns most efficiently through weakening of erroneously activated inputs. It was only after Ito[21] described the process of long-term depression (see **paragraph 1.2.2**) that experimental evidence was found for the Marr-Albus theory. In the classic Marr-Albus-Ito hypothesis, also known as the learning hypothesis, long-term depression at the parallel fiber synapse is sufficient to explain cerebellar associative motor learning[22]. Later a second

learning site was suggested: the mossy fiber – cerebellar nuclei synapse[23]. Medina[24] proposed that the first learning site (cortex) initiates learning, while the second (nuclei) is involved in long-term storage. The general idea of the learning hypothesis (depicted in **figure 1.4**) is that information about ongoing movement is conveyed to the Purkinje cells via the mossy / parallel fiber system. If an error occurs, i.e. sensory information in the inferior olive, this will be translated into climbing fiber activity. The effectiveness of the active parallel fiber will now be weakened by the climbing fiber activity. The signal of the Purkinje cells to the cerebellar nuclei is now altered and the cerebellar nuclei will relay a different signal to the pre motor centers than the original input of the mossy fiber system. There is also an alternative hypothesis that explains the functioning of the cerebellum, namely the timing hypothesis advocated by Llinas[25]. This hypothesis is based on the following three observations: (1) olivary neurons have a propensity to fire rhythmically[26-28]; (2) olivary neurons are dynamically electronically coupled by gap junctions so that different synchronous firing patterns can be generated by chemical synaptic inputs[29-31] and (3) synchronous olivary activity can be correlated to the initiation and performance of movements[29,32,33]. In the timing hypothesis, the inferior olive functions as an oscillating clock providing the appropriate timing of command signals for the cerebellum. The main difference between the learning and the timing hypothesis is the role of the inferior olive. In the learning hypothesis the olivary neurons give the cerebellum error signals, correcting the cerebellum until the motor behavior is appropriate; in the timing hypothesis the olivary neurons directly provide the correct information to the cerebellum. The pros and cons of these two theories are reviewed by de Zeeuw *et al.*[14].

1.2   CEREBELLAR ELECTROPHYSIOLOGY

In the next paragraph, I will discuss the electrophysiological properties of Purkinje cells and in **paragraph 1.2.2** and **paragraph 1.2.3** two processes, long-term depression (LTD) and long-term potentiation (LTP) that explain plasticity at the Purkinje cell synapse. Plasticity is the ability of a neuron to alter its responsiveness to certain inputs and one of the four generalizations[1] (see **paragraph 1**) describing learning. The cellular mechanisms that underlie these changes in responsiveness are believed to be the molecular pathways that are responsible for cerebellar learning.

1.2.1   Electrophysiological properties of Purkinje cells

The Purkinje cells are the most recorded cells in the cerebellar cortex for several reasons. They are the only cells projecting out of the cerebellar cortex, they have a high firing frequency and they have a unique firing pattern, because they fire simple and complex spikes. Purkinje cells fire simple spikes at approximately 50 Hz and complex spikes at 1 Hz. After a complex spike there is always a consistent pause in simple spike activity[34]. A simple spike is a normal action potential. A complex spike is a strong depolarization of the Purkinje cell caused by

climbing fiber activity. The characteristics of the complex spike are described by Schmolesky *et. al*[35] and the role of the complex spike is explained by De Zeeuw *et al.*[14]. The spontaneous activity of Purkinje cells is 50 Hz but this can be increased to 80 Hz during eye movements[36], to 150 Hz during arm movements[37] and *in vitro* studies show fire rates of almost 300 Hz[38]. Purkinje cells have a large range of frequencies to transfer information and Purkinje cells are able to integrate different inputs (climbing fibers and mossy fiber / parallel fiber input) to a new signal. Therefore, Purkinje cells seem an important candidate to mediate cerebel-

Figure 1.5
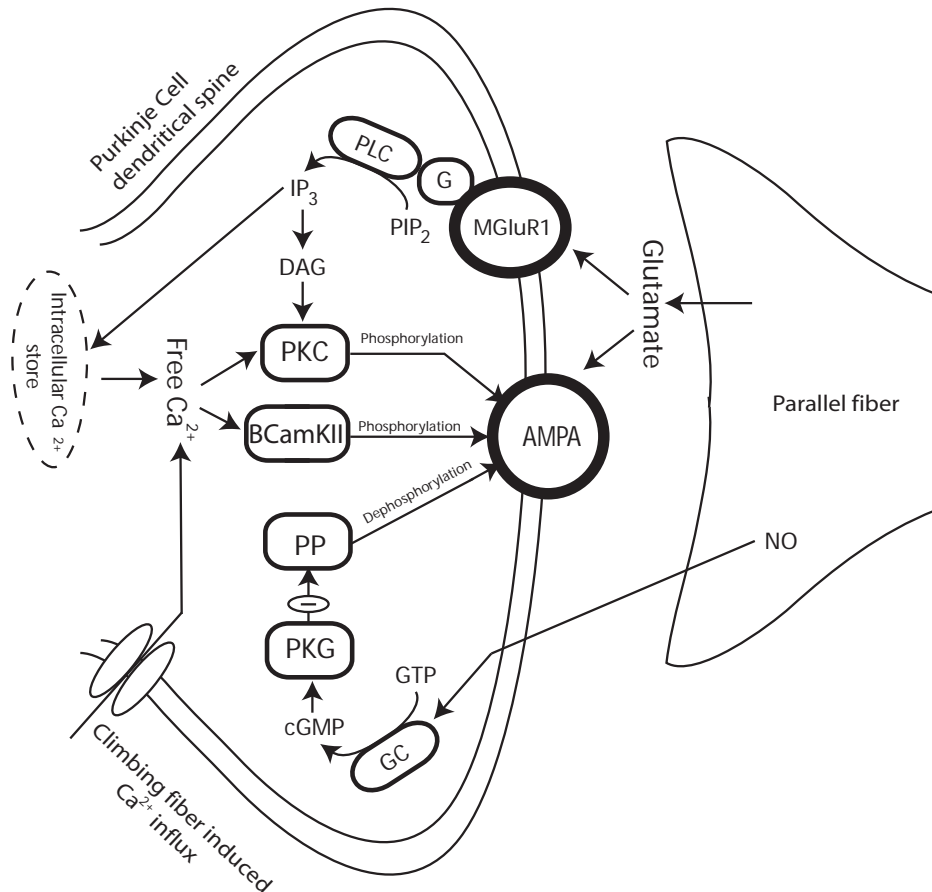
LTD normally requires simultaneous activation of AMPA and MGlu receptors together with a high intracellular free Ca2+. The latter is achieved by both the MGlur activation as well as climbing fiber induced depolarization. MGlur activation leads to production of DAG which together with high free Ca2+ activates PKC. The activation of PKC results in phosphorylation and internalization of AMPAr thereby making the Purkinje cell less excitable through this particular parallel fiber contact. AMPAr=α-amino-3-hydroxy-5-methylisoxazolproprionate receptors. CamKII=Ca2+/calmodulin-dependent protein kinase II. cGMP=cyclic guanosine-mono-phosphate. DAG=diacyl-glycerol. G=G-protein. GC=guanylyl-cylase. GTP=guanosine-tri-phosphate. IP3=inositol-tri-phosphate. MGlur=metabotropic glutamate receptors. NO= nitric oxide. PIP2= phosphatidyl-inositol-phosphate. PKC=protein kinase C. PKG=protein kinase G. PLC=phospholipase C. PP=protein phosphatase.

lar learning. The processes described below, Purkinje cell – parallel fiber LTD and LTP, are believed to underlie cerebellar learning. Plasticity at the parallel fiber – Purkinje cell synapse is reviewed by Jörntell and Hansel[39].

1.2.2   Long-term depression (LTD)

Purkinje cell parallel fiber-LTD is a long lasting reduction in synaptic efficacy and can be induced by pairing parallel fiber activity to climbing fiber activity[40,41]. The process of Purkinje cell parallel fiber-LTD is summarized in **figure 1.5**. Parallel fiber activation leads to the activation of α-amino-3-hydroxy-5-methylisoxazolproprionate receptors (AMPAr) and the metabotropic glutamate receptors (MGlur) on the dendritic synapse of Purkinje cells. Climbing fiber activation leads to a massive depolarization of the Purkinje cell and subsequently to a large increase of intracellular Ca^{2+}. Activation of mGluR1 leads to a G-protein coupled activation of phospholipase C (PLC), which produces diacyl-glycerol (DAG) and converts phosphatidyl-inositol-phosphate (PIP_2) into inositol-tri-phosphate (IP_3). IP_3 mediates release of intracellular Ca^{2+}. Increased intracellular Ca^{2+} and DAG activate protein kinase C (PKC), which acts on AMPA receptors by phosphorylating a serine residue. AMPA receptors with phosphorylated serine residues are internalized by clathrin-mediated endocytosis. Increased intracellular Ca^{2+} also activates CamKII (Calcium/Calmodulin-dependent Kinase type II), which acts in the same way on AMPA receptors as PKC. Thus, LTD causes a reduction in selected parallel fiber synapse efficacy by down-regulating the number of AMPA receptors on the postsynaptic membrane. A second pathway is mediated by nitric oxide (NO)[42,43]. NO is a short-living gas that through diffusion can influence about 4000 synapses in 10 milliseconds. NO acts on guanylyl-cylase (GC), which converts guanosine-tri-phosphate (GTP) into cyclic guanosine-mono-phosphate (cGMP). cGMP then activates protein kinase G (PKG), which results in inhibition of protein phosphatase (PP), thereby blocking dephosphorylation of AMPA receptors.

1.2.3   Long-term potentiation (LTP)

LTP is a physiological procedure pioneered in studies of the hippocampus[44] and is believed to engage the cellular mechanisms similar to those that underlie learning[45]. The most extensively studied form of LTP occurs in the CA1 region of the hippocampus and involves the interaction between presynaptic glutamate and two classes of postsynaptic receptors. First, glutamate binds to AMPA receptors and depolarizes the postsynaptic cell. The depolarization allows glutamate to bind to the N-methyl-D-aspartate (NMDA) class of receptors. Calcium then flows into the cell through the NMDA channel and triggers a host of intracellular events that ultimately result in gene induction and synthesis of new proteins[46].

LTD at cerebellar parallel fiber – Purkinje synapses (see **figure 1.5)** must be balanced to prevent saturation and allow reversal of associative motor learning. Cerebellar LTP is a candidate for this role. Lev-Ram[47] describes a form of postsynaptic LTP enhanced by chelating postsynaptic calcium and depends on NO but not on adenosine 3'5'-cyclic monophosphate

(cAMP) or cGMP, making it a possible reversal mechanism for cerebellar LTD, which is also postsynaptic. Coesmans *et al.*[48] showed that parallel fiber long-term plasticity (both LTD and LTP) is governed by calcium (see **figure 1.6**[48]), which is characterized by a high calcium threshold for LTD and a lower calcium threshold for LTP induction. Postsynaptic parallel fiber-LTP might work more locally than parallel fiber-LTD, because activation of neighboring parallel fibers would lead to an increase of Ca^{2+} and possibly to LTD. LTP may also be used to actively erase memory stored by parallel fiber LTD[49]**.** This would enable parallel fiber-LTD and parallel fiber-LTP to work in synergy, actively shaping Purkinje cell output: 'correctly activated' parallel fibers without climbing fiber activity are potentiated, whereas 'correctly activated' parallel fibers with climbing fiber activity are depressed[48].

Figure 1.6
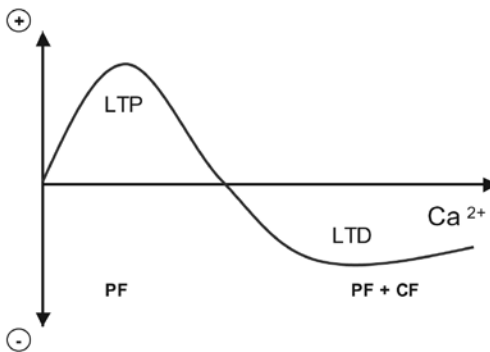
Parallel fiber plasticity is governed by calcium. For parallel fiber-LTD a higher calcium concentration is needed than for parallel fiber-LTP. Climbing fiber activity contributes sufficient calcium to reach the LTD threshold. LTD=Long-Term Depression. LTP=Long-Term Potentiation. PF= Parallel fiber activity. PF + CF=Parallel Fiber + Climbing Fiber activity.

1.3   CEREBELLAR BEHAVIORAL TASKS FOR MICE

In the paragraphs above a short overview was given of structures, cellular mechanisms and models that could explain cerebellar plasticity. Another way to investigate the cerebellum is by testing mice with defects in one of these abovementioned structures or mice lacking one of the abovementioned proteins in a cerebellar behavioral task. With the rapid advances in transgenic technologies, it has become routine to investigate cellular mechanisms using behavioral tasks. Mice are the preferred species for transgenic technologies, and therefore for behavioral testing, since there are several techniques available to manipulate their embryonic stem cells.

    A range of tasks have been developed to behaviorally phenotype (mutant) mice[50,51]. Tasks include grid walking, rope climbing, inclined plane, kinematic analysis, open-field tasks, gait analysis, measures of ground reaction forces, swimming, and accelerating rotarod[52]. The accelerating rotarod will be discussed in **paragraph 1.3.1**. Most of these tasks are easily

implemented and can be used to gauge motor performance. However, none provide information about associative motor learning. Associative motor learning in mice can be explicitly tested using several methods adapted for mice in our laboratory, including compensatory eye movements[53-55] (see **paragraph 1.3.2**) and eyeblink conditioning[56,57] (see **paragraph 1.3.3**). The neural circuitry of the cerebellum that is activated and modified during learning in each of these tasks is well-studied, providing a direct link between behavior and synaptic modification[58]; however, both tasks suffer in that they involve extensive surgical preparation (e.g. eye-coil or magnet placement), careful monitoring during experimental sessions, loss of some subjects during these sessions (e.g., due to broken or displaced coils/magnets) and significant post-hoc analysis. Although all of the abovementioned behavioral tasks have their merits for cerebellar research, I believe that a new cerebellar behavioral task for mice would be an asset. As such, we aimed to build a new behavioral task, the Erasmus Ladder (see **paragraph 1.3.4**) which had to meet the following requirements: (1) the task should be automated; (2) the task should be non-invasive; (3) the task should be more sensitive in detecting motor performance deficits than the accelerating rotarod; (4) the associative motor learning paradigm has to be dependent on the cerebellum and (5) the task should have the ability to distinguish between motor performance deficits and associative motor learning deficits. These requirements are the hypotheses that I will test in this thesis. In **chapter 6**, I will discuss to what extend we have been able to meet these requirements.

1.3.1   Accelerating rotarod

The accelerating rotarod (see **figure 1.7**, model 7650, Ugo Basile Biological Research Apparatus, Varese, Italy) is the most widely used apparatus to test motor behavior in mice. The mouse is placed on a cylinder and the speed of the cylinder rotation is gradually increased over a 5 minute interval. Latency to fall from the rotarod is recorded. Mice are normally tested for 4 sessions and with this accelerating rotarod, 5 mice can be tested at the same time (see **figure 1.7)**. This apparatus is easy to use and acquires data quickly; however the accelerating rotarod task can be compromised by mice. They do this by flatting themselves and holding tight to the rotating rod, thereby riding passively on it instead of running on top of it[59].

Some experimenters claim that you can test cerebellar motor learning with the accelerating rotarod, but I think you only measure motor performance and improvement of motor performance with the accelerating rotarod. For testing cerebellar motor learning you need a more complicated setup.

1.3.2   Compensatory eye movements

In our neuroscience department a cerebellar behavioral task was developed in which we could register compensatory eye movements in mice[60]. Compensatory eye movements are generated to drive the eye muscles to prevent retinal slip. Retinal slip, the slip of images over the retina resulting in a degraded image, is caused by head movements. In mice the two main

Figure 1.7
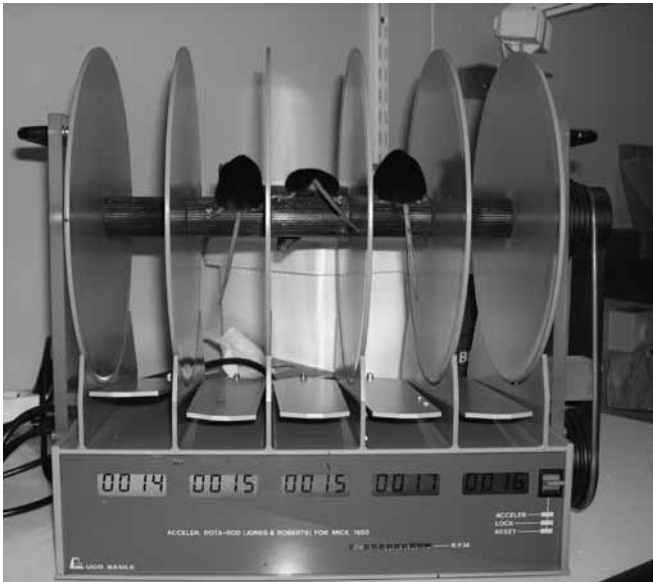
reflexes that compensate for head movement are the vestibuloocular reflex (VOR) and the optokinetic reflex (OKR). The VOR is a reflex based on head movement. The OKR generates eye movements based on retinal slip. Together VOR and OKR aim to minimize the retinal slip. Compensatory eye movements can be quantified in mice using various methods and can be used to make distinction between cerebellum-specific mouse mutants[55]. In **chapter 3** compensatory eye movements will be described in more detail.

1.3.3 Eyeblink conditioning

Another cerebellar task for mice we developed in our department was eyeblink conditioning[56]. This is a classical Pavlovion conditional task. Pavlov was studying the role of saliva in the digestive system. To collect saliva he presented food to dogs, a species that has a natural reflex to start salivating in the presence of food. After working a couple of days with a particular dog, Pavlov noticed that when he entered the room this dog would start to salivate even when there was no food present. The fact that a natural reflex could be affected by learning, made Pavlov switch from studying the digestive system to this interesting phenomenon. In this particular example the salivating in the presence of food is the unconditioned response (UR) and the food itself is the unconditioned stimulus (US). The salivating of the dog without food is the conditioned response (CR) and the entering of the room by Pavlov is called the conditioned stimulus (CS).

In eyeblink conditioning, mice get a puff of air (US) in their eye. This puff of air will cause immediately closure of the eye (UR). Prior to this air puff mice will hear a tone (CS). When mice learn to close their eye, solemnly based on this tone, the mice have made a CR. With

the MDMT technique[56] we use in eyeblink conditioning, we can measure the latency, peak amplitude, velocity and acceleration of eyelid responses. Therefore we can investigate in great detail how mice acquire a CR. Cerebellum-specific mutants[61] and Fmr1 knockout mice[57], have shown deficits in eyeblink conditioning. In **chapter 4**, eyeblink conditioning will be described in more detail. Since both compensatory eye movements and eyeblink conditioning involve invasive surgery, and significant post-hoc analysis, only a limited amount of mice can be measured. Therefore we developed a new cerebellar task that is easier to use.

1.3.4   The Erasmus Ladder

The Erasmus Ladder (see **figure 1.8**) is a horizontal ladder on which mice can perform several visually-guided stepping paradigms. Visually guided stepping has been used as a task for motor performance in rodents[52,62,63], cats[64-66], patients with cerebellar degeneration and control subjects[67]. To the best of my knowledge, visually guided stepping protocols have not been previously used to assess associative motor learning in mice, but our own research and several studies of neuronal firing patterns and locomotion in the cat, indicated that such an approach would be profitable. We have demonstrated that synaptic plasticity in the cerebellum is required for learning-dependent timing of the conditioned eyeblink response in mice[61]. The repeated presentation of an auditory tone (CS) just prior to an air puff to the

Figure 1.8
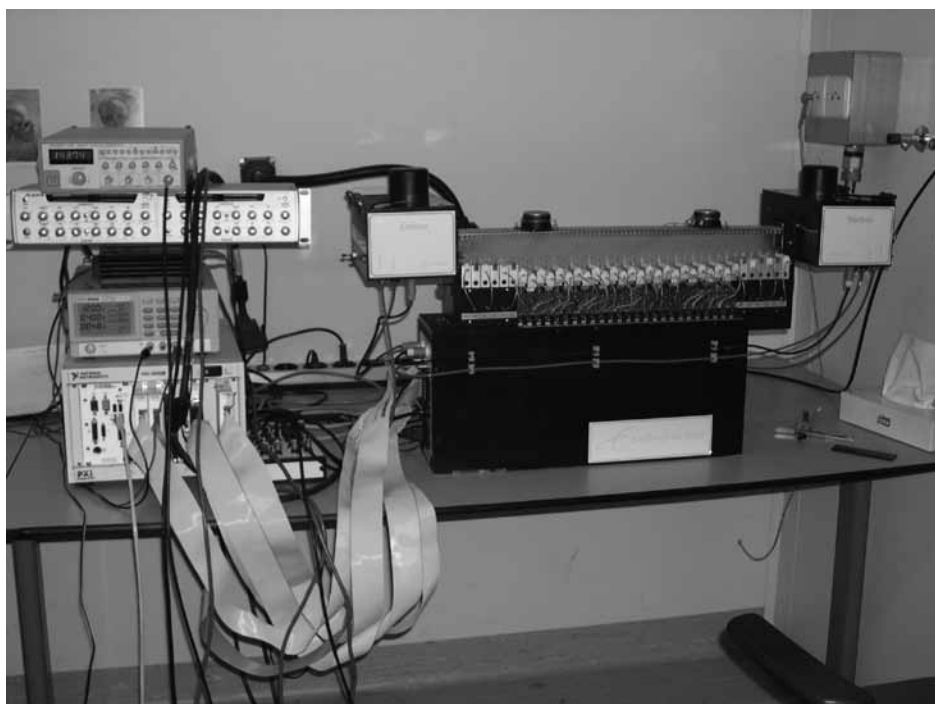
eye (US) ultimately results in acquisition of the conditioned response (a blink to the tone). We reasoned that the same type of classical conditioning could be performed on a horizontal ladder by presenting a tone just prior to raising or lowering a ladder rung in the path of the moving animal. Furthermore, evidence suggests that this form of associative motor learning would likely be cerebellum-dependent: unexpected ladder rung perturbation during visually guided stepping caused modulation of activity in the cat cerebellar cortex and deep cerebellar nuclei[68]. **Chapter 5** explains the used protocols, the analysis and the technical features of the Erasmus Ladder.1.4 Scope of the Thesis

In this introduction, I gave an overview of several ways to study the cerebellum. One of the ways to study the cerebellum is to test (mutant) mice in a behavioral task. We created a new behavioral task, the Erasmus Ladder (see **figure 1.8**), which had to meet the requirements mentioned in **paragraph 1.3**. In the paragraphs below I will describe all the mice, which I measured in **chapters 2**, **chapter 3** and **chapter 4**. **Chapter 5** explains the used protocol, the analysis and the technical features of the Erasmus Ladder. In **chapter 6**, I will discuss to what extend I have been able to meet the requirements of **paragraph 1.3**. In this chapter I will also suggest future improvements.

1.4.1 Expanded CGG mouse

In **chapter 2**, I will try to prove that the Erasmus Ladder can distinguish between motor performance deficits and associative motor learning deficits, which to my knowledge can not be done with any other behavioral task. I will do this by studying two different mouse models, the expanded CGG mouse and the Fmr1 knockout mouse (see **paragraph 1.4.2**). The expanded CGG mouse is a model for fragile-X-associated tremor/ataxia syndrome (FXTAS), a progressive neurodegenerative disorder associated with the fragile X premutation[69]. Male patients carrying a premutation may develop FXTAS at later stages in life (>50 years). FXTAS patients suffer from progressive action tremor, causing executive function deficits, cerebellar dysfunction, cognitive decline and Parkinsonism associated with generalized brain atrophy. Also autonomic dysfunction and peripheral neuropathy were reported[70,71]. There is one report that these mice have a motor performance deficit[72] and to my knowledge there are no reports that these mice have an associative motor learning deficit. Thus, I hypothesize that the expanded CGG mice will have a motor performance deficit but not an associative motor learning deficit on the Erasmus Ladder. FXTAS is a completely different syndrome than Fragile X syndrome, which I will describe below.

1.4.2 Fmr1 knockout mouse

Also in **chapter 2**, the data of the Fmr1 knockout mouse[73] are given. The Fmr1 knockout mouse is a model for fragile X syndrome. Fragile X syndrome has been recognized as the most common inherited form of mental retardation. Other clinical features include macroorchidism, autistic behavior, epileptic seizures, hyperactivity, attention deficits and mild craniofacial abnormalities[74]. In our lab we tested these mice for motor performance deficits and found no differences with wildtype littermates. We have shown that Fmr1 knockout mice have a deficit

in eyeblink conditioning[57]. Therefore, I hypothesize that these mice will have no motor performance deficits but will have an associative motor learning deficit on the Erasmus Ladder.

1.4.3   ßCamKII knockout mouse

In **chapter 3**, I will present data of the Ca^{2+}/calmodulin-dependent protein kinase II beta (βCaMKII) knockout mouse. CamKII is the most abundant kinase in the brain and the α-subunit is essential for neural plasticity in the hippocampus[75-77]. βCaMKII is highly expressed in the cerebellum and we have shown that mice lacking βCaMKII are ataxic and have altered parallel fiber-LTD and parallel fiber LTP[78]. In this chapter we tested if these mutants have an associative motor learning deficit and we measured the spontaneous firing of the Purkinje cells in these mutants. I will also try to make a correlation between the electrophysiological data and the behavioral data.

1.4.4   Cx36 knockout mouse

In chapter 4, I will present data of Connexin36 (Cx36) knockout mice. Cx36 is essential for the creation of gap junctions in neurons. Cx36 is expressed in the olfactory bulb, hippocampus, cerebral cortex, (hypo)thalamus and the inferior olive[79]. For most of these regions, the possible role of neuronal gap junctions has been determined at the cell-physiological level[80-82]. In these *in vitro* studies, a lack of Cx36 generally leads to an absence of electronic coupling and to changes in subthreshold activities[82-84]. Yet, the apparent behavioral phenotype is relatively mild and/or remains a topic for systems electrophysiological investigations[85-88]. In this chapter we will investigate if these mutant mice have an associative motor learning deficit and if the firing of the olivary cells of these mutants is affected. It is also interesting to see if the data of this chapter accumulate evidence for the learning hypothesis or for the timing hypothesis (see **paragraph 1.1.3**).

1.4.5   *Lurcher*

In **chapter 4**, I will also present data of *Lurchers*. *Lurchers* are mutant mice which are characterized by postnatal degeneration of Purkinje cells and their primary afferents, granule cells and olivary neurons[89]. All *Lurcher*s I measured were of such an age that they had no more functional Purkinje cells and all mice were visibly ataxic. These mice are the only cerebellum-specific mice of which data will be presented in this thesis. If *Lurchers* have a motor performance deficit or an associative motor learning deficit on the Erasmus Ladder, this will indicate that the Erasmus Ladder is a cerebellum-specific behavioral task.

1.5   REFERENCES

1.   I. Kupfermann, *Learning and Memory*, 3rd ed. (Elsevier, New York, 1991).
2.   L. Rolando, *Journal de Physiologie Expérimentale* 3, 95 (1823).
3.   L. Luciani, *Il cervelletto: Nuovi studi di fisiologia normale e patologica*. (Le Monnier, Firenze, 1891).

4. P. Flourens, *Recherches expérimentales sur les propriétés et les functions du système nerveuz dans les animaux vertrébés*. (Cervot, Paris, 1824).

5. J. Babinski, *Rev Neurol* 7, 806 (1899).

6. T.J.H. Ruigrok, *The role of the cerebellum*. (VU University Press, Amsterdam, 2007).

7. O. Larsell, *J Comp Neurol* 97 (2), 281 (1952).

8. J. D. Schmahmann, *Arch Neurol* 48 (11), 1178 (1991).

9. J. H. Gao, L. M. Parsons, J. M. Bower et al., *Science* 272 (5261), 545 (1996).

10. S. Ramón y Cajal, *Histologie du système nerveux de l'homme et des vertébrés*. (Maloine, Paris, 1911).

11. R. M. Napper and R. J. Harvey, *J Comp Neurol* 274 (2), 168 (1988).

12. J. C. Desclin, *Brain Res* 77 (3), 365 (1974).

13. C. I. De Zeeuw, J. C. Holstege, T. J. Ruigrok et al., *J Comp Neurol* 284 (1), 12 (1989).

14. C. I. De Zeeuw, J. I. Simpson, C. C. Hoogenraad et al., *Trends Neurosci* 21 (9), 391 (1998).

15. T.J.H. Ruigrok, *Precerebellar nuclei and red nucleus*, 3 ed. (Elsevier Academic Press, San Dieso, 2004).

16. I. Sugihara, *J Comp Neurol* 487 (1), 93 (2005).

17. F. Rossi, T. Borsello, E. Vaudano et al., *Neuroscience* 53 (3), 759 (1993).

18. J. Voogd, *The cerebellum of the cat: structure and fiber connection*. (Van Gorcum, Assen, 1964).

19. D. Marr, *J Physiol* 202 (2), 437 (1969).

20. J.S. Albus, *Math. Biosci.* 10, 25 (1971).

21. M. Ito and M. Kano, *Neurosci Lett* 33 (3), 253 (1982).

22. M. Ito, *The Cerebellum and Neural Control*. (Raven Press, New York, 1984).

23. J. F. Medina, K. S. Garcia, and M. D. Mauk, *J Neurosci* 21 (11), 4081 (2001).

24. J. F. Medina, J. C. Repa, M. D. Mauk et al., *Nat Rev Neurosci* 3 (2), 122 (2002).

25. R. Llinas, *Physiologist* 17 (1), 19 (1974).

26. R. Llinas and Y. Yarom, *J Physiol* 315, 549 (1981).

27. R. Llinas and Y. Yarom, *J Physiol* 315, 569 (1981).

28. R. Llinas and Y. Yarom, *J Physiol* 376, 163 (1986).

29. R. Llinas and K. Sasaki, *Eur J Neurosci* 1 (6), 587 (1989).

30. C. I. De Zeeuw, E. J. Lang, I. Sugihara et al., *J Neurosci* 16 (10), 3412 (1996).

31. T. H. Bullock, M. V. Bennett, D. Johnston et al., *Science* 310 (5749), 791 (2005).

32. J. P. Welsh, E. J. Lang, I. Suglhara et al., *Nature* 374 (6521), 453 (1995).

33. E. J. Lang, I. Sugihara, and R. Llinas, *J Neurophysiol* 76 (1), 255 (1996).

34. W. T. Thach, Jr., *J Neurophysiol* 30 (4), 675 (1967).

35. M. T. Schmolesky, J. T. Weber, C. I. De Zeeuw et al., *Ann N Y Acad Sci* 978, 359 (2002).

36. H. H. Goossens, F. E. Hoebeek, A. M. Van Alphen et al., *Eur J Neurosci* 19 (3), 687 (2004).

37. P. F. Gilbert and W. T. Thach, *Brain Res* 128 (2), 309 (1977).

38. Z. M. Khaliq and I. M. Raman, *J Neurosci* 25 (2), 454 (2005).

39. H. Jorntell and C. Hansel, *Neuron* 52 (2), 227 (2006).

40. D. J. Linden and J. A. Connor, *Annu Rev Neurosci* 18, 319 (1995).

41. M. Ito, *J Physiol* 81 (2001).

42. H. Daniel, N. Hemart, D. Jaillard et al., *Eur J Neurosci* 5 (8), 1079 (1993).

43. V. Lev-Ram, L. R. Makings, P. F. Keitz et al., *Neuron* 15 (2), 407 (1995).

44. T. V. Bliss and T. Lomo, *J Physiol* 232 (2), 331 (1973).

45. T. V. Bliss and G. L. Collingridge, *Nature* 361 (6407), 31 (1993).

46. E. R. Kandel, *J Cell Physiol* 173 (2), 124 (1997).

47. V. Lev-Ram, S. T. Wong, D. R. Storm et al., *Proc Natl Acad Sci U S A* 99 (12), 8389 (2002).

48. M. Coesmans, J. T. Weber, C. I. De Zeeuw et al., *Neuron* 44 (4), 691 (2004).

49.   M. Fujita, *Biol Cybern* 45 (3), 195 (1982).

50.   R. E. Brown, *Can J Exp Psychol* 61 (4), 328 (2007).

51.   J. N. Crawley, *Neuron* 57 (6), 809 (2008).

52.   B. J. Cummings, C. Engesser-Cesar, G. Cadena et al., *Behav Brain Res* 177 (2), 232 (2007).

53.   C. I. De Zeeuw, A. M. Van Alphen, S. K. Koekkoek et al., *Otolaryngol Head Neck Surg* 119 (3), 193 (1998).

54.   J. S. Stahl, A. M. van Alphen, and C. I. De Zeeuw, *J Neurosci Methods* 99 (1-2), 101 (2000).

55.   A. M. Van Alphen, T. Schepers, C. Luo et al., *Ann N Y Acad Sci* 978, 413 (2002).

56.   S. K. Koekkoek, W. L. Den Ouden, G. Perry et al., *J Neurophysiol* 88 (4), 2124 (2002).

57.   S. K. Koekkoek, K. Yamaguchi, B. A. Milojkovic et al., *Neuron* 47 (3), 339 (2005).

58.   C. I. De Zeeuw and C. H. Yeo, *Curr Opin Neurobiol* 15 (6), 667 (2005).

59.   D. Wahlsten, N. R. Rustay, P. Metten et al., *Trends Neurosci* 26 (3), 132 (2003).

60.   A. M. Van Alphen, J. S. Stahl, and C. I. De Zeeuw, *Brain Res* 890 (2), 296 (2001).

61.   S. K. Koekkoek, H. C. Hulscher, B. R. Dortland et al., *Science* 301 (5640), 1736 (2003).

62.   J. Cendelin, I. Korelusova, and F. Vozeh, *Behav Brain Res* 189 (1), 65 (2008).

63.   J. S. Soblosky, L. L. Colgin, D. Chorney-Lane et al., *J Neurosci Methods* 78 (1-2), 75 (1997).

64.   D. M. Armstrong, *Prog Neurobiol* 26 (4), 273 (1986).

65.   K. M. Friel, T. Drew, and J. H. Martin, *J Neurophysiol* 97 (5), 3396 (2007).

66.   D. E. Marple-Horvat, J. M. Criado, and D. M. Armstrong, *J Physiol* 506 (Pt 2), 489 (1998).

67.   D. E. Marple-Horvat and K. A. Crowdy, *Gait Posture* 21 (1), 39 (2005).

68.   D. E. Marple-Horvat and J. M. Criado, *J Physiol* 518 (Pt 2), 595 (1999).

69.   R. Willemsen, M. Hoogeveen-Westerveld, S. Reis et al., *Hum Mol Genet* 12 (9), 949 (2003).

70.   P. J. Hagerman and R. J. Hagerman, *Am J Hum Genet* 74 (5), 805 (2004).

71.   J. R. Brouwer, R. Willemsen, and B. A. Oostra, *Am J Med Genet B Neuropsychiatr Genet* (2008).

72.   D. Van Dam, V. Errijgers, R. F. Kooy et al., *Behav Brain Res* 162 (2), 233 (2005).

73.   E. J. Mientjes, I. Nieuwenhuizen, L. Kirkpatrick et al., *Neurobiol Dis* 21 (3), 549 (2006).

74.   R. J. Hagerman, *Fragile-X syndrome: diagnosis, treatment and research*. (The Johns Hopkins University Press, Baltimore, 2002).

75.   Y. Elgersma, N. B. Fedorov, S. Ikonen et al., *Neuron* 36 (3), 493 (2002).

76.   Y. Elgersma, J. D. Sweatt, and K. P. Giese, *J Neurosci* 24 (39), 8410 (2004).

77.   J. E. Lisman, *Proc Natl Acad Sci U S A* 82 (9), 3055 (1985).

78.   G. M. Van Woerden, F. E. Hoebeek, Z. Gao et al., *Nat Neurosci* (2009).

79.   C. I. De Zeeuw, E. L. Hertzberg, and E. Mugnaini, *J Neurosci* 15 (2), 1587 (1995).

80.   M. R. Deans, J. R. Gibson, C. Sellitto et al., *Neuron* 31 (3), 477 (2001).

81.   C. E. Landisman, M. A. Long, M. Beierlein et al., *J Neurosci* 22 (3), 1002 (2002).

82.   M. A. Long, M. R. Deans, D. L. Paul et al., *J Neurosci* 22 (24), 10898 (2002).

83.   D. L. Buhl, K. D. Harris, S. G. Hormuzdi et al., *J Neurosci* 23 (3), 1013 (2003).

84.   C. I. De Zeeuw, E. Chorev, A. Devor et al., *J Neurosci* 23 (11), 4700 (2003).

85.   M. Guldenagel, J. Ammermuller, A. Feigenspan et al., *J Neurosci* 21 (16), 6036 (2001).

86.   M. R. Deans, B. Volgyi, D. A. Goodenough et al., *Neuron* 36 (4), 703 (2002).

87.   C. Frisch, M. A. De Souza-Silva, G. Sohl et al., *Behav Brain Res* 157 (1), 177 (2005).

88.   M. A. Long, M. J. Jutras, B. W. Connors et al., *Nat Neurosci* 8 (1), 61 (2005).

89.   M. W. Vogel, J. Caston, M. Yuzaki et al., *Brain Res* 1140, 4 (2007).

CHAPTER II

The Erasmus Ladder: a new, automated system for precise phenotyping of motor behavior in mice

Alexander Cupido, Matthew T. Schmolesky, Rob Willemsen, Ben A. Oostra, Sebastiaan K. E. Koekkoek and Chris I. De Zeeuw

ABSTRACT

Here we describe in detail the Erasmus Ladder, which is a new system to measure motor behavior in mice. The main incentive for the creation of the Erasmus Ladder is that there are no behavioral tasks for mice available that can reliably separate motor performance deficits from associative motor learning deficits. Furthermore, we wanted to create a tool that is easy to use and does analysis automatically. We present data of two mouse models, one for fragile X syndrome (FXS) and one for fragile-X-associated tremor/ataxia syndrome (FXTAS). We also provide evidence that the Erasmus Ladder can be configured as a cerebellum-specific task.

INTRODUCTION

A central focus of neuroscientific research has been to study the genetic, cellular and physiological correlates of motor function and dysfunction. The fact that many neurological conditions involve the loss of motor coordination, performance, or learning lends urgency to this research. In this pursuit, a range of tasks have been developed to behaviorally phenotype (mutant) mice[1,2]. Tests of locomotion include grid walking, rope climbing, inclined plane, kinematic analysis, open-field tasks, gait analysis, measures of ground reaction forces, swimming and accelerating rotarod[3]. Most of these tasks are easily implemented and can be used to gauge motor performance. However, none provide information about associative motor learning. Associative motor learning in mice can be explicitly tested using several methods adapted for mice in our laboratory, including compensatory eye movements[4-6] and eyeblink conditioning[7,8]. The neural circuitry of the cerebellum that is activated and modified during learning in each of these tasks is well-studied, providing a direct link between behavior and synaptic modification[9]; however, both tasks suffer in that they involve extensive surgical preparation (e.g. eye-coil or magnet placement), careful monitoring during experimental sessions, loss of some subjects during these sessions (e.g., due to broken or displaced coils/magnets) and significant post-hoc analysis. Thus, we sought to develop a method for behaviorally phenotyping mice that would not require surgery, would be automated via software driven control, would provide real-time data analysis and would be capable of providing information on both motor performance and associative motor learning. At the same time, we wished to develop a method that would be suitable for testing associative motor learning that is likely to be dependent upon proper function of, and plasticity in, the cerebellum.

The Erasmus Ladder described herein offers each of these benefits by making use of a horizontal ladder and a visually-guided stepping paradigm. Visually guided stepping has been used as a test for motor performance in rodents[3,10,11], cats[12-14], patients with cerebellar degeneration and control subjects[15]. To the best of our knowledge, visually guided stepping protocols have not been previously used to assess associative motor learning in mice, but our own research, and several studies of neuronal firing patterns and locomotion in the cat, indicated to us that such an approach would be profitable. We have demonstrated that synaptic plasticity in the cerebellum is required for learning-dependent timing of the conditioned eyeblink response in mice[8]. The repeated presentation of an auditory tone (conditioned stimulus) just prior to an air puff to the eye (unconditioned stimulus) ultimately results in acquisition of the conditioned response (a blink to the tone). We reasoned that the same type of classical conditioning could be performed on a horizontal ladder by presenting a tone just prior to raising or lowering a ladder rung in the path of the moving animal. Furthermore, evidence suggests that this form of associative motor learning would likely be cerebellum-dependent: unexpected ladder rung perturbation during visually guided stepping caused modulation of activity in the cat cerebellar cortex and deep cerebellar nuclei[16]. Here we describe the development and implementation of the Erasmus Ladder and offer evidence that

it is capable of sensitive and automated phenotyping of mice, both for motor performance and associative motor learning.

RESULTS

All wildtype and mutant mice were tested for motor performance and associative motor learning using two different protocols of the Erasmus Ladder (see **figure 2.1a**). The Erasmus Ladder is composed of 2 X 37 rungs, which may be raised or lowered individually (see **figure 2.1b**). Prototype testing revealed an optimum forepaw displacement of 60 mm during a single step at medium to high velocity locomotion. Therefore, rungs were spaced 15 mm apart for highly flexible ladder configurations wherein the experimenter can lower or raise rungs at will to create varying degrees of difficulty. All experiments described herein used a configuration in which even numbered rungs on one side and odd numbered rungs on the other side were placed in the descended position (6 mm below the upright rungs) so as to create a distance of 30 mm between rungs (see **figure 2.1b**). This allowed extremely motorically compromised mice to finish the task, while the task was still challenging enough for wildtype mice. Each mouse was tested once per day, first in four motor performance sessions and then in four associative motor learning sessions.

Motor performance sessions

During the motor performance sessions a mouse was placed in one of the shelters. After 9-11 seconds the light was turned on (run cue 1) and automatically followed three seconds later by the pressurized air outlet (run cue 2) in this shelter (see **figure 2.1c**). When the mouse exited the shelter, a second pressurized air outlet (see **figure 2.1c**) was activated, providing a tailwind to encourage the animal to walk over the ladder to the opposite shelter at a consistent, and relatively high speed. It is worth noting that extensive pilot testing demonstrated that without a strong incentive (i.e. the pressurized air) to transit the ladder, mice would explore the rungs at leisure, often pausing and reversing directions. This variable exploratory behavior made it impossible to predict exactly when a mouse would place a paw on a given rung and therefore impossible to implement a precisely timed associative motor learning paradigm. Thus, the pressurized air tailwind proved to be a critical feature.

Every rung in the Erasmus Ladder system is equipped with a sensor composed of a Hall device that is actuated by a magnet embedded in the rung (see **figure 2.1d**). Rung movement threshold is set by adjusting the diameter of the hinge rod and rung press detection is performed by the Hall device. A National Instruments[17] (NI) computer system running a real-time operating system was programmed to read all sensors and store the data within a guaranteed 2 ms cycle. The computer itself is a NI PXI-8150[17] controller mounted in a PXI[17] chassis. The sensor readout is performed by digital IO hardware (3x PXI-6533[17]). Thus, the timing of every paw placement, and the overall pattern of stepping was recorded for each

trial in real-time. When the mouse arrived in the opposite shelter, the two pressurized air outlets were automatically switched off. After 9-11 seconds the protocol as described above was repeated. One trial was defined as a single ladder crossing from shelter to shelter and one session consisted of 72 trials.

After numerous pilot sessions in this configuration (see **figure 2.1a** and **figure 2.1b**) with several different (mutant) mice, we established that the step time, the time needed to transfer one paw from one rung to the next rung, is normally between 300 and 400 ms. Visibly ataxic mice have longer step times (see **chapter 3** and **chapter 4**). In **figure 2.2a** and **figure 2.3a** the step times are given of the motor performance sessions of the mutant mice described below and their wildtype littermates. As mice traversed the ladder, the number of missteps per trial was recorded (see **figure 2.2b** and **figure 2.3b**). A misstep was defined as any step on one of the descended half-rungs (see **figure 2.1b)**. The average number of missteps per trial in a given session was taken as a measure of motor performance. A decrease in the number of missteps per trial over the motor performance sessions is a measure of improved motor performance. To test the ability of the Erasmus Ladder to do automatic phenotyping on motor performance, we first compared 48-56 week old expanded CGG mice to their wildtype littermates. The expanded CGG mouse is a murine model for fragile-X-associated tremor/ataxia syndrome (FXTAS), a progressive neurodegenerative disorder associated with the fragile X premutation[18]. Male patients carrying this premutation may develop FXTAS at later stages in life (>50 years). Mice of 48-56 weeks old are comparable to humans at the age of 50. FXTAS patients suffer from progressive action tremor, causing executive function deficits, cerebellar dysfunction, cognitive decline and Parkinsonism associated with generalized brain atrophy. Also autonomic dysfunction and peripheral neuropathy were reported[19,20]. Traditional motor behavior phenotyping did not reveal any significant difference between 52 week old expanded CGG mice and their wildtype littermates on the accelerating rotarod[22]. In contrast, we found that expanded CGG mice made significantly more missteps at 48-56 weeks on the Erasmus Ladder than did their wildtype littermates in all motor performance sessions (see **figure 2.2b**). Further analysis revealed that both expanded CGG mice and wildtype littermates show significant improvement in motor performance over the motor performance sessions (see **figure 2.2b**). In **figure 2.2a** the step times are given for the expanded CGG mice and their wildtype littermates. Expanded CGG mice have over the motor performance sessions an average step time of 327 ms per step and their wildtype littermates a step time of 389 ms. Note that a low step time indicates a high speed. It is not surprising that the wildtype mice are a bit slower than the expanded CGG mice. Wildtype mice take more care in placing their paws on the rungs and therefore make significantly less missteps (see **figure 2.2b**). Finally, while expanded CGG mice demonstrated relatively poor motor performance compared to wildtype littermates, expanded CGG mice were still able to complete the task, and wildtype littermates found the task suitably challenging, even after four motor performance sessions they had an average of 2.04 missteps per trial (see **figure 2.2b**). Collectively, these
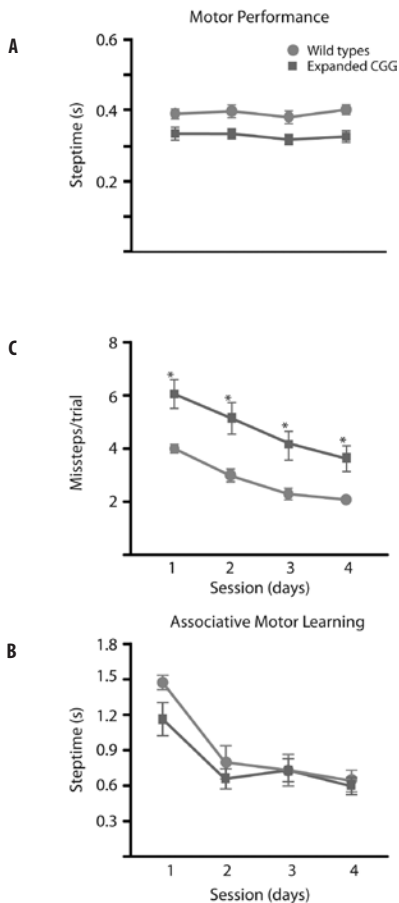
Figure 2.1
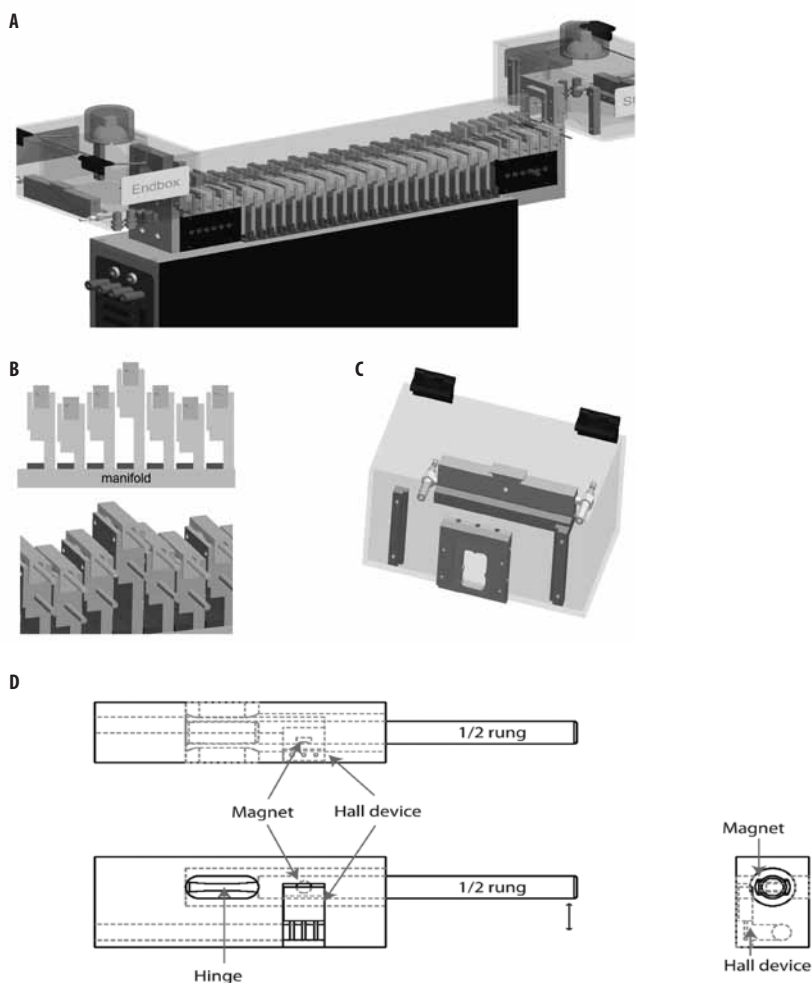
A General overview of the Erasmus Ladder. **B** The stepping pattern used throughout this study is depicted. The lowered rungs are 6 mm below the stepping surface. Here, the middle rung is raised 12 mm above the stepping surface and this is an example of the obstacle in the associative motor learning (see **figure 2.2c**, **figure 2.3c**, **figure 2.4a** and **figure 2.4b**). The distance between the rung and the manifold (40 mm) is significantly greater than the length of a mouse limb, thus a misstep is unpleasant for the animal. Thus, each half-rung was equipped with an "anti-escape" rod placed 12 mm below the rung itself. **C** One of the shelters is depicted. On the grayish block facing the rear, eight pressurized air outlets are strategically placed, which encourages the mouse to leave the shelter (run cue 2, see text). A bigger outlet is aimed at the stepping surface of the mouse and the strength of this outlet can be altered by a voltage controlled variable valve. The valve is controlled by LabView real-time software in such a way that when the mouse is on the stepping surface, it will always have a tailwind of 16 km p/h which encourages the mouse to traverse the stepping surface to the other shelter at a constant speed. The small valves have a diameter of 1mm and the large valve a diameter of 5 mm. The opening to the stepping surface is 25 mm wide and 40 mm high, the shelter itself is 135 mm wide, 104 mm high and 230 mm deep. **D** The sensor is constructed out of custom 3d printed polymer components. In principle it is a rod that connects to the outer housing with a flattened area. Movement threshold is set by adjusting the diameter of this flattened area. Rung press detection is performed by a Hall device that is actuated by a magnet embedded in the rung. This magnetic setup provides a system that is unaffected by the debris that inevitably builds up when mice are frequently crossing the Erasmus Ladder.

data indicate that the Erasmus Ladder is able to automate motor performance phenotyping, and is sensitive enough to reveal motor performance deficits not seen in traditional motor performance phenotyping.

Associative motor learning sessions

After the four motor performance sessions we subjected the mice to four associative motor learning sessions in which they were trained to avoid an obstacle using a tone as the conditioned stimulus (CS) and a rising rung in the swing phase of their right paw as the unconditioned stimulus (US). Proper associative conditioning requires precise timing of the CS-US presentation to achieve consistent and appropriate inter-stimulus intervals (ISI). During each trial, step sizes and step times were buffered in real-time and standard deviations (SD) were calculated for every three step combinations using custom written real-time LabView software[17]. The step time is the time needed to transfer the front paw from one rung to the

Figure 2.2

A Expanded CGG mice (squares, n=13) and their wildtype littermates (circles, n=7) have similar step times over the four sessions. No significant differences are found between the two strains. **B** Expanded CGG mice and their wildtype littermates both significantly improve their motor performance over time, but the expanded CGG mice are in each session significantly worse than their wild type littermates. One-way Anova: learning for both strains, p<0.001; Two-way Anova: difference between strains, p<0.05. Paired students t-test: all sessions p<0.05. **C** Expanded CGG mice and their wildtype littermates learn to adjust their walking pattern to the suddenly appearing obstacle in the same way. No significant differences are found between the two strains. Note that the average step times of the wild type expanded CGG mice are smaller (hence they step slower) than of wildtype Fmr1 knockout mice in **figure 4c**. This is likely due to the large age difference. The wildtype expanded CGG mice are 48-56 weeks old and the Fmr1 knockout mice are 12-16 weeks old.

next rung in the traveling path of the mouse; the step size is the distance between these two rungs. Whenever the SD of the step sizes equaled zero (so all three step sizes are the same) and the SD of the accompanying step times was smaller than 150 ms, the stepping pattern was reliable enough to predict when and where the mouse was going to place its right fore-paw. With this information, the real-time LabView[17] software calculated an appropriate time and place (i.e. specific half-rung) to present the US perturbation by raising the half-rung by 18 mm to create an obstacle of 12 mm above the stepping surface of the mice (see **figure 2.1b**). At a time point 285 ms before this US perturbation was going to take place the Erasmus Ladder presented a 90 dB, 15 kHz tone (lasting 285 ms) as the CS. The pressurized air outlets provided a background noise of 80 dB which prevented auditory startle reactions to the CS. The rung remained in the raised position until the mouse entered the opposing shelter, whereupon it was automatically lowered. The associative motor learning sessions consisted of nine blocks of eight trials; each block consisted of six CS-US paired trials, one US-Only trial, and one CS-Only trial. The key feature of the associative motor learning sessions is that the timing of the US is determined by the stepping pattern of each mouse individually.

Using the protocol described above, for each trial we calculated the step time directly after the CS in order to measure associative motor learning for the expanded CGG mice. The averages of these values across all CS-US paired trials are given in **figure 2.2c**. A decrease in step time directly after the CS over the sessions implies that mice learn to adjust their stepping pattern to the obstacle and is therefore a measure of associative motor learning. As shown in **figure 2.2c**, expanded CGG and wildtype mice both demonstrate associative motor learning and the rate of associative motor learning is not significantly different between the two groups of mice. Thus, we are able to measure motor performance and associative motor learning in mice using the Erasmus Ladder. In the case of the expanded CGG animals, the mutant mice clearly show a dysfunction in motor performance (see **figure 2.2b**), but not in associative motor learning (see **figure 2.2c**).

To further test the capabilities of the Erasmus Ladder, we chose to examine the Fmr1 knockout mouse[21], a model for fragile X syndrome (FXS). FXS has been recognized as the most common inherited form of mental retardation. Other clinical features include mac-roorchidism, autistic behavior, epileptic seizures, hyperactivity, attention deficits and mild craniofacial abnormalities[22]. The development of mouse models of FXS has facilitated cellular studies on the underlying molecular basis of this loss-of-function disorder. Fmr1 knockout mice recapitulate the typical characteristics of FXS, including behavioral abnormalities, learn-ing deficits and audiogenic seizures[23]. In this study, all mice were measured between an age of 12 and 16 weeks. The motor performance sessions revealed that Fmr1 knockout mice and their wildtype littermates do not show significant differences in step times, in missteps per trial or in motor performance improvement (see **figure 2.3a** and **figure 2.3b**), suggesting that motor performance in these mutants is normal. Since accelerating rotarod data from Fmr1 knockout mice with this background have not yet been published, we tested mice us-

ing this measure and found no differences between Fmr1 knockout mice and their wildtype littermates (data not shown). Next we conducted the associative motor learning sessions with these mice. The results of the CS-US paired trials indicate that learning occurs in the first two sessions for both strains and saturates in the following sessions (see **figure 2.3c**). Wildtype animals learn at a faster rate than their knockout littermates (see **figure 2.3c**). Put otherwise, the average Fmr1 knockout step time is significantly higher than of that of their wildtype littermates for sessions 2, 3, and 4 (see **figure 2.3c**). Note that the step times of the wildtype Fmr1 knockout mice (see **figure 2.3c**) are significantly lower than the step times of the wildtype expanded CGG mice (see **figure 2.2c**) in the associative motor learning sessions. This is likely due to the age difference between the groups. The expanded CGG mice are on average more than 8 months older than the Fmr1 knockout mice.

After establishing that there is a difference in the CS-US paired trials between Fmr1 knockout mice and their wildtype littermates, we analyzed this difference in more detail by looking
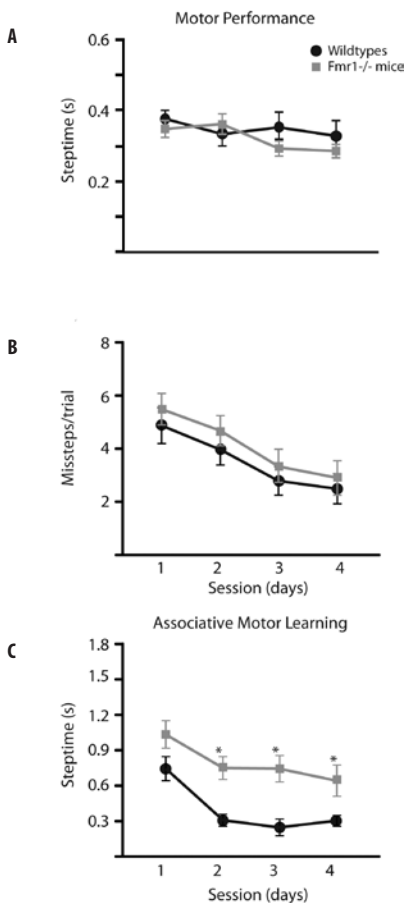
Figure 2.3

A Fmr1 knockout mice (squares, n=7) and their wildtype littermates (circles, n=9) have similar step times over the four sessions. No significant differences are found between the two strains. **B** Fmr1 knockout mice and their wildtype littermates have the same amount of missteps per trial over the four sessions. No significant differences are found between the two strains. **C** Fmr1 knockout mice do not learn to adjust their walking pattern to the suddenly appearing obstacle as quick as their wildtype littermates. In the first session the step time does not differ significantly, but the step time does differ significantly in sessions 2, 3 and 4. One-way Anova: learning for both strains, $p<0.001$. Two-way Anova: difference between strains, $p<0.001$. Students paired t-tests: session 1, $p=0.08$; session 2, $p=0.001$; session 3, $p=0.002$ and session 4, $p=0.018$.

at the US-Only trials. In **figure 2.4a,** we compared the US-Only trials with the CS-US paired trials for the Fmr1 knockout mice. As can be seen in **figure 2.4a** there is no difference between the two graphs. We can conclude from **figure 2.4a** that the associative motor learning the Fmr1 knockout mice showed in **figure 2.3c** is not based on the CS, but on other stimuli, most likely on visual stimuli, e.g. the movement of the rung becoming an obstacle itself or on the experience acquainted in previous trials. In **figure 2.4b** the CS-US paired trials of the wildtype littermates are compared to their US-Only trials and the difference between these two graphs is the associative motor learning based on the CS. This graph indicates that after two sessions the associative learning based on the CS is saturated, since in session 3 there are no differences between the CS-US paired trials and the US-Only trials. After establishing that there is a difference in associative motor learning between Fmr1 knockout mice and their wildtype littermates based on the CS, we wished to examine the CS-Only trials. The average
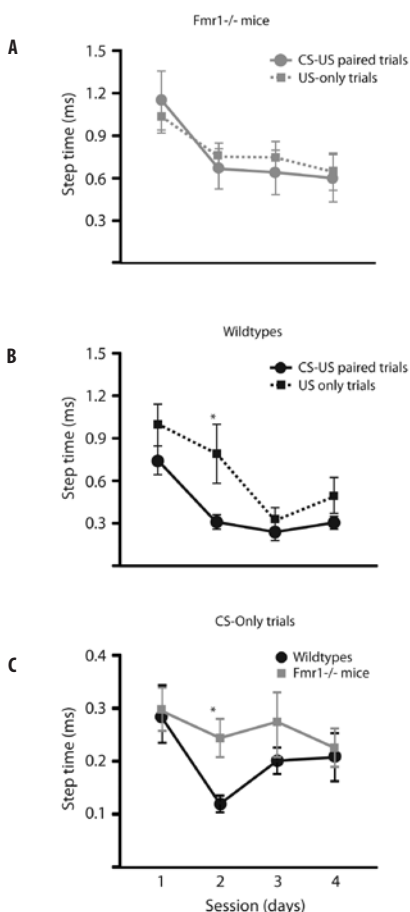
Figure 2.4

A Fmr1 knockout mice have similar step times in the CS-US paired trials as in the US-Only trials. No significant differences are found between the two different trials. This indicates that the Fmr1 knockout mice are unable to adjust to the perturbation by using the CS as a cue. **B** Wildtype mice have lower step times in the CS-US paired trials than in the US-Only trials. This indicates that wildtype Fmr1 knockout mice do use the CS as a cue to adjust to the upcoming perturbation. One way Anova: learning for both strains, $p<0.001$. Two-way Anova: difference between strains, $p<0.001$. Students paired t-tests: session 1, $p=0.180$; session 2, $p=0.026$; session 3, $p=0.526$ and session 4, $p=0.135$. **C** Wildtype mice have lower step times in the CS-Only trials than the Fmr1 knockout mice. The effect of the CS is especially prominent in the second session. After the second session other (most likely visual cues) may assist the animals in adjusting to the perturbation in time. Two-way Anova: difference between strains, $p<0.001$. Students paired t-tests: session 1, $p=0.900$; session 2, $p=0.005$; session 3, $p=0.526$ and session 4, $p=0.135$.

step time during motor performance session 4 was 320 ms for the Fmr1 knockout mice and 346 ms for the wildtype littermates (see **figure 2.3a**). As can be seen in **figure 2.4c**, the step time for wildtypes decreases to 125 ms in session 2, while the step time of Fmr1 knockout mice only decreases to 255 ms. The average step time differs significantly in session 2 (see **figure 2.4c**). The most logical explanation for the decrease in step time (increase in speed) is the following: the 285 ms CS-US interval does not give mice enough time to stop in front of the obstacle; even when mice attempt to stop completely, they will hit the obstacle, which is clearly aversive. Therefore, wildtype mice universally accelerate after the CS to avoid the obstacle. This is a successful tactic, since the Erasmus Ladder software presumes that the step times of the mice remain constant. In **figure 2.4c** every wildtype mouse (n=9) had decreased its step time with more than 50% (an increase of speed of more than 50%). Not one of the knockout mice (n=7) decreased its speed with more than 50%. Two knockout mice were even slower in associative motor learning session 2 than in motor performance session 4. Note again that this graph shows that after two sessions the associative motor learning related to the CS is saturated.

DISCUSSION

We have created a new behavioral task for mice that can detect subtle motor performance deficits and associative motor learning deficits, which to our knowledge is not possible with any other behavioral task for mice. The Erasmus Ladder task can be completed by visibly ataxic mice (see **chapter 3** and **chapter 4**) and is still too difficult for wildtype mice to perform without missteps. This makes the Erasmus Ladder a better tool to analyze motor performance than the accelerating rotarod, because there are limitations in the range of scores possible on the accelerating rotarod, since some mice achieve the maximum score, i.e. they will stay on the accelerating rotarod at its highest speed and others will score the minimum, i.e. they will fall off immediately[24]. The Erasmus Ladder does not produce minimum scores (all mice finish the task) nor maximum scores (no mouse ever had a session without a misstep) and therefore can detect more subtle motor performance deficits in mice than the accelerating rotarod.

In eyeblink conditioning, associative learning is measured as the improvement of correct (conditioned) responses to CS-Only trials over time[7,8]. Correct responses from CS-Only trials prove that the mice make an association between the tone (CS) and the air puff (US), because the mice close their eyes at the appropriate moment even without an US. With the associative motor learning paradigm on the Erasmus Ladder it is not possible to show an improvement in correct responses. Moreover, the US (the obstacle) in the Erasmus Ladder task, unlike eyeblink conditioning, cannot be reflexively avoided, but has to be avoided by changing their stepping pattern.

Fmr1 knockout mice have an associative motor learning deficit, since we found no difference between their CS-US paired trials and their US-Only trials (see **figure 2.4**). The associa-

tive motor learning Fmr1 knockout mice did show was not related to the CS, but to other cues. All mice use other cues than the CS to avoid the obstacle, most likely the raise of the rung itself and probably also the experience from previous trials. Interestingly, the associative motor learning related to the CS is already saturated after two sessions, unlike other cerebellar associative motor learning tasks, implicating that another part of the cerebellum is involved in the motor learning paradigm on the Erasmus Ladder than in conventional cerebellar behavioral tasks[4-8].

An important question to answer is: how cerebellum-specific is the associative motor learning paradigm of the Erasmus Ladder? The best way to prove that this paradigm is cerebellum-specific is by testing cerebellum-specific mutants, which have no motor performance deficits but do have deficits in the associative motor learning paradigm. Unfortunately, all cerebellum-specific mutants we tested so far demonstrated motor performance deficits or no deficits at all. However, there is a lot of evidence that the associative motor learning paradigm is cerebellum-specific: (1) as mentioned before unexpected ladder rung perturbation during visually guided stepping caused modulation of activity in the cat cerebellar cortex and deep cerebellar nuclei[16]; (2) although this mouse is not a cerebellum-specific mutant, Fmr1 is highly expressed in Purkinje cells[25] and (3) we also measured wildtype mice with the associative motor learning paradigm that were either injected with mefloquine or only with the vehicle (see **chapter 4**). Mefloquine blocks the functioning of gap junctions in the inferior olive[26]. The inferior olive only projects to the cerebellum[27]. Since the mice injected with mefloquine were significantly impaired in the associative motor learning sessions and the mice injected with just the vehicle were not impaired, this points to the cerebellum-specificity of the associative motor learning paradigm.

Finally, we would like to summarize the main advantages of the Erasmus Ladder: (1) the Erasmus Ladder can be operated by an inexperienced person; (2) the Erasmus Ladder is completely automated and (3) the Erasmus Ladder can detect subtle motor performance and associative motor learning deficits in mice.

METHODS

The Erasmus Ladder consists of two shelter boxes connected by a horizontal ladder composed of computer-controlled rungs that can be raised or lowered at will. Here we will describe each of the Erasmus Ladder system components in turn.

Shelters

Each shelter is a black PVC box (see **figure 2.1c**) with a small opening on the side and a hinged roof equipped with a bright white LED spotlight. Inside this box a second clear PVC box can be placed. This clear box also has a small opening, which lines up with the opening in the outer box thereby creating a doorway for the mouse to leave the shelter. The clear box

enables easy transport of the mice to and from their cages. An air flow system (see below) is located on the back wall facing the doorway of the black box.

Horizontal ladder

The ladder is made of 37 rungs placed 15 mm apart from each other. Each rung is split in the middle and each half consists of a specially developed sensor (see below) placed on top of a high-speed, air-pressure sliding actuator (see below). The first and last 6 rungs have no actuators; these rungs provide a platform for the mice to accelerate and decelerate.

Sensors and actuators

The sensor design is depicted in **figure 2.1d**. Movement threshold is set by adjusting the diameter of the hinge rod. Rung press detection is performed by a Hall device that is actuated by a magnet embedded in the rung. The actuators (see **figure 2.1c**) are high speed, air pressure slides (Pneumax). These slides (15x40x80 mm) have a maximal travel distance of 18 mm. A TTL pulse to the controller controls slide pressure (on, off), which in itself controls slide position (up, down). Reaction time from onset of TTL to completion of slide movement is 52 ms with a movement time of 8 ms.

Air flow system

Strategically located pressurized air nozzles are used to encourage the mouse to leave the shelters when necessary and cross the ladder at constant velocity. Mice generally learn very quickly to react to these cues, which then results in fully automated ladder crossings at constant velocity. In addition it prevents unauthorized ladder exploration. The air flow system is constantly adjusted to the direction and position of the mouse to create a constant 16 km/h tailwind until the mouse completely traverses the ladder and enters the shelter box. Headwind is turned on at full force (30 km/h) from the opposite direction when a mouse leaves one of the shelters at an unauthorized time, usually causing the mice to immediately return to the shelter.

Controller and software

The Erasmus Ladder is a fully automated system that automatically completes mouse phenotyping on motor performance and associative motor learning. A National Instruments[17] computer system running a real-time operating system is programmed to read all sensors, make all decisions, execute all interventions and store the data within a guaranteed 2 ms cycle. The programs were custom written using the LabView[17] programming language with the real-time module. The computer itself is a PXI-8150[17] controller mounted in a PXI[17] chassis. The sensor readout is performed by digital IO hardware (3x PXI-6533[17]) and the actuators are controlled by a 64 channel relay switch card (PXI-2567[17]). The air flow system is controlled by an M-Dac card (PXI-6229[17]) which provides analogue in and analogue out channels. The tone

system is a custom made PXI[17] card that contains a precise sine wave generator and 3 voltage controlled gain amplifiers. Ladder rung positions are controlled by custom written LabView virtual instruments[17], which runs on a real time operating system installed on a dedicated NI-PXI 8150 controller[17].

MICE

All mice were bred and raised in our own facilities. National and institutional guidelines were followed for all animal care and experimentation. Mice were entrained to a light schedule of 12 hours light – 12 hours dark and provided with food and water *ad libitum*. All mice were measured for 8 consecutive days at the same point in their light phase. All wildtype mice were littermates of the mutants described below. We only used male mice.

Expanded CGG mice

This is a mouse model for fragile-X-associated tremor/ataxia syndrome[18]. All mice were of a mixed C57BL6 / OLA129 background and were measured between 48-56 weeks of age. Thirteen mice carried the CGG repeat; we used seven wildtype littermates as controls. The length of the CGG repeats varied between 150 and 200 and was analyzed as previously described[28].

Fmr1 knockout mice

This is a mouse model for fragile X syndrome[21,25]. All mice were of a mixed C57BL6 / FVB background and were measured between 12-16 weeks of age. Seven mice carried the null mutation; we used nine wildtype littermates as controls. We established for all 16 mice that they were not blind.

ACKNOWLEDGEMENTS

REFERENCES

1. R. E. Brown, *Can J Exp Psychol* 61 (4), 328 (2007).
2. J. N. Crawley, *Neuron* 57 (6), 809 (2008).
3. B. J. Cummings, C. Engesser-Cesar, G. Cadena et al., *Behav Brain Res* 177 (2), 232 (2007).
4. C. I. De Zeeuw, A. M. van Alphen, S. K. Koekkoek et al., *Otolaryngol Head Neck Surg* 119 (3), 193 (1998).
5. J. S. Stahl, A. M. van Alphen, and C. I. De Zeeuw, *J Neurosci Methods* 99 (1-2), 101 (2000).

6.   A. M. Van Alphen, T. Schepers, C. Luo et al., *Ann N Y Acad Sci* 978, 413 (2002).

7.   S.K.E. Koekkoek, W. L. Den Ouden, G. Perry et al., *J Neurophysiol* 88 (4), 2124 (2002).

8.   S. K. Koekkoek, K. Yamaguchi, B. A. Milojkovic et al., *Neuron* 47 (3), 339 (2005).

9.   C. I. De Zeeuw and C. H. Yeo, *Curr Opin Neurobiol* 15 (6), 667 (2005).

10. J. Cendelin, I. Korelusova, and F. Vozeh, *Behav Brain Res* 189 (1), 65 (2008).

11. J. S. Soblosky, L. L. Colgin, D. Chorney-Lane et al., *J Neurosci Methods* 78 (1-2), 75 (1997).

12. D. M. Armstrong, *Prog Neurobiol* 26 (4), 273 (1986).

13. K. M. Friel, T. Drew, and J. H. Martin, *J Neurophysiol* 97 (5), 3396 (2007).

14. D. E. Marple-Horvat and J. M. Criado, *J Physiol* 518 (Pt 2), 595 (1999).

15. D. E. Marple-Horvat and K. A. Crowdy, *Gait Posture* 21 (1), 39 (2005).

16. D. E. Marple-Horvat, J. M. Criado, and D. M. Armstrong, *J Physiol* 506 (Pt 2), 489 (1998).

17. National Instruments, www.ni.com.

18. R. Willemsen, M. Hoogeveen-Westerveld, S. Reis et al., *Hum Mol Genet* 12 (9), 949 (2003).

19. P. J. Hagerman and R. J. Hagerman, *Am J Hum Genet* 74 (5), 805 (2004).

20. J. R. Brouwer, R. Willemsen, and B. A. Oostra, *Am J Med Genet B Neuropsychiatr Genet* (2008).

21. E. J. Mientjes, I. Nieuwenhuizen, L. Kirkpatrick et al., *Neurobiol Dis* 21 (3), 549 (2006).

22. R. J. Hagerman, *Fragile-X syndrome: diagnosis, treatment and research*. (The Johns Hopkins University Press, Baltimore, 2002).

23. R. F. Kooy, *Trends Genet* 19 (3), 148 (2003).

24. D. Wahlsten, N. R. Rustay, P. Metten et al., *Trends Neurosci* 26 (3), 132 (2003).

25. *Cell* 78 (1), 23 (1994).

26. S. J. Cruikshank, M. Hopperstad, M. Younger et al., *Proc Natl Acad Sci U S A* 101 (33), 12364 (2004).

27. C. I. De Zeeuw, J. I. Simpson, C. C. Hoogenraad et al., *Trends Neurosci* 21 (9), 391 (1998).

28. J. R. Brouwer, K. Huizer, L. A. Severijnen et al., *J Neurochem* 107 (6), 1671 (2008).

Chapter 2

CHAPTER III

Absence of βCamKII leads to deficits in cerebellar motor learning and disturbed cell firing in Purkinje cells

Alexander Cupido, Freek E. Hoebeek, Geeske M. Van Woerden, Sebastiaan K.E. Koekkoek, Ype Elgersma, Marcel T.G. de Jeu and Chris I. De Zeeuw

ABSTRACT

Absence of βCamKII (Calcium/Calmodulin-dependent Kinase type II) leads to ataxia and to deficits in long-term depression (LTD) and long-term potentiation (LTP). Here we show that βCamKII knockout mice have impaired learning on the Erasmus Ladder and have impaired eye movement adaptation. We also show that the simple spike and complex spike firing of these mutants is highly irregular. Since βCamKII knockout mice have numerous deficits, we have to test cell-specific βCamKII knockout mice to further elucidate the role of βCamKII.

INTRODUCTION

Long-term changes in synaptic strength are thought to be one of the cellular mechanisms underlying learning and memory. Marr[1], Albus[2] and Ito[3] proposed that long-term depression (LTD) in the parallel fiber – Purkinje cell synapse might underlie cerebellar learning and memory. In order to prevent saturation, LTD at the cerebellar parallel fiber – Purkinje synapse is likely to be balanced by cerebellar long-term potentiation (LTP). Parallel fiber long-term plasticity (both LTD and LTP) is governed by the intracellular calcium concentration, which is indicated by a high calcium threshold for LTD and a lower calcium threshold for LTP[4]. Recently we reported that absence of βCamKII (Calcium/Calmodulin-dependent Kinase type II) inverses the effects of low and high calcium concentrations[5]. βCamKII is the most predominant isoform of CamKII in the cerebellum. We showed that a widely used LTD-inducing protocol resulted in LTP, whereas an LTP-inducing protocol resulted in LTD at the parallel fiber – Purkinje cell synapse. Furthermore, we reported that this knockout mouse is ataxic, but we did not test if cerebellar learning is affected[5]. Here, we will analyze cerebellar learning of these mutants in two different behavioral tasks: the Erasmus Ladder and eye movement adaptation. Since it is believed that intact parallel fiber – Purkinje cell plasticity is required for eye movement adaptation[6], it is our hypothesis that βCamKII knockout mice have impaired learning. However, it is unlikely that an alteration in parallel fiber – Purkinje cell plasticity alone can explain the severe motor performance deficits, since several mutant mice with deficits in parallel fiber – Purkinje cell plasticity have no motor performance deficits[7,8]. Changes in Purkinje cell firing have been shown to affect motor performance[9]. Therefore, we recorded Purkinje cell activities in awake βCamKII knockout mice and wildtype littermates to elucidate the underlying mechanism of the disturbed motor behavior of these mutants.

RESULTS

Erasmus Ladder

We tested the βCamKII knockout mice and their wildtype littermates on the Erasmus Ladder. In this behavioral task, mice have to walk over a horizontal ladder consisting of 37 rungs divided in a left and a right side. All rungs are equipped with pressure sensors, which are continuously monitored. To assess the motor behavior deficits, the mice were trained on the Erasmus Ladder with the left side even numbered rungs and the right side odd numbered rungs descended 13 mm. We computed the number of missteps. A misstep was defined as a touch of one of the descended rungs. As shown in **figure 3.1a**, βCamKII knockout mice made significantly more missteps as compared to wildtype littermates (genotype: $F_{1,21}=187$, p<0.001; training x genotype: $F_{4,84}=1.3$, p=0.3 repeated measures Anova). But in contrast to the accelerating rotarod[5], additional training resulted in significant improvement of the βCamKII knockout mice ($t_8=2.7$ p<0.05; Paired students t-test motor performance 1 vs. motor

Chapter 3

performance 5). Nevertheless, βCamKII knockout mice still make significant more missteps than wildtype mice after 5 motor performance sessions (p<0.001, Post hoc Fisher's PLSD).

Next, we tested the same mice in an associative motor learning paradigm. In this paradigm a randomly selected descended rung, which will interfere with the stepping pattern of the mouse, raises 18 mm. This rise (the unconditioned stimulus) is preceded by a tone (the conditioned stimulus), 90 ms before the rising rung will interfere with the stepping pattern of the mouse. The ascending rung will interfere with the next front paw step of the mouse, unless a corrective paw movement is made. Interestingly, although βCamKII knockout mice showed more missteps (**figure 3.1a**) the time needed to place the front paw from one rung to the other (step time) was not significantly different between βCamKII knockout mice and their wildtype littermates during the first associative motor learning session ($F_{1,23}$=2.1, p=0.2; Anova). Thus unlike the accelerating rotarod and the motor performance sessions (**figure 3.1a)**, mutant and wildtype mice now start at the same performance level, allowing us to look more accurately at motor learning. Introduction of the elevated rung significantly slowed down the step time for both βCamKII knockout mice and their wildtype littermates (βCamKII knockout mice: t_9=4.1, p<0.01; wild-type: t_{14}=3.1, p<0.01; Paired students t-test between motor performance session 5 and associative motor learning session 1). However, wildtype mice quickly learned to readjust their paw movements, since step time at the second associative motor learning session was similar to that of the last motor performance session (t_{14}=1.1, p=0.3; Students paired t-test). βCamKII knockout mice also showed some improvement in the associative motor learning paradigm, but they were still not back at the motor performance sessions level at the final associative motor learning session (t_8=2.9 p<0.05; Students paired t-test, motor performance session 5 vs. associative motor learning session 3). These

Figure 3.1
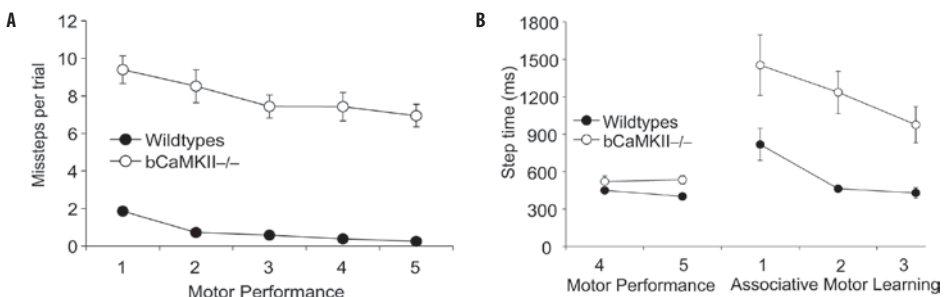
A Mice were trained to walk over the ladder and the number of missteps per trial was determined. Each training block consists of 72 trials. βCamKII$^{-/-}$ mice made significantly more missteps than their wildtype littermates. Number of mice used: wildtypes (15); βCamKII$^{-/-}$ (10). **B** In this paradigm the step time is computed as a measure of associative motor learning. During the motor performance sessions, no significant difference was seen in step time between βCamKII$^{-/-}$ and wildtype mice. However, a marked difference is observed in the associative motor learning paradigm. Number of mice used: wildtypes (15); βCamKII$^{-/-}$ (10).

Figure 3.2
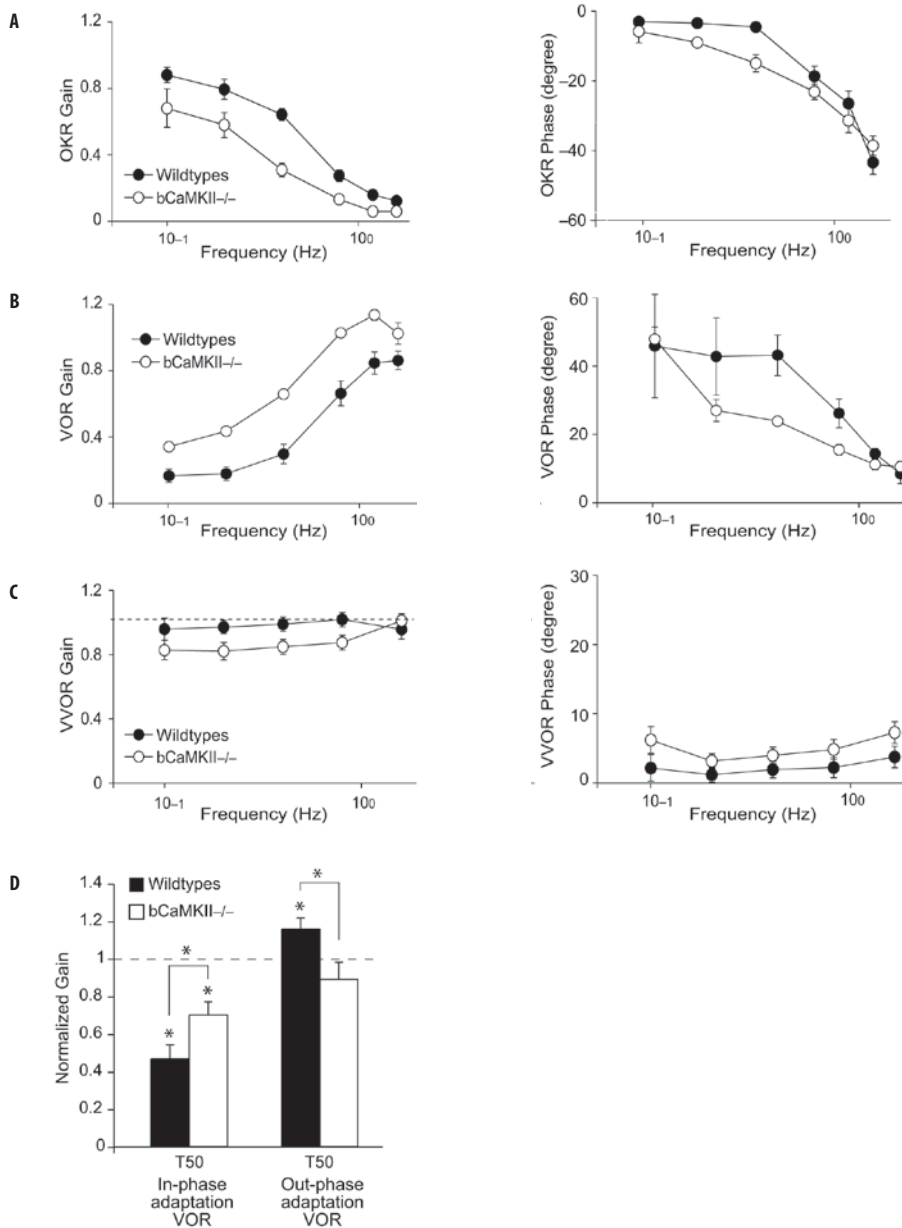
ABC Bode-plots of the OKR, VOR and VVOR performance. Gain and phase were monitored during sinusoidal optokinetic and vestibular stimulation at different frequencies. The OKR was evoked by rotating an illuminated surrounding screen. The VOR was evoked by turning the mouse (in the dark). For VVOR measurements, both the illuminated surrounding screen and the turntable holding the mouse are turned. Number of mice used: wildtypes (6); βCamKII^{−/−} (6). **D** Effect of 50 minutes visuo-vestibular training on VOR adaptation of wildtype and βCamKII^{−/−} mutants. Gains shown are after 50 minutes of training and normalized to the T0 values. Both the in-phase and out of phase VOR are impaired in βCamKII^{−/−} mutants. Number of mice used: wildtypes (6); βCamKII^{−/−} (6).

Chapter 3

experiments show that βCamKII knockout mice have impairments in motor performance and in associative motor learning.

Eye movement performance

The motor impairments of the βCamKII knockout mice as described above could in principle arise from malfunctioning of several brain areas. However, given the remarkable resemblance with the motor performance deficits of cerebellar degeneration mutants[10] and the high expression of βCamKII in the cerebellum, it is conceivable that dysfunction of the (olivary) cerebellar system strongly contributes to this phenotype. The vestibulo-ocular (VOR) and optokinetic reflexes (OKR) work together to stabilize images on the retina during head movements and cerebellar dysfunction can be more specifically studied by measuring eye movements induced by vestibular and optical stimuli[6,11]. Using this technique we demonstrated that αCaMKII is required for VOR and OKR gain adaptation but not for VOR and OKR performance[7]. In contrast, performance of the βCamKII knockout mice in these paradigms was markedly affected, since OKR gain values were significantly reduced (**figure 3.2a**; OKR gain: $F_{1,10}=12$, $p<0.01$ ANOVA). Notably, whereas OKR gain values were decreased, VOR gain values were significantly increased (VOR gain: $F_{1,10}=25$, $p<0.001$; ANOVA; **figure 3.2b**), suggesting a VOR compensation mechanism as has been observed in other cerebellar mutants as well[12]. Conversely, the OKR phase is significantly increased and the VOR phase is significantly decreased in the βCamKII knockout mice (OKR phase: $F_{5,50}=3.4$, $p<0.05$; VOR phase: $F_{5,50}=2.5$, $p<0.05$; ANOVA genotype x frequency; **figure 3.2a** and **figure 3.2b.** Whether the VOR compensation is sufficient to counterbalance the optokinetic deficit can be studied by measuring the visually enhanced VOR (VVOR), which should approximately be a summation of the OKR and VOR values. Wildtype mice showed VVOR gain values that were not significantly different from the ideal value of one ($p>0.2$ for each frequency; one-sample t-test). However, βCamKII knockout mice still showed a significant impairment ($p<0.05$ for all frequencies except the highest frequency; one-sample t-test). In addition, VVOR phase values were still significantly larger in the βCamKII knockout mice as compared to their wildtype littermates (VVOR phase: $F_{1,9}=5.1$, $p<0.05$; repeated measures ANOVA). Thus, the absence of βCamKII results in impaired OKR, VOR and VVOR performance.

The vestibulo-ocular reflex can be modified by subjecting the mice to a visuo-vestibular mismatch training, in which visual stimuli are provided that are in conflict with the vestibular stimulus. This adaptation has been shown to be dependent on cerebellar plasticity[6,11]. To test whether this form of cerebellar learning was impaired, we determined gain and phase adaptation of the VOR following a short-term visuo-vestibular training period of 50 minutes. Upon VOR in-phase training, wildtype mice and βCamKII knockout mice showed a significant decrease of the gain (**figure 3.2d**; wildtype: $t_7=8.4$, $p<0.001$; βCamKII knockout mice: $t_5=4.2$, $p<0.01$ one sample t-test). However, gain adaptation of wildtype mice was significantly stronger than the gain adaptation of βCamKII knockout mice ($t_{12}=2.4$, $p<0.05$ Student's t-test). VOR

Figure 3.3
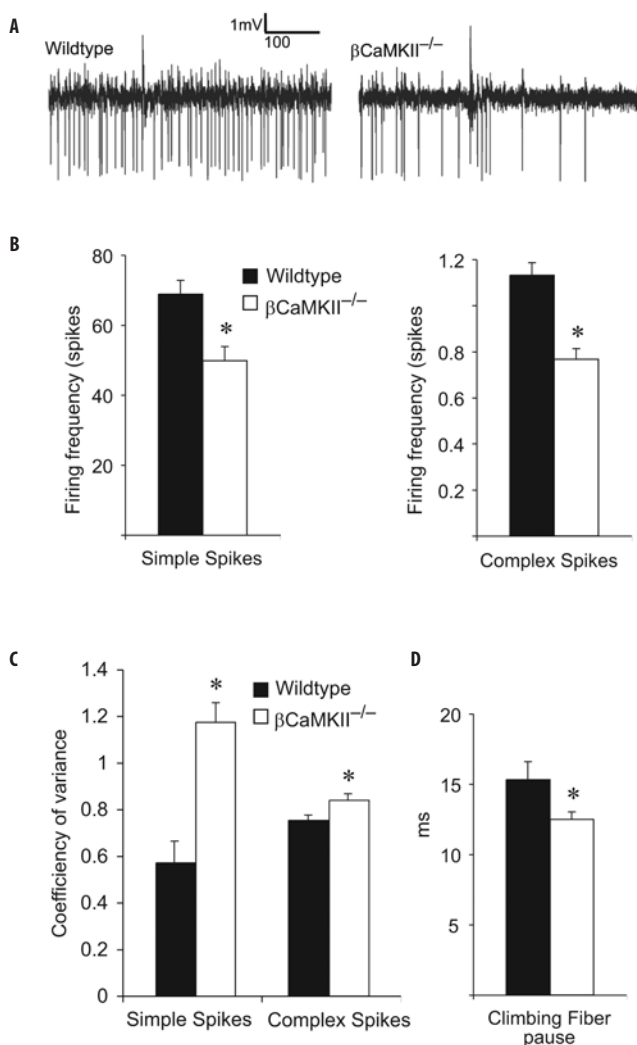
A Typical example of extracellular recordings of spontaneous Purkinje cell activity in wildtype and βCamKII$^{-/-}$ mice. Note that the firing of the βCamKII$^{-/-}$ mice is very irregular. **B** Firing frequency of both the complex and the simple spikes is reduced in the βCamKII$^{-/-}$ mutants compared to their wildtype littermates. **C** Irregularity can be defined by the coefficiency of variance. **D** The increase in irregularity is also reflected in the shorter climbing fiber pause. Number of mice/cells measured: wildtype (3/22); βCamKII$^{-/-}$ (3/30).

out-phase training resulted in a significant gain adaptation increase in wildtype mice (t_6=2.8, p<0.05 one sample t-test) but not in mutants (t_5=1.2, p=0.3) and mutants were significantly different from wildtype mice (t_{11}=2.6, p<0.05 student's t-test). Phases were not significantly different between wildtype and βCamKII knockout mice in either paradigm (data not shown).

The absence of βCamKII results in impaired gain adaptation of the VOR in both directions, suggesting a more general deficit in cerebellar plasticity.

Disturbed purkinje cell firing in βCamKII knockout mice

We recorded extracellular Purkinje cell activity in awake βCamKII knockout mice and wild-type mice. This revealed a drastically disturbed firing pattern (**figure 3.3a**). βCamKII knockout mice show highly irregular simple spike firing, as measured by the coefficient of variance (t_{50}=4.6, p<0.001 Student's paired t-test; **figure 3.3b**). In addition, the firing frequency of the simple spike was significantly reduced (t_{50}=3.2, p<0.01; Student's paired t-test; **figure 3.3c**). The increased firing irregularity in βCamKII knockout mice was also reflected in the shorter climbing fiber pause. The climbing fiber pause is defined by the period between the start of the complex spike and the first following simple spike (t_{50}=2.2, p<0.05; Student's paired t-test; **figure 3.3d**).

DISCUSSION

Despite the lack of morphological changes in the cerebellum of the βCamKII knockout mice, these mice showed clear signs of ataxia[5]. The βCamKII knockout mice did show motor learning on the Erasmus Ladder. However, this learning is comparable to the motor learning of the Fmr1 knockout mice described in **chapter 2** and is not cerebellar learning. Consistent with the experimental support that parallel fiber – Purkinje cell LTD is required for increasing the VOR, we also found that both LTD[5] and VOR increase adaptation were affected in the βCamKII knockout mice. Beside that, LTP was also severely affected in the β CaMKII knockout mice[5], which might explain the reduced VOR decrease learning in these mutants[5]. In contrast to αCaMKII knockout mice[13], βCamKII knockout mice also showed impaired basal OKR and VOR performance, as well as ataxia and locomotion deficits[5]. In addition, βCamKII knockout mice showed striking changes in simple spike and complex spike firing, which could explain why these mutants are so ataxic, since Tottering mice[9], which are also very ataxic, also have altered simple and complex spike firing. Thus, cerebellar function in βCamKII knockout mice is much more affected than in αCaMKII knockout mice. What could be the reason for this difference? Unlike αCaMKII, βCamKII is expressed in most cells of the cerebellar circuitry[7] (inferior olive, granule cells, Purkinje cells, vestibular nuclei). Thus, synaptic function or other neuronal properties of these cells could potentially be affected. In fact, the role of CaMKII in regulating the intrinsic excitability of the vestibular nuclei cells has been demonstrated[14].

Since βCamKII knockout mice have so many deficits and βCamKII is expressed throughout the cerebellum, it is almost impossible to point out how the absence of βCamKII affects the cellular mechanisms in the cerebellum and the different behavioral tasks. In future studies, we should test cell-specific βCamKII knockout mice to further elucidate the role of βCamKII.

METHODS

Erasmus Ladder

The Erasmus Ladder is a fully configurable horizontal ladder with at both ends a shelter box. In each shelter there are two small air nozzles for pressurized air delivery. The horizontal ladder has 37 rungs. Each rung consists out of a left and a right pressure sensor attached to a 12 x 3 mm (length x diameter) rod. Separation between the opposing rods is 2 mm. The distance between the individual rungs is 15 mm and each alternating rung is descended 13 mm. On the left side the even rungs and on the right side the odd rungs are descended thereby creating an alternated stepping pattern with 30 mm gaps. Each rung is fixed to a high-speed pneumatic slide that provides vertical position control of the rung. A computer system running a real-time operating system is programmed to record sensor data, adjust air pressure, predict future touches, calculate interventions, reposition slides and store data in a time fixed 2 ms cycle. Mice were trained with the following protocol. A mouse was placed in one the shelters. After 10 seconds, the bottom air nozzles in this shelter were activated, after which the mouse usually left the shelter immediately. When the mouse touched the first rung on the ladder, a pressurized air nozzle was activated, which is oriented in the same direction as the travel path of the mouse. Air pressure was adjusted constantly to achieve a 16 km/h tailwind. This encouraged the animal to walk quickly over the ladder to the opposite shelter. When the mouse arrived in the opposite shelter, the pressurized air nozzles were switched off. After 10 seconds the protocol as described above was repeated. One session lasted 72 trials (ladder crossings). Mice which did not cross the ladder with a constant speed after the first session where excluded. Mice were conditioned to avoid an ascending rung in three associative motor learning sessions. One of the descended rungs quickly rose 18 mm (randomly chosen, when mouse is walking constantly), 90 ms after the moment the mouse had heard the tone. The tone was 15 kHz tone (90 dB, smooth onset). The conditioning sessions consisted of 9 blocks of 8 trials. The blocks consisted of 6 CS-US paired trials, 1 US-Only trial and 1 CS-Only trial. The data in **figure 3.1b** are all CS-US paired trials. Number of mice used: wildtypes (15); βCamKII knockout mice (10).

Eye movement recordings

These experiments were done as described previously[7]. OKR and VVOR were evoked by rotating an illuminated surrounding cylindrical screen (diameter 63 cm) with a random-dotted pattern. In case of the VVOR, the turntable holding the mouse was turned as well. VOR measurements were similar as VVOR measurements, but in entire darkness to avoid optokinetic input. VOR adaptation was induced by 50 minutes in-phase or out-phase training. During in-phase training the surrounding screen and turntable rotated exactly in phase with each other, whereas during out-phase training the surrounding screen and turntable rotated

180° out of phase of each other. Number of mice used: basic eye movements (wildtypes / mutants), OKR (6/6); VOR (8/6); VVOR (6/6); VOR adaptation paradigm: (7/6).

Single-cell recordings

Extracellular recordings were performed as described previously[9]. Purkinje cells of the left hemisphere were recorded during spontaneous activity in the dark. Signals were amplified, filtered (Cyberamp, Cambridge Electronic Devices, Cambridge, UK), digitized (CED1401 digitizer, CED) and stored for offline analysis. Purkinje cells were identified by their brief pause in simple spike activity following each complex spike[9,15]. Offline analysis of neuronal firing rates during single Purkinje cell recordings was performed in MATLAB analysis[9]. Simple spikes and complex spikes were discriminated using custom made routines based in cluster analysis[15]. Cumulative probabilities of simple spike interspike intervals were calculated by grouping all interspike intervals per stimulus conditions. Igor Pro (Wavemetrics, Inc., OR, USA) was used to fit EPSC decays with single-exponential functions. Number of mice/cells measured: wildtypes (3/22); βCamKII knockout mice (3/30).

REFERENCES

1. D. Marr, *J Physiol* 202 (2), 437 (1969).
2. J.S. Albus, *Math. Biosci.* 10, 25 (1971).
3. M. Ito, *The Cerebellum and Neural Control*. (Raven Press, New York, 1984).
4. M. Coesmans, J. T. Weber, C. I. De Zeeuw et al., *Neuron* 44 (4), 691 (2004).
5. G. M. Van Woerden, F. E. Hoebeek, Z. Gao et al., *Nat Neurosci* (2009).
6. C. I. De Zeeuw and C. H. Yeo, *Curr Opin Neurobiol* 15 (6), 667 (2005).
7. C. Hansel, M. de Jeu, A. Belmeguenai et al., *Neuron* 51 (6), 835 (2006).
8. S. K. Koekkoek, H. C. Hulscher, B. R. Dortland et al., *Science* 301 (5640), 1736 (2003).
9. F. E. Hoebeek, J. S. Stahl, A. M. van Alphen et al., *Neuron* 45 (6), 953 (2005).
10. R. Lalonde, A. N. Bensoula, and M. Filali, *Neurosci Res* 22 (4), 423 (1995).
11. A. H. Gittis and S. du Lac, *Curr Opin Neurobiol* 16 (4), 385 (2006).
12. A. M. Van Alphen, T. Schepers, C. Luo et al., *Ann N Y Acad Sci* 978, 413 (2002).
13. Y. Elgersma, N. B. Fedorov, S. Ikonen et al., *Neuron* 36 (3), 493 (2002).
14. A. B. Nelson, A. H. Gittis, and S. du Lac, *Neuron* 46 (4), 623 (2005).
15. H. H. Goossens, F. E. Hoebeek, A. M. Van Alphen et al., *Eur J Neurosci* 19 (3), 687 (2004).

CHAPTER IV

Role of Olivary Electrical Coupling in Cerebellar Motor Learning

Alexander Cupido, Ruben S. Van Der Giessen, Sebastiaan K. E. Koekkoek, Stijn van Dorp, Jornt R. De Gruijl, Sara Khosrovani, Bjorn R. Dortland, Kerstin Wellershaus, Joachim Degen, Jim Deuchars, Elke C. Fuchs, Hannah Monyer, Klaus Willecke, Marcel T.G. De Jeu and Chris I. De Zeeuw

ABSTRACT

Many brain regions contain neurons that are coupled by electrical synapses allowing signals to traverse directly from one neuron to the other with minimal delay. In mammals the level of coupling in the inferior olive is probably higher than in any other brain region. Yet, the functional role of this phenomenon in cerebellar motor control remains to be determined. Here, we subjected mice that lack coupling among their olivary neurons to paradigms that require learning-dependent timing. Cx36 knockout mice showed impaired timing of both locomotion and eyeblink responses that were conditioned to a tone. The timing of spike activities generated in the olive of coupling-deficient mice was abnormal in that their latencies in response to the unconditioned stimulus were significantly more variable than those in wildtypes. Whole cell recordings of olivary neurons *in vivo* showed that the differences in spike timing result at least in part from altered interactions with their sub-threshold oscillations. These results, combined with analyses of olivary activities in computer simulations at both the cellular and systems level, suggest that electrotonic coupling among olivary neurons is essential for proper timing of their action potentials and thereby for learning-dependent timing in cerebellar motor control.

INTRODUCTION

More than a century ago in 1906 Santiago Rámon y Cajal received the Nobel Prize for the neuron doctrine stating that neurons operate as anatomically and functionally distinct cellular units in the mammalian brain. This tenet still holds, but over the past decade the neuron doctrine has been complemented by new discoveries about the constitution, distribution and cell physiological functions of neuronal gap junctions that can establish cytoplasmic continuity among large ensembles of neurons[1]. Importantly, in 1998 groups led by Condorelli[2] and Willecke[3] cloned the first gap junction protein, i.e. Connexin36 (Cx36), that is predominantly expressed by neurons. The identification of this protein allowed several groups to study the distribution of Cx36 and/or to create mouse mutants to investigate the cellular consequences of a lack of Cx36 in the brain[4,5]. To date, Cx36 and neuronal gap junctions are widely distributed in regions such as the olfactory bulb, hippocampus, cerebral cortex, (hypo)thalamus and inferior olive[6]. For most of these regions the possible role of neuronal gap junctions has been determined at the cell physiological level[7-10]. In these *in vitro* studies a lack of Cx36 generally leads to an absence of electrotonic coupling and to changes in sub-threshold activities[9,11,12]. Yet, for most of the brain systems mentioned above the apparent behavioral phenotype is relatively mild and/or remains a topic for systems electrophysiological investigations[7,10,13-15]. With regard to the olivocerebellar system previous behavioral studies on Cx36 knockout mice showed no ataxia and a relatively normal motor performance[16]. This lack of a clear phenotype during natural motor behavior is remarkable, because in mammals the density of gap junctions in the inferior olive is probably higher than in any other brain region[6]. Here we show that although Cx36 knockout mice have no prominent general motor deficits, they do show problems when challenged to perform a learning-dependent motor task such as the Erasmus Ladder or eyeblink conditioning. In these learning tasks the timing of the motor responses is modified by conditioning the movement to a conditioned stimulus (CS) that starts before, but co-terminates with, an unconditioned stimulus (US)[17-19]. The CS is probably conveyed by the mossy fiber - parallel fiber system to the Purkinje cells in the cerebellar cortex, while the US is conveyed by their climbing fibers originating from the inferior olive[20,21]. Thus, in the current study we investigated the hypothesis that appropriate timing of conditioned motor responses critically depends on the precise temporal coding of the activities of coupled neurons in the inferior olive.

RESULTS

Deficits on the Erasmus Ladder

To quantify their general level of motor performance Cx36 knockout mice (C57BL/6 background; n = 16) and wildtype littermates (n = 18) were tested on the Erasmus Ladder. The Erasmus Ladder is formed by 2 x 37 rungs positioned between a startbox and an endbox

across which the mice can run back and forth. Each rung on both the left and right side is equipped with a pressure sensor, which is continuously monitored. Based on instantaneous analysis of the activities of these sensors, the walking pattern of the mice can be predicted in the millisecond range, and, if wanted, interrupted by moving each individual rung up or down. The mice were trained with the even numbered rungs on the left side and the odd numbered rungs on the right side in a descended position so as to create an alternated stepping pattern with 30 mm gaps. In this paradigm the Cx36 knockout mice and wildtype littermates had similar step times, which was defined as the time needed to place the front paw from one rung to the other (358 ms ± 29 SD for Cx36 knockout mice and 339 ms ± 23.5 SD for wildtypes) and a comparably number of missteps, which were identified by touches on the descended rungs (**figure 4.1a**). For comparison we also tested *Lurchers* (C57BL/6 background; n=9), which lack Purkinje cells and which are known to show ataxia[22,23]. Indeed, these spontaneous mouse mutants showed longer step times (589 ms ± 49 SD; p<0.01 for each sessions; t-tests) and 3 to 4 times more missteps than the Cx36 knockout mice or their wildtype littermates (p<0.001 and p<0.001 for each session; t- tests). Thus, in line with previ-ous rotarod tests[14,16], we conclude from this test on the Erasmus Ladder that Cx36 knockout mice show, in contrast to *Lurchers*, a relatively normal motor performance.

To find out whether the ability for motor learning is affected in Cx36 knockout mice, we subjected them to a conditioning paradigm in which they were trained to make a new locomotion movement using a 15 kHz tone as the CS and a rising rung as the US (ISI of 90 ms). A training session consisted of 9 blocks of 8 trials, which were separated by an inter-trial interval of 9 to 11 seconds. As described above the step time was not different among Cx36 knockout mice and their wildtype littermates. However, in the conditioned motor learning paradigm, the step time in the mutants increased significantly compared to that of the wildtypes (p<0.05; t-test). In fact, this increase in step time was comparable to that observed in *Lurchers* (**figure 4.1b**). The difference among Cx36 knockout mice and wildtypes remained when we prolonged the inter-stimulus (CS – US) intervals from 90 ms to 285 ms (p<0.001; t-test; **figure 4.1c** and **figure 4.1d**). Since the Cx36 knockout mice lack Cx36 from early on and may therefore show compensations within the olivary neurons[12], we also tested the same associative motor learning paradigm in wildtype mice following application of drugs that can block olivary coupling instantaneously[24-28]. We either applied carbenoxolone systemically (40 mg/kg) just before the two motor performance sessions and just before the first of a series of three associative motor learning sessions (n=5), or we made intra-olivary injections with mefloquine (150 µM) one day before a series of associative motor learning sessions (n=4). For impact of dosages of drugs see references 60 and 61. In these experiments we also found a significantly greater increase in step time of the coupling deficient animals after, but not before, conditioning than in control animals (n=6 and n=5, respectively) which received injections with vehicle only (p<0.01 and p<0.001, respectively; t-tests; **figure 4.2a**, **figure 4.2b** and **figure 4.2c**). In the case of carbenoxolone the impact of the drug on con-

Figure 4.1
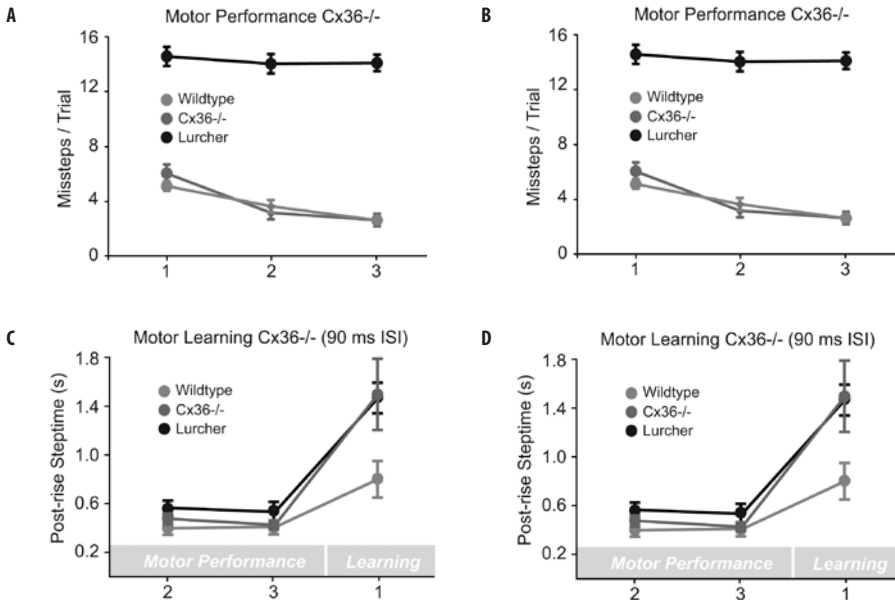
A Motor performance level is revealed by the amount of descended rungs touched, which represents the number of missteps. Cx36 mutants (red) and wildtype littermates (blue) show normal motor performance, while *Lurchers* (black) show deficits in performance during all sessions. **B** Motor learning level is revealed by the change in steptime after and before learning. During learning trials, a randomly selected rung rises 12 mm above the walking surface to create a perturbation; this unconditioned stimulus occurs after 90 ms after the onset of the conditioned stimulus (a 15 kHz tone). Both Cx36 mutants and *Lurchers* reveal difficulties in motor learning. **CD** While the data obtained in **B** have been obtained with an ISI of 90 ms, these data have been obtained with an ISI of 285 ms. Note that the deficits in learning-dependent timing are just as pronounced with this longer ISI, regardless whether they are revealed in an absolute (**C**) or normalized (**D**) fashion.

ditioning tapered off more quickly than that observed after the mefloquine injections (at session 4 $p<0.05$; t-test); this difference may be due to a relatively strong and fast clearance of carbenoxolone[25,29].

Taken together, the experiments on the *Lurchers* and on the animals subjected to intra-olivary injections described above showed that the Erasmus Ladder allows us to detect specific deficits in both motor performance (*Lurchers*) and motor learning (pharmaceutical manipulation of the olive). We can therefore conclude that genetic or pharmaceutical blocking of olivary coupling mediated by Cx36 has relatively little affect on motor performance, while it probably does affect motor learning in that the learning is slowed down substantially.

Deficits in eyeblink conditioning

Analysis of the Erasmus Ladder described above suggests that learning-dependent timing is affected in Cx36 knockout mice. However, in this paradigm the movements are analyzed in discrete steps, which makes it virtually impossible to identify the exact deficits over time. Thus,
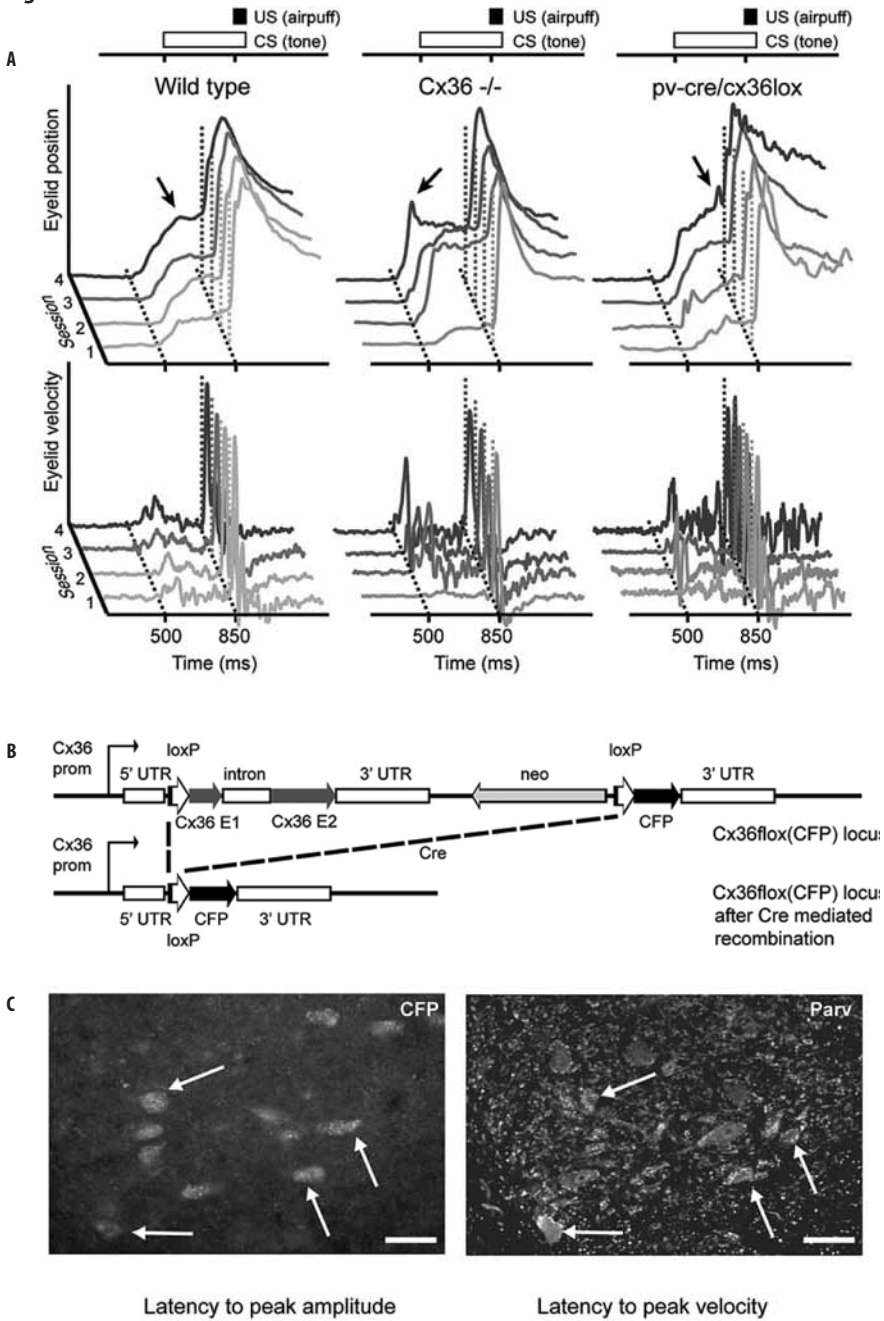
Figure 4.2
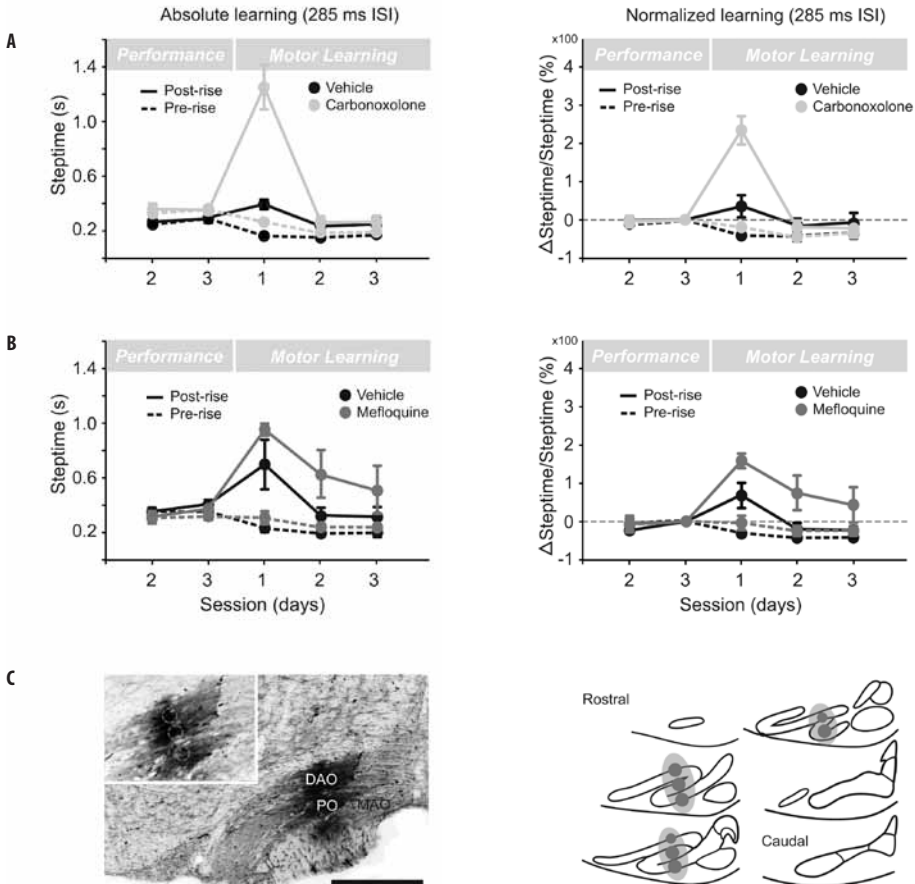
A Carbonoxolone was injected i.p. just before the two motor performance sessions and just before the first of a series of three learning sessions. B Mefloquine was injected bilaterally inside the inferior olive 1 day before the series of the three learning sessions. C Example of one of the reconstructions of the injection site in the olive following BDA labeling.

to further investigate the potential role of Cx36 in learning-dependent timing, we compared the Cx36 mutants with wildtype littermates in an eyeblink conditioning paradigm. For this paradigm, the motor responses can be continuously measured using the magnetic distance measurement technique (MDMT)[30]. We subjected adult Cx36 knockout (n=8) and wildtype littermates (n=8) to a conditioning paradigm using a tone as the CS and an air puff as the US and an inter-stimulus intervals (ISI) of 350 ms. The 8 daily training blocks consisted of 8 trials (1 US-Only, 6 CS-US-paired, and 1 CS-Only). After four paired training sessions (T-1 to T-4) the percentage of conditioned responses and their average peak amplitude in wildtypes reached levels of 77 % and 0.48 mm, respectively, while those in Cx36 knockout mice had values of 78 % and 0.56 mm. These values were not significantly different (p>0.9 and p>0.5; MANOVA for

Figure 4.3

Latency to peak amplitude

Latency to peak velocity

Figure 4.3

D
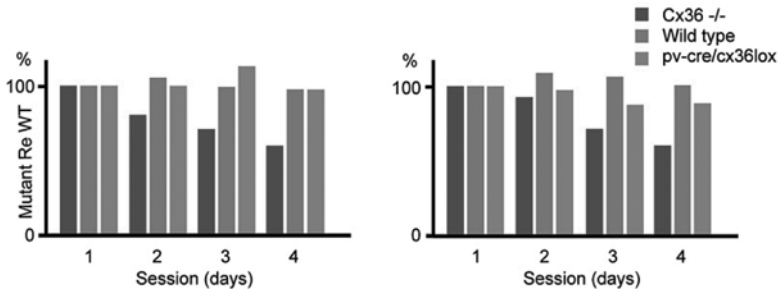
A Representative examples of eyeblink traces in a wildtype (blue), global Cx36 mutant (red) and Cx36 del(lacZ)/flox(CFP):parvalbumin-Cre mouse (green). They all show conditioned eyeblink responses after four training sessions using a tone as the conditioned stimulus (CS) and an air puff as the unconditioned stimulus (US). However, while the timing of the learned response in wildtype and floxed-Cre mice improves over the sessions, that in the global Cx36 mutants gets worse (see arrows). **B** Genetic design of floxed-Cx36 mutants crossbred with parvalbumin-Cre mice, which were used as controls. **C** The Cx36 del(lacZ)/flox(CFP): parvalbumin-Cre mice showed CFP staining in their cerebellar nuclei neurons, demonstrating that Cx36 has been floxed in these neurons and thus not expressed. Immunostaining for parvalbumin of the same sections (right panel) showed that most of the cerebellar nuclei neurons indeed express parvalbumin (arrows) and that they would otherwise in the non-floxed situation express Cx36. Thus, the Cx36 del(lacZ)/flox(CFP):parvalbumin-Cre mice do not express Cx36 in their cerebellar nuclei, while their expression in the relevant olivary subnuclei is normal (data not shown). Punctate labeling in neuropil of the right panel reflects staining of axonal fibers. **D** While the latency to peak amplitude (left panel) in the global knockouts of Cx36 (red) got worse during the training sessions, that in the Cx36 del(lacZ)/flox(CFP): parvalbumin-Cre mice (green) was indistinguishable from that in their unaffected littermates (blue). Similarly, the average latency to peak velocity (right panel) in the mutants was also significantly reduced (p < 0.01; t test).

repeated measures; adjusted for multiple comparisons via Bonferroni correction). In contrast, the timing properties of the conditioned responses differed dramatically among the wild-types and Cx36 knockout mice as the training proceeded. While in wild types the average latency to peak amplitude of the conditioned eyelid responses was appropriately fixed at the moment when the US occurs, the timing in mutants got worse during the four training sessions (**figure 4.3a**). At the end of the training the average latency to peak amplitude in the mutants preceded the moment of the US by 196 ms (± 27 SD), which was significantly different from that in wild types (80 ms ± 24 SD; p < 0.01; t-test; **figure 4.3d**). These data indicate that coupling-deficient mutants cannot appropriately time their movements when challenged in a conditional task.

Still, these eyeblink experiments on the global Cx36 mutants do not directly demonstrate that the behavioral phenotype can be attributed solely to a lack of coupling in the inferior olive. GABAergic neurons in many brain regions including those in the cerebellar nuclei also show a prominent expression of Cx36[31,32], and a lack of this expression may therefore in principle also affect any cerebellar conditioning paradigm[33]. To address this potential caveat, we generated mutant mice in which the expression of Cx36 is ablated in the GABAergic neurons of the brain, while that in the relevant olivary neurons, which are all non-GABAergic, is normal (**figure 4.3b** and **figure 4.3c**). These mutants (n=4), which were cross-breedings of floxed-Cx36 mutants and parvalbumin-Cre mice, lacked expression of Cx36 in for example

the GABAergic neurons of the thalamus, olfactory bulb, cerebral cortex, hippocampus and cerebellar nuclei that express parvalbumin[34], whereas the neurons in the dorsal accessory olive that are involved in eyeblink conditioning showed a normal level of Cx36. The pv10 cre/cx36lox cross-bred mutants showed the same conditioned eyeblink responses as the wildtypes, i.e. without any deficits in their timing (**figure 4.3a** and **figure 4.3d**). These data indicate that in the global Cx36 knockout it is most likely the deficits in the olive that are responsible for the abnormalities in learning-dependent timing. For the same argument, it is also particularly relevant to find out whether the coupling among the stellate cells in the cerebellar cortex is affected in both the global and floxed-Cx36 mutant mice[35]. We therefore investigated the constitution of the gap junctions between these cells. It turned out that the vast majority of these inter-neuronal gap junctions are formed by Connexin45[32] rather than Cx36[31]. Thus, we conclude that Cx36 knockout mice show deficits in learning-dependent timing and that this behavioral deficit is likely due to an impairment of electrotonic coupling in the inferior olive.

Abnormal temporal pattern of climbing fiber responses

If the deficits in learning-dependent timing are due to a lack of coupling between the olivary neurons, one expects that the timing properties of the activities in these neurons are disrupted in Cx36 knockout mice. To investigate these properties we recorded the climbing fiber activities of Purkinje cells in the cerebellar cortex that reveal the olivary signals of the US during eyeblink conditioning[36,37]. The climbing fiber activities of Purkinje cells, also called complex spikes, generally reflect the temporal coding of olivary neurons rather precisely, because they are generated in an all-or-none fashion[38]. We found that the Purkinje cells that respond well to air puff stimulation are in the mouse situated in an area covering both lobulus simplex in the hemisphere and the adjacent part of lobule VI in the posterior lobe (**figure 4.4a**). In awake wildtypes (n=9) the air puff stimulation evoked virtually only short-latency climbing fiber responses; these responses had an average peak latency of 29 ms $\pm$ 9 (SD) over 879 successful stimulations (>70% successful). In contrast, in all Purkinje cells recorded in the Cx36 knockout mice (n=10) the same peri-oribital stimulation evoked both short-latency responses (average to peak of 30 + 7 ms) and long-latency responses (101 ms $\pm$ 17; **figure 4.4b**). Of all successful stimulations (n=1036; >75% successful) in the mutants 60% and 34% resulted in pure short-latency and pure long-latency responses, respectively, while 6% resulted in both a short-latency and long-latency response. These differences in the temporal distribution patterns following peripheral stimulation were highly significantly different among wildtypes and mutants (p<0.001; t-tests). Similarly, during spontaneous activity in the awake state the Cx36 knockout mice showed significantly (p<0.01; t-test) more doublets of two or three climbing fiber responses occurring within 200 ms (12% + 6 $\pm$,) than wild types (5% $\pm$ 2; **figure 4.4c**, upper panel), while their mean interspike interval within a doublet was significantly smaller (123 ms $\pm$ 11 ms in Cx36 knockout mice re 140 ms $\pm$ 12 in

Figure 4.4
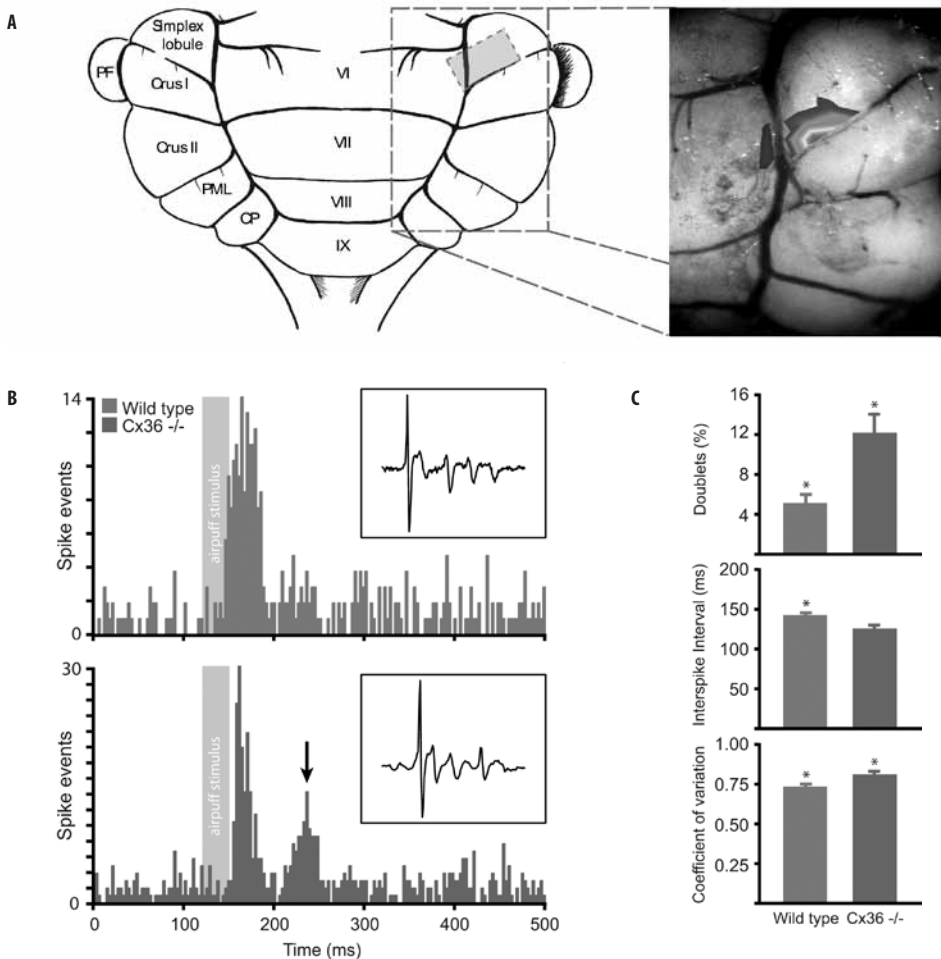
A Purkinje cells that responded well to air puff stimulation were situated in an area covering the lobulus simplex in the hemisphere and adjacent part of lobule VI in the posterior lobe. Color codings correspond to the percentage of Purkinje cells that responded with complex spike activities to air puff stimulation; red, yellow, green, light blue, and dark blue indicate success rates of 50%, 40%, 30%, 20%, and 10%, respectively. **B** Air puff stimulation evoked only short-latency climbing fiber responses in awake wildtype mice (blue) (latency of 29 ± 9 ms), while in the Cx36 mutants (red) the same peri-oribital stimulation evoked both short-latency (30 ± 7 ms) and long-latency responses (101 ± 17 ms) (arrow). Note that in both cases units on the y-axis represent two spikes. Insets show typical complex spike responses in wildtypes (top) and mutants (bottom); no differences were observed in the shape. **C** During spontaneous activity in the awake state, the Cx36 mutants showed significantly more doublets of two or three complex spikes occurring within 200 ms ($p < 0.01$, t-test), a significantly smaller mean interspike interval within these doublets ($p < 0.01$, t-test), and a general increased coefficient of variation for spike intervals ($p < 0.05$, t-test).

wild types; $p < 0.01$; t-test; **figure 4.4c**, middle panel). This difference was also reflected by a generally increased coefficient of variation for spike intervals ($p < 0.05$; t-test; **figure 4.4b**, bottom panel). All these differences in complex spike activities were not influenced by differences in average firing frequencies, because the average complex spike frequency was not

significantly different among wild types and Cx36 knockout mice (0.94 ± 0.19 re 1.00 ± 0.26[39]). Likewise, the shape of the climbing fiber responses and the average number of spikelets within the complex spikes (**figure 4.4b**) as well as the average firing rate (67 ± 13 re 69 ± 14) and coefficient of variation (0.68 ± 0.2 re 0.57 ± 0.2) of simple spike activities of the mutants were also not different from those in wildtypes. Thus, Purkinje cells in awake mice lacking Cx36 show robust differences in the temporal pattern of their climbing fiber responses, but not in the average firing frequencies of their ongoing activities.

Altered correlation between spiking activities and sub-threshold oscillations

To explain the differences in latencies and spiking patterns following peri-orbital stimulation described above, we investigated the activities of olivary neurons using whole-cell recordings *in vivo* in anaesthetized animals (see **table 4.1**). The majority of the neurons in wildtypes showed pronounced sub-threshold oscillations that either had a clear sinusoidal appearance, a more complex rhythmic shape, which probably corresponds to the activation of low threshold calcium conductances[40], or both types of sub-threshold activities[41] (**figure 4.5a**). In the mutants the same types of oscillating cells were observed, but they showed significantly more cells that did not oscillate (p<0.01; t-test) and the occurrence of their oscillations depended significantly stronger on the membrane potential (p<0.01; t-test) as previously described for *in vitro* conditions[9,12] (**figure 4.5b** and **figure 4.5c**). Power spectra of the oscillating sub-threshold activities showed that the frequencies of the oscillations

Tabel 4.1

Parameter	Wildtype	n	Cx36 mutant	n	Statistics
Cells Expressing Spontaneous STOs					
Resting membrane potential (mV)	-55 ± 1	53	-55 ± 1	16	0.31
Input resistance (MΩ)	40.1 ± 3.8	53	45.2 ± 4.3	14	0.24
Membrane capacitance (pF)	188.7 ± 11.8	53	233.0 ± 37.0	14	0.07
Firing rate (Hz)	0.64 ± 0.05	50	0.54 ± 0.09	14	0.15
Coefficient of variation for spike intervals	0.72 ± 0.02	50	0.83 ± 0.05	14	0.02
STO frequency (Hz)	3.1 ± 0.3	53	3.4 ± 0.6	16	0.32
STO amplitude (mV)	8 ± 1	53	8 ± 1	16	0.44
% Cells expressing depolarizing sag	24	58	62	14	0.01
% Cells expressing rebound depolarization	62	58	92	14	0.05
% Cells expressing afterhyperpolarization	19	45	45	12	0.26
Cells Expressing No Spontaneous STOs					
Resting membrane potential (mV)	-52 ± 2	9	-58 ± 1	12	0.11
Input resistance (MΩ)	42.3 ± 5.2	9	48.3 ± 15.5	12	0.32
Membrane capacitance (pF)	159.6 ± 19.1	9	100.6 ± 3.9	12	0.07
Firing rate (Hz)	0.54 ± 0.11	9	0.92 ± 0.35	12	0.10
Coefficient of variation for spike intervals	0.68 ± 0.13	9	0.68 ± 0.04	12	0.49
% Cells expressing depolarizing sag	0	8	0	12	1.00
% Cells expressing rebound depolarization	60	8	100	12	0.29
% Cells expressing afterhyperpolarization	40	8	0	12	0.29

Chapter 4

occurred in both wildtypes and mutants mostly in the range of 1 to 3 Hz or in the range of 6 to 9 Hz (**figure 4.5d**). Similarly, action potentials of olivary cells in both wildtypes and mutants showed a so-called capacity to reset the sub-threshold oscillation[41-43]. Still, the olivary activities differed in that the oscillations of the wildtype neurons often showed dynamic crescendo amplitudes starting directly after the generation of an action potential (crescendo amplitudes were defined as at least a 3-fold increase of the amplitude over 5 cycles), while those in the mutants showed significantly more ($p<0.05$; t-test) constant amplitudes (**figure 4.5a**). Moreover, the relationship between the preferred frequencies of the sub-threshold oscillations and those of the olivary spiking activities was less tight in the Cx36 knockout mice (mean residual scores of 1.33 re 0.63; $p<0.01$; t-test; **figure 4.5d**). Interestingly, this reduced correlation is in line with the observation that the olivary spikes occurred significantly more often ($p<0.05$; t-tests) during the peak period of an oscillation in wildtypes than in mutants (peak period is defined as the period plus or minus 90 degrees from the peak; right panel in **figure 4.5c**; see also arrows in **figure 4.5a**). These differences in interactions between spike generation and sub-threshold oscillations also occurred following peripheral stimulation as used in the conditioning paradigms described above (**figure 4.5e**). Following peripheral stimulation the frequency of the subsequent oscillations in the mutant cells was significantly less stable ($p<0.05$; t-test) than in the wildtypes (for quantification of first four cycles after stimulus see **figure 4.5f**). Thus, peripheral sensory stimulation can indeed induce and modify the sub-threshold activities and such modulation can influence the timing of subsequent spiking activities of olivary neurons when they are appropriately coupled. Therefore, the altered timing of the climbing fiber signals mediating the US in the coupling-deficient Cx36 knockout mice can at least in part be explained by altered interactions with their sub-threshold oscillations.

How may a lack of coupling among olivary neurons in the Cx36 knockout mice lead to altered spiking?

If the lack of coupling between olivary neurons indeed leads to altered timing of their action potentials due to altered interactions with their sub-threshold oscillations, we should be able to find similar relations and characteristics in a simulation of olivary neurons. To this end we used a modified version of a two-compartmental olivary cell model by Schweighofer *et al.*[44] (**figure 4.6**). Since direct responses to depolarizing pulses in the olive are generally not delayed for periods of time near 100 ms[41], while long-latency responses due to reverberating loops can be readily found when the network is affected[45,46], the secondary response found in Cx36-deficient mice is probably caused by another input. Therefore, we applied to both the normal and coupling-deficient situation depolarizing currents timed ~100 ms apart, of which the second was assumed to be caused by a reverberating loop. In both wildtype and Cx36 knockout mice mutant cells, the modeled reverberating loop stimulation was in itself,

Figure 4.5
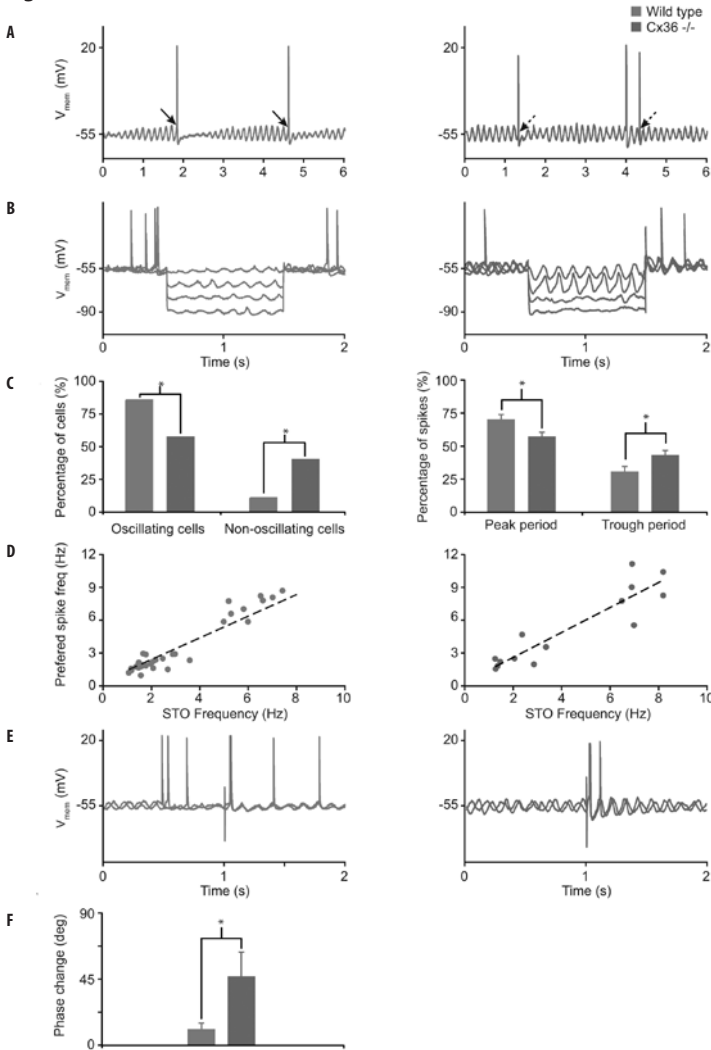
A Examples of whole-cell recordings of olivary neurons in a wildtype (blue) and Cx36 mutant (red) *in vivo*. Most of the olivary spikes in the wildtype occurred around the peak of the oscillations (solid arrows), while those in the mutant frequently also occurred in the trough area (dashed arrows). **B** Sub-threshold oscillations also occurred during hyperpolarizing steps (100 pA) in both wildtypes and mutants; however, the oscillations in the mutants depended more strongly on the membrane potential. **C** (Left panel) Percentages of oscillating and non-oscillating cells differed significantly among wildtypes and Cx36 mutants ($p < 0.01$, χ^2-test). (Right panel) When oscillating, the percentage of spikes that occurred in the peak period was significantly lower in Cx36 mutants, while that in the trough period was significantly higher ($p < 0.05$, t-tests). **D** Power spectra showed that the frequencies of both the oscillations and spikes occurred in both wildtypes and mutants mostly in the range from 1 to 3 Hz and from 6 to 9 Hz. However, the correlation between the preferred frequency of the oscillations and that of the spiking activities was significantly stronger in wildtypes ($p < 0.01$, t-test). **E** Examples of action potentials and sub-threshold oscillations in wildtypes (left) and Cx36 mutants (right) before and after peripheral stimulation. In both types of animals, the peripheral stimulation had a resetting effect in that the oscillations after the occurrence of the stimulus were in phase with each other, while they were out of phase before the oscillations. However, while the phase of the sub-threshold oscillation remained stable in the wildtype, it was unstable in the mutant. **F** The average phase change within the first four cycles of ten different traces of an individual cell following peripheral stimulation was significantly greater in Cx36 mutants than in wildtypes ($p < 0.05$, t-test).

i.e. without the priming induced by the first input, never strong enough to generate an action potential.

The single-cell behavior of the model closely resembled that of its biological counterpart as described in the current and previous work[12]. Both cell models oscillate at ~9 Hz, have preferred firing windows on the upward slopes of sub-threshold oscillations, exhibit differentially damped oscillations after an action potential and undergo a phase change (resetting effect) upon stimulation (**figure 4.6a**). The Cx36-deficient cells exhibited sub-threshold oscillations with a slightly larger amplitude than that of the wildtype cells and had an increased chance of generating doublets (12% instead of 0% in simulated wildtypes). Due to dendritic leak currents, the wildtype cells were less excitable and had smaller firing windows.

In the multiple-cell simulations electrotonic coupling allowed the ensembles of wildtype cells to gradually build up a charge as pulses come in and to synchronize their action potentials on the first input (**figure 4.6b** and **figure 4.6c**, left panels). Still, the coupled wildtype neurons did not respond to the reverberant input. In contrast, the Cx36 knockout network depended on increased excitability to be able to respond with at least some level of synchrony, reacting as quickly as possible as pulses to different cells arrive in presumably rapid succession (**figure 4.6b**, right panel). Simulations of Cx36-deficient networks showed a dual response as the reverberating loop stimulation was in this case sufficiently effective (**figure 4.6b** and **figure 4.6c**, right panels). Thus when the first input arrived outside the firing window, the second pulse could elicit a response in an uncoupled cell, but not in coupled cells (**figure 4.6b**). Due to the rebound spikes, dual responses and a wide spread in timing of the action potentials in the Cx36-deficient cells, the sub-threshold oscillations of ensembles of these cells did not synchronize, despite single-cell resetting effects. As a result, the variance in timing of these networks responses remained high.

How may altered spiking patterns lead to changes in learning-dependent timing?

Our data on evoked climbing fiber activities and the model of olivary activities described above indicate that the temporal firing patterns of olivary cells are destabilized when the cells are not coupled by functional gap junctions. Considering that electrotonic coupling of olivary neurons by Cx36 gap junctions also synchronizes climbing fiber activities of ensembles of Purkinje cells within the same parasagittal zone[16,39], one can appreciate that the overall defect in the temporal patterns of complex spike activities within the olivocerebellar modules must be substantial. To find out how impaired synchrony of climbing fiber responses may lead to deficits in learning-dependent timing, we created and tested a model of the olivocerebellar system controlling conditioned responses (**figure 4.7**). The model is in line with the hypothesis that plasticity associated with learning a conditioned eyeblink response is distributed among the cerebellar cortex and cerebellar nuclei, which may encode the timing of the response and store a representation of the amplitude of the response[18,19,47,48]. Since

Figure 4.6
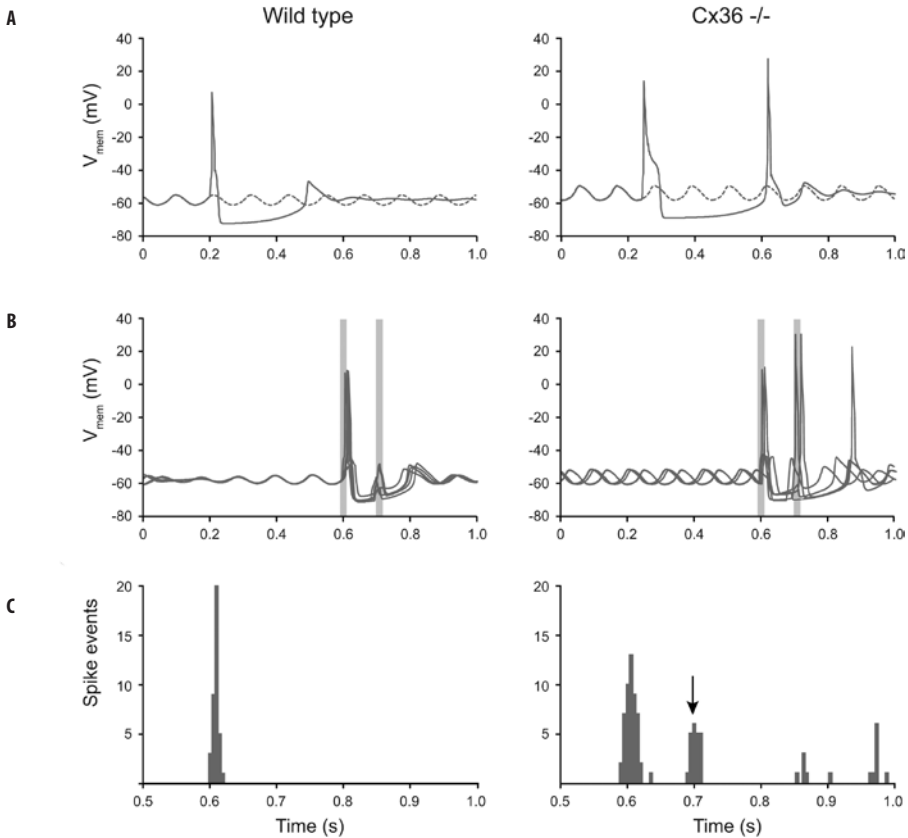
A 1000 ms trace of a wildtype cell and a Cx36-deficient cell. Five mA/cm² depolarizing currents are applied for 15 ms. The wildtype cell generates a spike and shows temporarily damped oscillations afterward. The Cx36-deficient cell responds with a doublet, despite the fact that stimulation occurred in the trough. **B** Five traces of 1000 ms from one of the wildtype cell ensemble simulations and a Cx36-deficient cell simulation. Due to the random initialization and coupling, the sub-threshold oscillations in the wildtype cells are damped at first and increase in amplitude as they become more synchronized (compare with **figure 4.5a**). Two depolarizing 15 ms currents (gray bars) are applied at 600 ± 10 ms (4.5 mA/cm²) and 700 ± 10 ms (2.5 mA/cm²). Exact onset of the currents was randomly determined per cell. The spike responses of the wildtype cells occur in a narrow time window, and the second input does not give rise to any action potentials. Thus, the wildtype network retains its synchronized oscillations. In contrast, due to a lack of coupling, the Cx36-deficient cells do not synchronize their oscillations. Their spike responses are not timed closely together, the second pulse also gives rise to action potentials, and doublets occur. Because of these factors, the Cx36-deficient network does not synchronize. **C** Temporal distribution of spikes in the wildtype and Cx36-deficient networks. The first depolarizing current was applied at 600 ± 10 ms and the second at 700 ± 10 ms. The coupled wildtype networks synchronize the first volley of spikes and do not respond to the second pulse. In the Cx36-deficient network, the first band consists of approximately the same number of spikes as the wild-type response indicated above, but due to a lack of coupling, the spikes are not as synchronized. Because of the increased excitability, Cx36-deficient cells also exhibit responses to the second pulse and an increased number of doublets.

a properly functioning cerebellar cortex has been shown to be required for the acquisition and expression of a well-timed conditioned response[19], the inability of Cx36-deficient mice to learn an appropriately timed eyeblink response might be partly due to incorrect guidance

of plasticity in the cerebellar cortex, which is known to be under climbing fiber control[49]. We therefore investigated the possibility of a causal link between absence of properly synchronously timed climbing fiber activities and impaired cortical plasticity in a network model of an olivocerebellar module[20,46]. The model initially analyzes the stability of the strengths of parallel fiber to Purkinje cell synapses during periods when active learning is not taking place and when plastic changes of synaptic strengths may occur due to uncorrelated parallel fiber and climbing fiber background activity. Subsequently, the impact of synaptic instability is explored in the situation when associative conditioning occurs, as post-learning (in)stability of parallel fiber synaptic strength might be directly related to the retention of cortical memory. The following assumptions form the principles of the model: (1) the olivocerebellar system is topographically organized, with Purkinje cells, neurons of the cerebellar nuclei and neurons of the inferior olive connected in discrete closed-loop modules in which the Purkinje cells converge onto the nuclei[50] (**figure 4.7a**); (2) the strengths of parallel fiber to Purkinje cell synapses can reversibly increase or decrease, depending for each activated granule cell on the width of the time interval to the climbing fiber stimulus[49,51] and (3) neurons tend to be more active as their excitatory inputs increase and less active as their inhibitory inputs increase[52,53].

Based upon these assumptions, one can deduce that adaptive changes of synaptic strengths within the olivocerebellar feedback loop can provide a feedback to control activity in the inferior olive around a stable equilibrium value[52] and that such equilibrium in activities of olivary neurons may in turn be necessary for synapses in the loop to remain stably fixed at their current strength. In the cerebellar loop it is probably not directly possible for a Purkinje cell to provide a one-to-one feedback to its own climbing fiber, due to the strong convergence of Purkinje cells onto deep cerebellar nuclei neurons (**figure 4.7a**). To enhance the efficiency of this feedback, specific sets of olivary neurons may be selectively coupled. In other words, selective coupling of olivary neurons, which together innervate the complete microzone of the Purkinje cells that converge onto the cerebellar nuclei neurons that provide the GABAergic input to the very same olivary neurons, can stabilize the activities in an entire olivocerebellar module.

Thus, the model shows how gap junction coupling in the inferior olive could help to stabilize the weights of parallel fiber to Purkinje cell synapses by synchronizing climbing fiber feedback to Purkinje cells (**figure 4.7b**). When the activity of inferior olivary neurons is not synchronized, as is the case in Cx36-deficient mutants, incorrect feedback through the cerebellar loop causes parallel fiber to Purkinje cell synaptic strengths to drift and finally saturate at their minimum or maximum strengths (**figure 4.7c** and **figure 4.7d**). Such saturation prevents efficient induction and maintenance of synaptic plasticity, which is required for learning and retention of a timed response. More specifically, impairment of cortical plasticity might lead to inadequate modulation of the activities in the cerebellar nuclei[53]. The development of a rectangular 'amplitude' response in the nuclei might then prevent an optimal closure of the eyelid at the moment when the unconditioned stimulus is about to take place[19,53] (**figure 4.7e**; compare to experimental data shown in **figure 4.3a**).

Figure 4.7
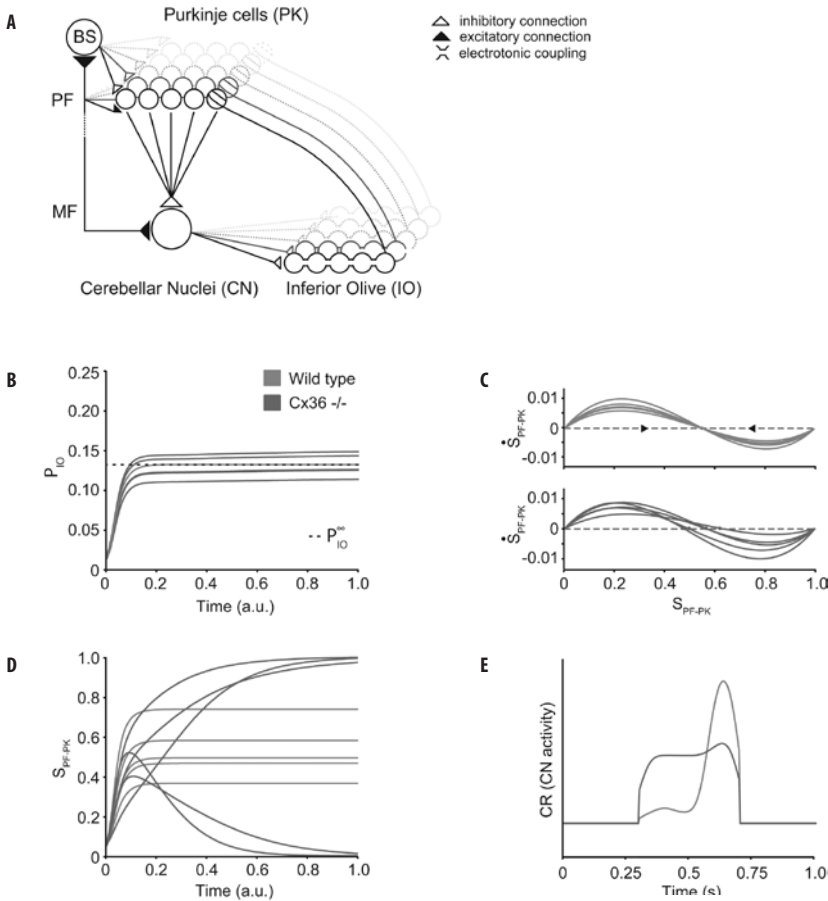
For panels **A**–**D**, a mathematical model was used to analyze the stability of parallel fiber to Purkinje cell synapses as a function of the average background spike probabilities of parallel fibers and climbing fibers. Panel **E** displays results from a real-time simulation, which incorporates the findings of the mathematical model in a conditioning paradigm. In the simulations, synaptic weights are adjusted according to coincidence rules for parallel fiber and climbing fiber activity. Neural spike probabilities are represented as linear sums of inhibitory and excitatory synaptic inputs, which are defined as the product of presynaptic average activity and synaptic strength. **A** Connectivity within a cerebellar module; Purkinje cells (PK), neurons of the cerebellar nuclei (CN), and neurons of the inferior olive (IO) form a closed loop. A key feature is the strong convergence of Purkinje cells onto CN neurons. MF, PF and BS indicate mossy fibers, parallel fibers, and basket cell cells, respectively. **B** Measure for the spike probability of five IO neurons as a function of time. Two different situations are investigated: a synchronized IO, in which IO neurons activate collectively due to coupling (wildtypes, blue) and an asynchronous IO, in which each neuron fires independently (Cx36 mutants, red). Wildtype curves all settle at the same equilibrium value, while mutant curves remain above or below this value. **C** Phase plots of the average PF to PK synaptic strength S of five Purkinje cells. The derivative of S represents the plastic change of S at each time step due to synaptic plasticity. PF activity determines the rate at which plasticity occurs, while the ratio of depression versus potentiation depends on the frequency of climbing fiber activation. Synaptic strengths are stable when the derivative of S equals zero. (Top panel) A synchronous IO produces synchronous climbing fiber activation, such that all Purkinje cells share a common stable state. (Bottom panel) In an asynchronous IO, each neuron fires at its own specific rate, resulting in different depression versus potentiation ratios in each Purkinje cell. Thus, in this situation each individual Purkinje cell strives for a different state of the network in order to stabilize its synaptic strengths. **D** Development of synaptic strengths in time for a synchronous IO (blue) and an asynchronous IO (red). Wildtype

Figure 4.7
Purkinje cells all receive the same stabilizing climbing fiber input, at which depression and potentiation exactly cancel each other over time. Their synaptic strengths therefore remain stable. Cx36 mutant Purkinje cells receive climbing fiber inputs that are either above or below equilibrium, resulting in too much depression or potentiation, respectively. Synapses therefore saturate at their minimum or maximum strengths. **E** Eyeblink responses of wildtypes (blue) and Cx36 mutants (red) resulting from a real-time simulation of the architecture in panel **A**. An additional plasticity rule was incorporated at the MF to CN synapse, allowing for the development of the "block" response in the CN. In wildtypes, inhibitory input from the cortex modulates the "block" activity in the CN to produce a well-timed response. In Cx36 mutants, saturation of PF to PK synaptic strengths prevents induction and maintenance of the right levels of depression and potentiation, resulting in insufficient cortical modulation.

DISCUSSION

Revealing the electrophysiological mechanisms that underlie the behavioral phenotypes of Cx36-deficient animals remains a topic of intense investigations[4,5,8,10,11,13,14,16]. Here, we showed that a lack of electrotonic coupling in the inferior olive leads to abnormal firing patterns of its neurons, which in turn can contribute to deficits in the timing of conditioned responses. The behavioral deficits in the global Cx36 mutants could be prominently revealed in different paradigms in which either a locomotion response or an eyeblink response was conditioned to a tone. In both cases conditioned responses occurred, but the timing that had to be learned to make the response optimal was aberrant. On the Erasmus Ladder Cx36 knockout mice were impaired in learning to avoid a bar that rose after a fixed period after the onset of the tone. Likewise, in the eyeblink test the coupling-deficient mutants showed after four training sessions a mismatch in their latency to peak amplitude of approximately 200 ms with respect to the onset of an air puff. This period stands in marked contrast to the 10 to 20 ms delay that can be observed in the basic eye movement responses of Cx36 null-mutants to optokinetic stimulation[16] or in the tremorgenic, limb and body movements of coupling-deficient rats treated with replication-incompetent lentiviral vectors[54]. The behavioral deficits in learning-dependent timing in the Cx36 knockout mice were robust despite secondary compensations that may occur[12]. Moreover, we observed the same type of deficits in the conditioning process following application of carbenoxolone and mefloquine, which are known to block olivary coupling in an acute fashion[24-26]. Although one cannot rule out short-term compensations or side effects with this approach either[27,28], still the behavioral effects were significant and similar to those in the global mutants, while they cannot be due to the potential long-term compensations that may occur in the Cx36 knockout mice. Importantly, the effect of mefloquine could be readily observed after injection into the inferior olive itself indicating that it is probably the coupling in the olive that is essential for learning-dependent timing of motor responses. These data in turn were supported by the finding that the abnormal timing of the conditioned eyeblink responses in the global Cx36 knockout mice was not observed in floxed Cx36 knockout mice, in which Cx36 is normally expressed in the relevant olivary sub-nuclei, but not in most other Cx36 expressing neurons in the brain. Together, these findings indicate that the role of coupling between inferior olivary neurons becomes apparent when the olivocerebellar system is challenged in a cerebellar motor learning task

and that it serves to facilitate learning-dependent timing in response to unexpected events rather than timing of movements per se.

In combination with modeling studies of both olivary neurons and the olivocerebellar system as a whole our electrophysiological recordings demonstrated that a lack of precision in the timing of the climbing fiber responses mediating the US signals as well as a reduction in synchrony of climbing fiber activities during spontaneous activity[16,39] are probably responsible for the behavioral deficits in the coupling-deficient Cx36 mutants. The lack of precision in timing is due to increased variety in the responses after the US, which in turn probably results from altered interactions with the sub-threshold oscillations in the inferior olive of Cx36 mutants. Our whole cell recordings of olivary neurons *in vivo* did not only demonstrate that Cx36mutants show less frequently sub-threshold oscillations and that the stability of the remaining oscillations is reduced, but also that the incidence of spikes occurring in the trough of these oscillations is significantly higher, while the correlation between their preferred spiking pattern and the frequency of their oscillations is generally weaker. The robust appearance of sub-threshold oscillations of olivary neurons has recently also been shown *in vivo* in rats with the use of sharp electrode recordings[55], while the contribution of electrotonic coupling to the occurrence of sub-threshold oscillations in olivary cells has recently also been addressed in rats with the use of lentiviral knockdown of Cx36 or pharmacological blockage of gap junctions[26,43]. Thus, together with the current findings we conclude that coupling supports the oscillations in the inferior olive *in vivo* and that the impact of oscillations on spiking patterns is reduced in uncoupled olivary neurons, which results in a more random timing of their spikes in relation to the oscillations.

The question remains as to how dynamic regulation of electrotonic coupling in the olive may contribute to learning-dependent timing[33,44,46,56]. Llinas and colleagues have provided strong evidence that the GABAergic input from the cerebellar nuclei, which terminates strategically at the coupled dendrites in olivary glomeruli[46], can uncouple the olivary neurons[56,57]. According to our model such a mechanism would counteract learning-dependent timing of the conditioned responses, because it desynchronizes the climbing fiber inputs that mediate the signals of the US. Interestingly, Mauk and colleagues recently demonstrated that the GABAergic projection to the olive is necessary for extinction of the conditioned responses by reducing the firing rate of the relevant olivary neurons below resting level[58]. Thus, in this respect the mechanism of uncoupling and the mechanism of reducing the firing rate of olivary neurons may serve the same effect in that they both actively counteract the conditioning process.

Chapter 4

METHODS

Animals

Global Cx36 knockout mice and wild type mice were generated and characterized as described by Guldenagel *et al.*[13]. The mutants that lacked Cx36 in their cerebellar nuclei neurons were cross-breedings of floxed-Cx36 mutants and parvalbumin-Cre mice. In contrast to the mouse published in Degen *et al.*[31], the current conditional Cx36 deficient mouse has the 5′ loxP site inserted in the 5′UTR of Cx36 and not in the intron, leading to functional expression of the floxed Cx36 allele. Furthermore, after Cre mediated deletion a cyan fluorescent protein (CFP) was expressed instead of the floxed Cx36 allele (**figure 4.3b**). Transfection of embryonic stem cells, creation of cell cultures, screening for homologously recombined HM-1 cell clones, and injections of blastocysts were performed as described by Theis *et al.*[59]. Subsequently Cx36+/flox(CFP) mice were mated to Cx36+/del (lacZ): Parvalbumin-Cre mice to obtain cerebellum deleted offspring with the genotype Cx36del(lacZ)/flox(CFP): parvalbumin-Cre. For the experiments described in the present study offspring from a parvalbumin-Cre founder with multicopy integration of the transgene was used. All experiments mentioned here and below were conducted in accordance with the European Communities Council Directive (86/609/EEC) and approved by the Dutch, British and/or German national ethics committee.

Immunofluorescence

Cx36-/flox: parvalbumin-Cre mice and Cx36-/flox(CFP) littermate controls were anesthetized and perfused with 4% paraformaldehyde in PBS. The brains were removed and cut on a vibratome (Leica, U.K.), and the sections were immersed in rabbit anti-GFP (1:1000, Invitrogen, U.K). Sections were washed in PBS and incubated in donkey anti-rabbit Cy3 (1:1000, Jackson ImmunoResearch, USA) prior to mounting (Vector Labs, U.K). Cy3 was viewed with a custom filter set and Alexa488 with FITC filters (Nikon E600 microscope) and images were captured directly from the slide using an Acquis Image Capture system (Synoptics, U.K).

Erasmus Ladder

The Erasmus Ladder is a fully automated system to screen both motor performance and motor learning capabilities of mutant mice in a non-invasive manner at a medium-throughput level. It consists of a horizontal ladder in between two shelter boxes, which are equipped with two pressurized air outlets (Pneumax, 171E2B.T.A.0009) to control the moment of departure and speed of the mouse. The ladder has 2 x 37 rungs for the left and right side, which are separated 2 mm apart. The rungs are 12 mm long and 3 mm in diameter, and the distance between two rungs on one side is 15 mm. All rungs are equipped with pressure sensors (produced at Erasmus MC), which are continuously monitored and which can be used to register and analyze the walking pattern of the mouse instantaneously. Moreover, based upon the prediction of the walking pattern the rungs can be moved up or down by a high-speed pneu-

matic slide (Pneumax, 2141.52.00.36.91) with a maximum of 18 mm at any moment in time. The computer system (National Instruments, PXI-1000B) that runs the real-time system to record sensor data, adjust air pressure, predict future touches, calculate interventions, reposition slides and store data, operates in a fixed cycle of 2 ms. In the associative motor learning paradigm, a 15 kHz tone (Voltcraft 7202), which gradually increases over 20 ms to 100 dB and which lasts up to 285 ms, was used as the CS, while a rising rung, which ascends 18 mm, was used as the US. The trials were separated by a random inter-trial interval ranging from 9 to 11 sec. Pharmacological interventions were done with either Carbenoxolone injections i.p. or Mefloquine injections into the olive, and the results obtained with the use of these applications were compared to the effects of vehicle injections. Carbenoxolone injections (40 mg/kg in 0.9% NaCl) were applied half an hour before each session. Bilateral mefloquine injections (150 μM in 0.2% DMSO) were applied in a surgical procedure directly after the last motor performance session, which meant one day before the first conditioning session. Dosages were chosen so as to make sure that impact on coupling was warranted, while side-effects were minimized[24,27,60,61]. For this surgery the mice were anaesthetized with a mixture of ketamine/xylazine (80 mg/kg and 2 mg/kg) and placed in a stereotaxic headholder, while their body temperature was kept at 37-38 °C using a heating pad. Following a dorsal craniotomy the atlanto-occipital membrane and dura were opened, and the inferior olive was identified using electrophysiological recordings[62]. Subsequently, the recording pipette was replaced by a glass pipette (tip diameter: 10-12 μm) filled with mefloquine or in two additional cases for histological verification a mixture of mefloquine and 2% BDA (Molecular Probes, Leiden, The Netherlands) and pressure injections of 50-100 nl were made within the olivary complex (**figure 4.2c**). After the conditioning sessions, the animals were anaesthetized with an overdose of pentobarbital (200 mg/kg i.p.) and perfused transcardially with flushes of saline and paraformaldehyde (4% in phosphate buffer). The brains were collected, embedded in gelatin, cut at 40μm transverse sections and mounted[63]. In case of the BDA injections selected sections were processed according to a BDA protocol using ABC-elite™ (Vector Laboratories) and DAB histochemistry[64].

Eyeblink conditioning

Wildtype and mutant mice were prepared for eyeblink conditioning according the MDMT procedure[30,65]. Mice are anaesthetized using nitrous oxide and isoflurane, and a dental acrylic pedestal was placed on the skull. On each day the MDMT measurement system was attached to the pedestal, while a magnet was glued on the lower eyelid. Mice were subjected to either a paired or a randomly paired procedure; both procedures lasted 4 days during each of which 1 session (64 trials grouped in 8 blocks) was conducted. The trials were separated by a random inter-trial interval ranging from 20 to 40 sec. Eyelid movements were considered as a significant eyelid response when its amplitude was greater than the mean + 3 SD of the amplitude of the movements that occurred in the 500 ms period before the onset of the CS.

Chapter 4

Extracellular recordings

To investigate the temporal aspects of climbing fiber activities (i.e. complex spikes) mice were prepared by placing a pedestal on the head and by placing a recording chamber above the simplex lobule and adjacent areas. During experiments the animals were immobilized using a restrainer. Extracellular Purkinje cell activities were recorded in the eyeblink region of awake animals with glass micro-electrodes using a Multiclamp 700A and Digidata 1322A from Axon Instruments. Complex spike responses were recorded during 1Hz air puff stimulation to the eye and analyzed off-line. A voltage threshold was used to detect complex spikes, and the time and waveform of the voltage records were used for off-line analysis (IGOR analysis software; WaveMetrics, OR).

Whole-cell recordings in vivo

Mice were prepared for experiments under isoflurane or ketamine/xylazine anesthesia[41]. Recordings were amplified with the use of a MultiClamp 700A and DIGIDATA 1322A (Axon Instruments, CA). All membrane potentials were corrected for the junction potential (8 mV). In current-clamp experiments, we measured voltage responses to a series of negative current steps (100 pA). Cells expressing IH-current were determined by the presence of an increasing depolarizing sag in more than three sequential hyperpolarization steps. Likewise, rebound depolarizations were only counted if present following more than three hyperpolarization steps. In general health of the cells was examined by checking input resistance, stability of membrane potential, and quality of the amplitude and waveform of action potentials. Corre-lations between the sub-threshold oscillation frequencies and preferred spiking frequencies were determined by analyzing autocorrelograms (clampfit9.0 software, Axon Instruments, CA). Bursts with a significant Poisson surprise value (>5) were correlated to the correspond-ing sub-threshold oscillation (STO) frequency extracted from the power spectrum of the recordings.

Model and simulations of olivocerebellar system

In the model, variable synaptic strengths are governed by coincidence rules for parallel fiber and climbing fiber activity probabilities. Synapses are accordingly described by differential equations, which are coupled by linear relations that represent the olivocerebellar loop. This formulation directly allows producing the phase plots shown in **figure 4.7c**. The equations were solved by numerical integration using MATLAB's function ode45, which is a 4th order Runge-Kutta solver. Resulting time-trajectory plots of synaptic strengths are shown in **figure 4.7d**. The model equations were then implemented in real-time simulations running with a 5 ms time-step (performed in MATLAB). In these real-time simulations inferior olivary neurons were simulated as spiking neurons. A training paradigm consisting of paired inputs repre-senting conditioned stimulus and unconditioned stimulus was used to train the network, both in case of synchronous and asynchronous inferior olive activity (**figure 4.7e**).

ACKNOWLEDGMENTS

REFERENCES

1. T. H. Bullock, M. V. Bennett, D. Johnston et al., *Science* 310 (5749), 791 (2005).
2. D. F. Condorelli, R. Parenti, F. Spinella et al., *Eur J Neurosci* 10 (3), 1202 (1998).
3. G. Sohl, J. Degen, B. Teubner et al., *FEBS Lett* 428 (1-2), 27 (1998).
4. M. V. Bennett and R. S. Zukin, *Neuron* 41 (4), 495 (2004).
5. B. W. Connors and M. A. Long, *Annu Rev Neurosci* 27, 393 (2004).
6. C. I. De Zeeuw, E. L. Hertzberg, and E. Mugnaini, *J Neurosci* 15 (2), 1587 (1995).
7. M. R. Deans, J. R. Gibson, C. Sellitto et al., *Neuron* 31 (3), 477 (2001).
8. C. E. Landisman, M. A. Long, M. Beierlein et al., *J Neurosci* 22 (3), 1002 (2002).
9. M. A. Long, M. R. Deans, D. L. Paul et al., *J Neurosci* 22 (24), 10898 (2002).
10. M. A. Long, M. J. Jutras, B. W. Connors et al., *Nat Neurosci* 8 (1), 61 (2005).
11. D. L. Buhl, K. D. Harris, S. G. Hormuzdi et al., *J Neurosci* 23 (3), 1013 (2003).
12. C. I. De Zeeuw, E. Chorev, A. Devor et al., *J Neurosci* 23 (11), 4700 (2003).
13. M. Guldenagel, J. Ammermuller, A. Feigenspan et al., *J Neurosci* 21 (16), 6036 (2001).
14. C. Frisch, M. A. De Souza-Silva, G. Sohl et al., *Behav Brain Res* 157 (1), 177 (2005).
15. M. R. Deans, B. Volgyi, D. A. Goodenough et al., *Neuron* 36 (4), 703 (2002).
16. W. M. Kistler, M. T. De Jeu, Y. Elgersma et al., *Ann N Y Acad Sci* 978, 391 (2002).
17. K. S. Garcia and M. D. Mauk, *Neuropharmacology* 37 (4-5), 471 (1998).
18. S. K. Koekkoek, H. C. Hulscher, B. R. Dortland et al., *Science* 301 (5640), 1736 (2003).
19. S. P. Perrett, B. P. Ruiz, and M. D. Mauk, *J Neurosci* 13 (4), 1708 (1993).
20. C. I. De Zeeuw and C. H. Yeo, *Curr Opin Neurobiol* 15 (6), 667 (2005).
21. G. Hesslow, P. Svensson, and M. Ivarsson, *Neuron* 24 (1), 179 (1999).
22. E. Porras-Garcia, J. Cendelin, E. Dominguez-del-Toro et al., *Eur J Neurosci* 21 (4), 979 (2005).
23. A. M. Van Alphen, T. Schepers, C. Luo et al., *Ann N Y Acad Sci* 978, 413 (2002).
24. T. A. Blenkinsop and E. J. Lang, *J Neurosci* 26 (6), 1739 (2006).
25. F. C. Martin and A. Handforth, *Mov Disord* 21 (10), 1641 (2006).
26. D. G. Placantonakis, A. A. Bukovsky, S. A. Aicher et al., *J Neurosci* 26 (19), 5008 (2006).
27. S. J. Cruikshank, M. Hopperstad, M. Younger et al., *Proc Natl Acad Sci U S A* 101 (33), 12364 (2004).
28. R. Rozental, M. Srinivas, and D. C. Spray, *Methods Mol Biol* 154, 447 (2001).
29. J. E. Saffitz, J. G. Laing, and K. A. Yamada, *Circ Res* 86 (7), 723 (2000).
30. S. K. Koekkoek, W. L. Den Ouden, G. Perry et al., *J Neurophysiol* 88 (4), 2124 (2002).
31. J. Degen, C. Meier, R. S. Van Der Giessen et al., *J Comp Neurol* 473 (4), 511 (2004).
32. R. S. Van Der Giessen, S. Maxeiner, P. J. French et al., *J Comp Neurol* 495 (2), 173 (2006).
33. F. Bengtsson and G. Hesslow, *Cerebellum* 5 (1), 7 (2006).
34. A. Seto-Ohshima, P. C. Emson, M. W. Berchtold et al., *Exp Brain Res* 75 (3), 653 (1989).

Chapter 4

35. P. Mann-Metzer and Y. Yarom, *J Neurosci* 19 (9), 3298 (1999).

36. G. Hesslow, *J Physiol* 476 (2), 229 (1994).

37. M. D. Mauk, J. E. Steinmetz, and R. F. Thompson, *Proc Natl Acad Sci U S A* 83 (14), 5349 (1986).

38. W. T. Thach, Jr., *J Neurophysiol* 30 (4), 675 (1967).

39. S. P. Marshall, R. S. van der Giessen, C. I. de Zeeuw et al., *Cerebellum*, 1 (2007).

40. R. Llinas and Y. Yarom, *J Physiol* 315, 549 (1981).

41. S. Khosrovani, R. S. Van Der Giessen, C. I. De Zeeuw et al., *Proc Natl Acad Sci U S A* 104 (40), 15911 (2007).

42. E. Leznik, V. Makarenko, and R. Llinas, *J Neurosci* 22 (7), 2804 (2002).

43. E. Leznik and R. Llinas, *J Neurophysiol* 94 (4), 2447 (2005).

44. N. Schweighofer, K. Doya, and M. Kawato, *J Neurophysiol* 82 (2), 804 (1999).

45. T. J. Ruigrok and J. Voogd, *Eur J Neurosci* 7 (4), 679 (1995).

46. C. I. De Zeeuw, J. I. Simpson, C. C. Hoogenraad et al., *Trends Neurosci* 21 (9), 391 (1998).

47. M. D. Mauk and N. H. Donegan, *Learn Mem* 4 (1), 130 (1997).

48. J. L. Raymond, S. G. Lisberger, and M. D. Mauk, *Science* 272 (5265), 1126 (1996).

49. M. Coesmans, J. T. Weber, C. I. De Zeeuw et al., *Neuron* 44 (4), 691 (2004).

50. J. Voogd and M. Glickstein, *Trends Neurosci* 21 (9), 370 (1998).

51. S. S. Wang, W. Denk, and M. Hausser, *Nat Neurosci* 3 (12), 1266 (2000).

52. G. T. Kenyon, J. F. Medina, and M. D. Mauk, *J Comput Neurosci* 5 (1), 17 (1998).

53. J. F. Medina and M. D. Mauk, *Nat Neurosci* 3 Suppl, 1205 (2000).

54. D. G. Placantonakis, A. A. Bukovsky, X. H. Zeng et al., *Proc Natl Acad Sci U S A* 101 (18), 7164 (2004).

55. E. Chorev, Y. Yarom, and I. Lampl, *J Neurosci* 27 (19), 5043 (2007).

56. R. Llinas and K. Sasaki, *Eur J Neurosci* 1 (6), 587 (1989).

57. E. J. Lang, I. Sugihara, and R. Llinas, *J Neurophysiol* 76 (1), 255 (1996).

58. J. F. Medina, W. L. Nores, and M. D. Mauk, *Nature* 416 (6878), 330 (2002).

59. M. Theis, T. M. Magin, A. Plum et al., *Methods* 20 (2), 205 (2000).

60. P. Gareri, D. Condorelli, N. Belluardo et al., *Neuropharmacology* 49 (4), 551 (2005).

61. D. G. Margineanu and H. Klitgaard, *Brain Res Bull* 71 (1-3), 23 (2006).

62. T. J. Ruigrok and J. Voogd, *J Comp Neurol* 426 (2), 209 (2000).

63. T. J. Ruigrok and R. Apps, *Nat Protoc* 2 (8), 1869 (2007).

64. A. Pijpers, J. Voogd, and T. J. Ruigrok, *J Comp Neurol* 492 (2), 193 (2005).

65. S. K. Koekkoek, K. Yamaguchi, B. A. Milojkovic et al., *Neuron* 47 (3), 339 (2005).

CHAPTER V

The Erasmus Ladder
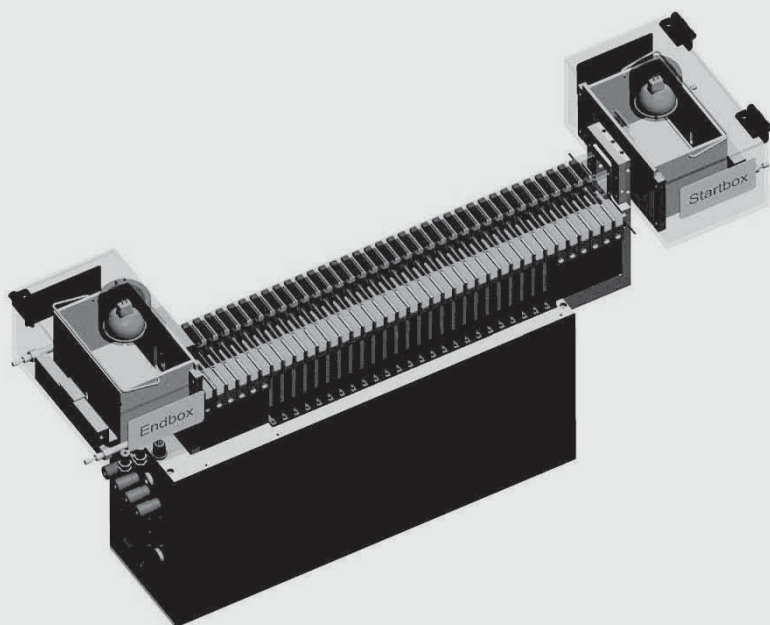
The overall design is depicted in the figure on the first page of this chapter. In general the Erasmus Ladder consists of two shelters connected by a horizontal ladder. Here we will dissect the Ladder in its components and describe each accordingly.

SHELTERS

Each shelter is a black PVC box (lxwxh, 13x23x10 cm, figure 5.1a) with a small opening on one of the sides and a hinged roof equipped with a bright white LED spotlight. Inside this box a second clear PVC box can be placed. This clear box also has a small opening, which lines up with the opening in the outer box and which can be closed with a slide thereby creating a flexible doorway for the mouse to leave the shelter. The clear box enables easy transport of the mice to and from their cages. An enforcement (see below) system is located on the back wall facing the doorway of the black box.

Figure 5.1
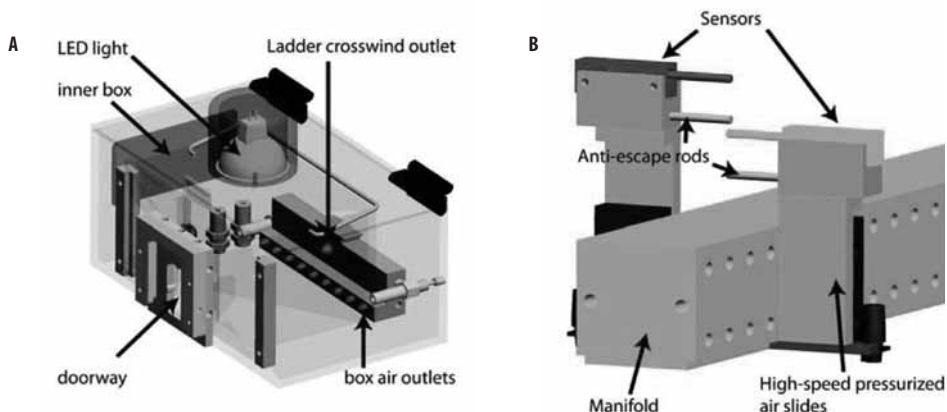
A depicts one of the two shelters of the Erasmus ladder. Clear plastic inner boxes are used as a barrier between mice and system components. Note the strategically located air nozzles which form the enforcement system. **B** depicts one rung of the ladder. It consists of two halves (red and green, illustration purpose only) each of which is placed on a separate actuator (high-speed pressurized air slides). Each actuator is connected to the air pressure system through a custom made aluminum manifold block. Anti-escape rods are placed under each sensor to prevent mice from accessing the area under the rungs.

LADDER

The ladder is made of 37 rungs placed 15 mm apart from each other. Prototype testing revealed an optimum step distance of 6 cm forepaw displacement during a single step, at medium velocity. Thus the use of 15 mm rung spacing provides highly flexible ladder configurations in that multiple rung patterns with varying degree of difficulty can be presented by lowering and raising rungs. In addition the 15 mm spacing allows ataxic mice to cross the ladder without too much difficulty. Each rung is split in the middle and each half-rung consists of a specially developed sensor placed on top of a high-speed, air-pressure sliding

actuator (figure 5.1b). This setup enables automatic configuration of the ladder, detection of rung pressures for each side individually and online reconfiguration of the ladder pattern based on feedback through online walking pattern prediction analysis. Experiments presented in this thesis have been performed with an alternated pattern configuration. On the green side all the even rungs (2, 4 ... 36) and on the red side all the odd rungs (1, 3 ...37) were lowered 6 mm. This configuration provided an alternating stepping pattern with 6 mm deep gaps in between. Each lowered rung could be raised 18 mm by the system to provide an unexpected obstacle of 12 mm.
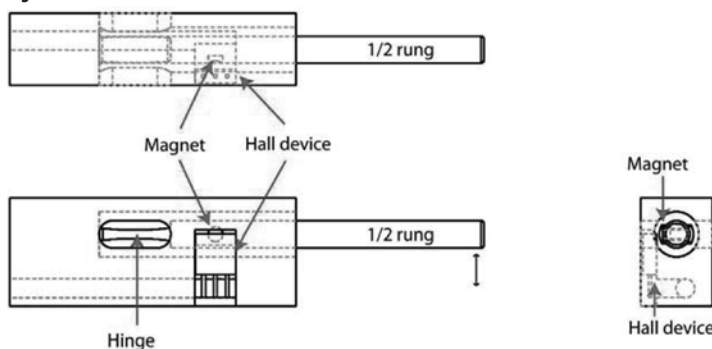
SENSORS

The sensors are constructed of custom 3d printed polymer components and electrical components. The basic idea is depicted in **figure 5.2**. Movement thresholds are determined by adjusting the diameter of the hinge rod, while rung pressures are detected by a Hall device, which is actuated by a magnet embedded in the rung. This magnetic setup provides a system that is unaffected by the debris that inevitably builds up when mice are frequently crossing the ladder.

ACTUATORS

The actuators are high speed, air pressure slides (Pneumax). These slides (lxwxh, 15x40x80 mm) have a maximal travel distance of 18 mm. A TTL pulse to the controller controls slide pressure (on, off), which in itself controls slide position (up, down). Reaction time from onset of TTL to completion of slide movement is 52 ms with an actual movement time of 8 ms. We

Figure 5.2

The sensors are constructed out of custom 3d printed polymer components and electrical components. In principle it is a rod that connects to the outer housing with a flattened area. Movement threshold is set by adjusting the diameter of this flattened area. Rung press detection is performed by a Hall device that is actuated by a magnet embedded in the rung. This magnetic setup provides a system that is unaffected by the debris that inevitably builds up when mice are frequently crossing the ladder.

use distance pieces to enable a variety of ladder configurations. The first and the last 6 rungs have no actuators, these rungs provide a platform for the mice to accelerate and decelerate.

ENFORCEMENT SYSTEM

Strategically located pressurized air nozzles (**figure 5.1a**) are used to stimulate the mouse to leave the shelters when needed and cross the ladder at constant velocity. In addition they are used to prevent the mouse from leaving the shelters and cross the ladder at other moments. Mice generally learn very quickly to react to these cues making fully automated ladder crossings at constant velocity. This operation enables a precise recording of motor performance and motor learning since all encounters of the mice with the motor task can be precisely controlled and measured. In addition, it prevents unauthorized ladder exploration. Ladder crosswind, which is constantly adjusted in each cycle (2 ms) to the direction and position of the mouse, is turned on at full force (30 km/h) from the opposite direction when a mouse leaves one of the shelters unauthorized; this wind usually causes the mice to immediately return to the shelter. In contrast, authorized ladder crossing is accompanied by a tailwind that is kept constant at a 16 km/h at the actual position of the mouse until the opposite shelter has been reached. Extensive testing with a variety of protocols has demonstrated that this resulted in a medium speed ladder crossing, without exploration episodes and very constant stepping patterns in wildtype mice.

CONTROLLER

The Erasmus ladder is a fully automated system that completes the mouse training automatically. Prototype testing revealed a mean stepping time of 350 ± 30 ms (forepaw to forepaw placement). A National Instruments (NI) computer system running a real-time operating system is used and programmed to read all sensors, make all decisions, execute all interventions and store the data within a guaranteed 2 ms cycle. The programs were custom written using the LabView (NI) programming language with the real-time module (see below). The computer itself is a National Instruments PXI-8150 controller mounted in a PXI chassis. The sensor readout is performed by digital IO hardware (3x PXI-6533) and the actuators are controlled by a 64 channel relay switch card (PXI-2567). The enforcement system is controlled by a M-Dac card (PXI-6229), which provides analog in and analog out channels. The tone system is a custom made PXI card that contains a precise sinewave generator and 3 voltage controlled gain amplifiers.

SOFTWARE

The Erasmus ladder is controlled by customly written LabView (NI) virtual instruments, which run on a real-time operating system (LabView) installed on a dedicated NI-PXI 8150 controller. Figure 5.3 depicts a basic flow schematic of the program. The basic control has a state machine architecture. Every 2 ms a program cycle starts and the valid state for that cycle is determined. During all states the sensors are read out, but the information processing depends on the active state. The machine has five states including a resting state, escape state, first leaving state, second leaving state and run sate. (1) Resting State: a particular trial always starts with the resting state, during which the mouse has to stay in the box. In the protocols described in this thesis the duration of state 1 ranges from 9 to 11 seconds; (2) Escape State: if the mouse leaves the box before state 1 has ended, state 2 is activated. Headwind is immediately turned on at full force from the opposite direction. This causes a return to the shelter after which state 1 recommences. (3) First Leaving State: the light is switched on in the shelter. If the mouse leaves the shelter, state 5 is activated; however if after

Figure 5.3
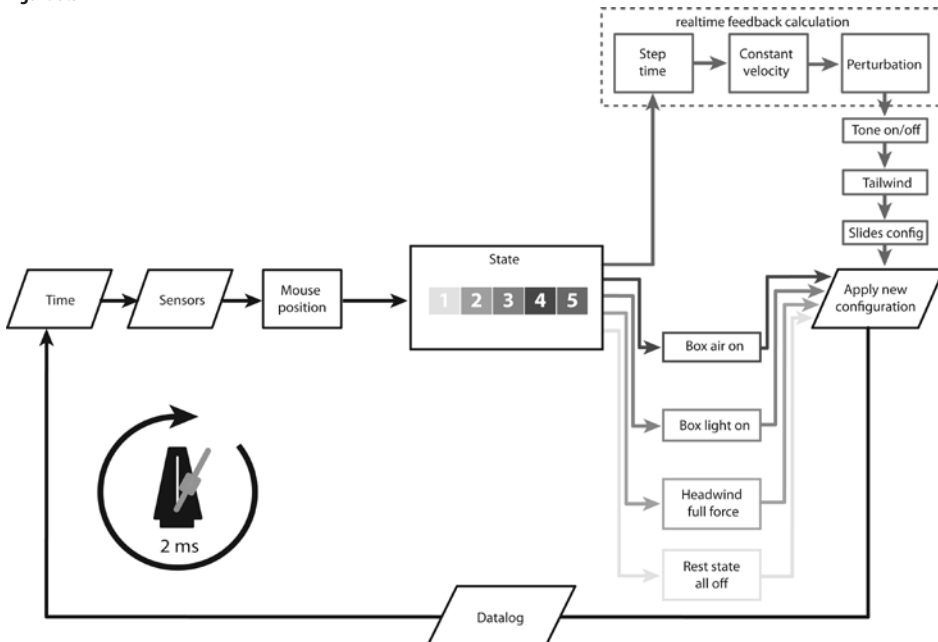
The software that controls the Erasmus ladder has a state machine architecture as depicted here. Different states (1-5) are plotted in different colors. The cycle is under real-time control and guaranteed to start every 2 ms. State 5 is the actual run state and is plotted in red. Input / output actions (skewed boxes) and processes / decisions (straight boxes) that belong to the main flow are plotted in black. Every cycle sensors are read out and it is determined what the mouse position is. This position subsequently is input as one of the cues which determines the new state of the system, after which the system acts accordingly. At the end of the cycle all configuration decisions are applied and data is logged after which the new cycle starts.

3 seconds the mouse has not yet left the shelter, state 4 is activated. (4) Second Leaving State: the 5 pressurized air nozzles located near the bottom on the back wall of the shelter (figure 5.1a) are activated until the mouse leaves the shelter. (5) Run State: the mouse is crossing the ladder, perturbations can be made based on readouts from previous cycles during this state, tailwind is adjusted to position to maintain 16km/h. When the mouse reaches the opposite shelter this state is ended and state 1 is activated thereby completing the cycle.

DATA MANAGEMENT

Every 2 ms cycle the sensors are read out digitally. This results in a 74 bit representation of the ladder, which is converted into a string. Whenever a change in state or a change in the 74 bit ladder pattern is detected, an entry in a file is saved, which consists of timestamp, state, mouse number, run number, etc. After each session this file is automatically fed into a relational database (MicrosoftAccess). With the use of SQL and SQL capable software data can be sorted, filtered and analyzed as required.

EXPERIMENTAL PROTOCOLS

Each mouse receives 4 motor performance sessions and associative motor learning sessions. During the motor performance sessions a mouse is placed in one of the shelters. After 10 seconds the shelter light is turned on (run cue 1) followed 3 seconds later by the pressurized air outlet in this shelter (run cue 2); cue 2 usually encourages the mouse to leave the shelter. The occasional mouse (<5%) that did not follow the protocol after the first motor perfor-mance session was removed from the experiment. When the mouse is on the ladder, a second pressurized air outlet is activated, which is directed in the same direction as the traveling path of the mouse. This encourages the animal to walk over the ladder to the opposite shelter at medium speed. When the mouse arrives in the opposite shelter, the two pressurized air outlets are switched off. After 10 seconds the protocol as described above is repeated. One trial is one run from shelter to shelter. One session consists of 72 trials. Two simple protocols were chosen for the associative motor learning sessions: (1) 90 ms ISI: prior to each run, the position of the obstacle was randomly chosen by the system. At the moment the mouse touched the preceding rung on the obstacle side a 90 ms, 90dB, 15 kHz tone was presented as a conditioned stimulus followed at the end by the sudden appearance of the obstacle. The pressurized air outlets provided a background noise of 80dB at15 kHz, which prevented auditory startle reactions to the tone. In these sessions the mice were trained to avoid an ascending rung during daily training sessions of 9 blocks of 8 trials, which included 1 CS-Only trial, 1 US-Only trial and 6 US-CS paired trials; (2) 285 ms ISI: during each run the last 3 step sizes and step times of the forepaw that was to be perturbed (right side only) were buffered and standard deviations (SD) were calculated. Whenever the SD of the step sizes equaled zero

and the SD of the step times was smaller than 150 ms the pattern was reliable enough to pre-
dict when and where the mouse was going to place its right forepaw. With this information
the time and place of the perturbation was calculated. Before this perturbation was going to
take place an 285 ms, 90dB, 15 kHz tone was presented as a conditioned stimulus.

ANALYSIS

For the motor performance I counted the number of times the mouse touched the descended
rungs. For the motor learning I extracted from the database per trail the time in ms of the
rung pressures as well as the time and place of the perturbation (**figure 5.4**). After step 1
only the first time that a particular sensor was touched remained. In step 2 decreasing rung
numbers were removed leaving us with front paw touches only. In step 3 time differences
were calculated and the pre and post-rise values were determined.
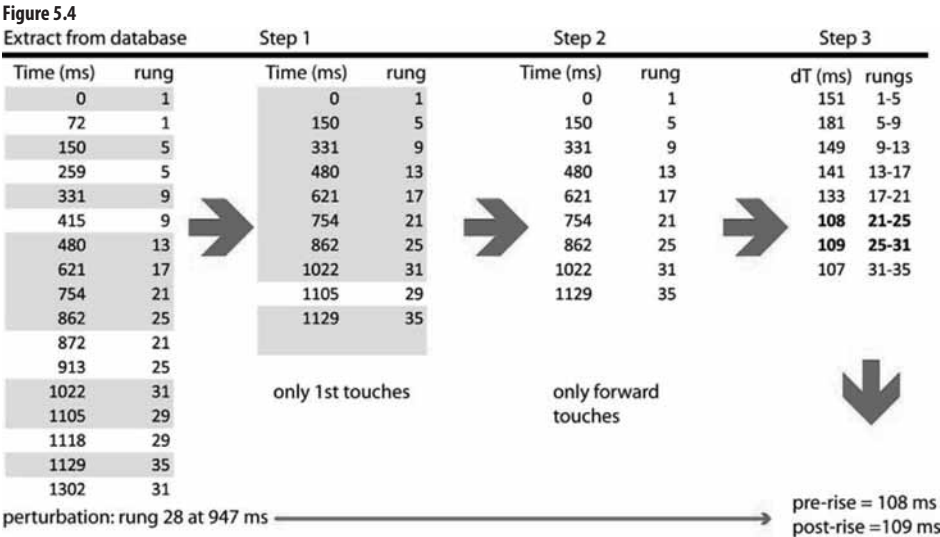
Figure 5.4

Analysis of step time is shown in this figure. Each sub-table is the result of an analytical step. In gray are the values that were taken to the next
sub-table. Values in white were discarded as non-relevant. Basically analytical step 1 and 2 are performed to filter the data such that only front
paw touches in the forward direction are taken to analytical step 3. Note that the extracts are generated using SQL queries and that a selection
is made for right side data only.

CHAPTER VI

General Discussion

GENERAL DISCUSSION

I aimed to build a new behavioral task with the following requirements: (1) the task should be automated; (2) the task should be non-invasive; (3) the task should be more sensitive in detecting motor performance deficits than the accelerating rotarod; (4) the associative motor learning paradigm has to be dependent on the cerebellum and (5) the task should have the ability to distinguish between motor performance deficits and associative motor learning deficits. Below I will discuss to what extend I have been able to meet these requirements with the Erasmus Ladder and at the end of this thesis I will suggest future improvements to make the Erasmus Ladder a better task than it already is.

6.1 HAS THE ERASMUS LADDER MET THE REQUIREMENTS?

The Erasmus Ladder has met requirements (1) and (2). The task is automated (see **chapter 5**) and the task is non-invasive. The other three requirements will be discussed in more detail below.

6.1.1 Is the task more sensitive in detecting motor performance deficits than the accelerating rotarod?

The Erasmus Ladder task can be completed by visibly ataxic mice (ßCamKII knockout mice see **chapter 3** and *Lurchers* see **chapter 4***)* and is still too difficult for wildtype mice to perform flawlessly (without missteps). This makes the Erasmus Ladder a better task to analyze motor performance than the accelerating rotarod because there are limitations in the range of scores possible on the accelerating rotarod, since some mice achieve the maximum score, i.e. they will stay on the accelerating rotarod at its highest speed and others will score the minimum, i.e. they will fall off immediately[1]. The Erasmus Ladder does not produce minimum scores (all mice finish the task) nor maximum scores (no mouse ever had a session without a misstep). In **chapter 2** this advantage of the Erasmus Ladder is highlighted: expanded CGG mice have a motor performance deficit on the Erasmus Ladder but not on the accelerating rotarod. Another advantage of ataxic mice finishing the task is that we can now measure if these mice are capable of associative motor learning, which to my knowledge cannot be done by any other behavioral task.

6.1.2 Is the associative motor learning paradigm dependent on the cerebellum?

In eyeblink conditioning, associative learning is measured as the improvement of correct (conditioned) responses to CS-Only trials over time[2,3]. Correct responses from CS-Only trials prove that the mice make an association between the tone (CS) and the air puff (US), because the mice close their eyes at the appropriate moment even without an US. With the associative motor learning paradigm on the Erasmus Ladder it is not possible to show an improvement

in correct responses. Moreover, the US (the obstacle) in the Erasmus Ladder task, unlike eye blink conditioning, cannot be reflexively avoided, but has to be avoided by a visually guided step.

The best way to prove that the associative motor learning paradigm is cerebellum-specific is by testing cerebellum-specific mutants, which have no motor performance deficits but have deficits in the associative motor learning paradigm. Unfortunately, all the cerebellum-specific mutants we tested so far either had motor performance deficits or no deficits at all.

However, there is evidence that the motor learning paradigm is cerebellum-specific. The Fmr1 knockout mouse has no motor performance deficit but has an associative motor learning deficit (see **chapter 2)**. Although this mouse is not a cerebellum-specific mutant, Fmr1 is highly expressed in Purkinje cells[4], making it likely that the found deficit is due to malfunctioning of the cerebellar circuit.

I also measured wildtype mice with the associative motor learning paradigm that were either injected with mefloquine or only with the vehicle (see **chapter 4**). Mefloquine blocks the functioning of gap junctions in the inferior olive[5]. The inferior olive only projects to the cerebellum[6]. Since the mice injected with mefloquine were significantly impaired in the associative motor learning paradigm and the mice injected with just the vehicle were not impaired, this points to the cerebellum-specificity of the associative motor learning paradigm.

6.1.3 Is the Erasmus Ladder able to distinguish between motor performance deficits and associative motor learning deficits?

In **chapter 2** I showed that expanded CGG mice have a motor performance deficit but not a motor learning deficit and Fmr1 knockout mice do not have a motor performance deficit but have a motor learning deficit. Therefore we can conclude that the Erasmus Ladder can detect differences between motor performance deficits and motor learning deficits. The expanded CGG mouse has a mild motor performance deficit, but the ßCamKII knockout mouse (**chapter 3**) and the *Lurcher* (**chapter 4**) have more severe motor performance deficits. Both these mice also show a deficit in the associative motor learning paradigm. Thus, for ataxic mice the Erasmus Ladder can not distinguish between motor performance deficits and associative motor learning deficits but for mice with a mild motor performance deficit the Erasmus Ladder can distinguish between motor performance deficits and motor learning deficits.

6.2 FUTURE IMPROVEMENTS

The goal of this project was to build a cerebellum-dependent associative motor learning task for mice, which is non-invasive, easy to operate and fully automated. I decided to make a horizontal ladder in which the height of the rungs could be altered. Since synaptic plasticity in the cerebellum is required for learning-dependent timing of the conditioned eyeblink response in mice[3,7], which also uses repeated presentation of an auditory tone as the CS, we

reasoned that the same type of classical conditioning could be performed on the Erasmus Ladder by presenting a tone (CS) just prior to raising a ladder rung in the path of the moving animal (US). The most important prerequisite for the associative motor learning paradigm is that the Erasmus Ladder system has to predict very accurately where the mouse will be at any moment. The only way that this can be achieved is if the mice step with a constant speed from shelter to shelter. Extensive pilot testing, with all the rungs in the standard position and no incentive to transit the ladder, revealed that mice would explore the rungs at leisure, often pausing and reversing directions. This variable exploratory behavior made it impossible to predict exactly when a mouse would place a paw on a given rung and, therefore, also impossible to implement a precisely timed associative motor learning paradigm. In the paragraphs below, I will discuss the most important improvements we made to the system, which led to a more constant stepping pattern and suggest future improvements.

6.2.1   Incentive

We choose the air flow system which I described in **chapter 5** as an incentive for the mice to transit the Erasmus Ladder because of the following two reasons. Firstly, the air flow system is very aversely for the mice. This will limit their exploratory behavior on the Erasmus Ladder and therefore will lead to a more constant stepping pattern. Secondly, I programmed the air flow system in such a way that regardless the position of the mouse, the mouse is always subjected to a tailwind of 16 km p/h. This makes the speed with which mice cross the ladder less variable and therefore it will be easier to predict where mice will be at any given moment.

However, the fact that the air flow system is very aversely for the mice is not ideal. Another way to encourage the mice to walk from shelter to shelter is by giving them a food reward when they arrive in the other shelter. What effect this incentive has on the consistency of the stepping pattern can only be determined with new experiments.

6.2.2   Rung configuration

After extensive pilot testing, we choose to use the rung configuration described throughout this thesis (see **chapter 5**). We used this configuration for two reasons. Firstly, with this configuration it is very easy to determine the motor performance and the improvement in motor performance, because you can simply count the number of steps on the descended rungs. Secondly, it is much easier to predict where the mouse will step in the associative motor learning paradigm, since with this configuration mice are forced to make steps with step size 2 or 4. But even with this configuration, it sometimes happens that the raised rung (US) in the associative motor learning paradigm is not in the path of the mouse. It is possible to change the associative motor learning paradigm in such a way that you do not need any predictions from the Erasmus Ladder system anymore. Instead of using the rising of the rung as an US, the Erasmus Ladder system changes the entire rung configuration as an US. Now, the mice will always have to adjust its walking pattern, even if it is standing still, decelerating or ac-

celerating. Their ability to adapt their stepping pattern just after the CS will be the measure of associative motor learning. Again new experiments will have to be conducted to see if this is profitable approach.

6.2.3   Sensors

The sensors in the rungs of the Erasmus Ladder are set to detect a force of 5 grams or more, so as to only detect paw touches and not tail touches (an adult mice weighs on average 25 grams). These sensors give an all-or-nothing signal. However, with this signal it is impossible to establish if a sensor is touched by a front paw, a hind paw or both paws. Mice normally put their hind paw on the same rung as they have put their front paw before they move their front paw to the next rung**.** Therefore it is not possible to reliably divide the step time into stance time and swing time with the current sensors. This is why we are developing a new sensor, which measures pressure in a 2d plane. Apart from this new parameter, with these new sensors we can now also analyze stance time and swing time and look specifically at hind paw and front paw characteristics. This will give us the opportunity of determining animal specific stepping patterns and will improve our chances of detecting even more subtle phenotypes.

6.2.4   High-speed video camera system

Another improvement that has to be made is setting up a high-speed video camera system, which records all the movements of the mice. With this it will be able to determine how the mice exactly avoid the obstacle.

6.3   REFERENCES

1.   D. Wahlsten, N. R. Rustay, P. Metten et al., *Trends Neurosci* 26 (3), 132 (2003).
2.   S.K.E. Koekkoek, W. L. Den Ouden, G. Perry et al., *J Neurophysiol* 88 (4), 2124 (2002).
3.   S. K. Koekkoek, K. Yamaguchi, B. A. Milojkovic et al., *Neuron* 47 (3), 339 (2005).
4.   *Cell* 78 (1), 23 (1994).
5.   S. J. Cruikshank, M. Hopperstad, M. Younger et al., *Proc Natl Acad Sci U S A* 101 (33), 12364 (2004).
6.   C. I. De Zeeuw, J. I. Simpson, C. C. Hoogenraad et al., *Trends Neurosci* 21 (9), 391 (1998).
7.   S. K. Koekkoek, H. C. Hulscher, B. R. Dortland et al., *Science* 301 (5640), 1736 (2003).

Chapter 6

SUMMARY

Which parts of the brain are involved in learning? How and where is the information stored? Neuroscientists would like to answer these questions. In this thesis, I try to answer these questions by studying the cerebellum, a part of the brain that plays an important role in motor learning. There are several ways to study the cerebellum: the anatomy can be studied, molecular pathways can be elucidated, electric currents of cerebellar neurons can be recorded, and models can be made about the functioning of the cerebellum. The most direct way to investigate the functioning of the cerebellum is by testing (mutant) mice in a cerebellar behavioral task. With the rapid advances in transgenic technologies, it has become routine to investigate cellular mechanisms using behavioral tasks. Mice are the preferred species for transgenic technologies, and therefore for behavioral testing, since there are several techniques available to manipulate their embryonic stem cells.

A range of tasks has been developed to behaviorally phenotype (mutant) mice. Tasks include grid walking, rope climbing, inclined plane kinematic analysis, open-field tasks, gait analysis, measures of ground reaction forces, swimming, and accelerating rotarod. Most of these tasks are easily implemented and can be used to gauge motor performance. However, none provide reliable information about associative motor learning. Associative motor learning in mice can be explicitly tested using several methods adapted for mice in our laboratory, including compensatory eye movements and eyeblink conditioning. The neural circuitry of the cerebellum that is activated and modified during learning in each of these tasks is well-studied, providing a direct link between behavior and synaptic modification; however, both tasks suffer in that they involve extensive surgical preparation (e.g. eye-coil or magnet placement), careful monitoring during experimental sessions, loss of some subjects during these sessions (e.g., due to broken or displaced coils/magnets) and significant post-hoc analysis.

Although all of the abovementioned behavioral tasks have their merits for cerebellar research, I believe that a new cerebellar behavioral task for mice would be an asset. As such, I created a new behavioral task, the Erasmus Ladder paradigm, which had to meet the following requirements: (1) the task should be automated; (2) the task should be non-invasive; (3) the task should be more sensitive in detecting motor performance deficits than the accelerating rotarod; (4) the associative motor learning paradigm has to be dependent on the cerebellum; and (5) the task should have the ability to distinguish between motor performance deficits and associative motor learning deficits.

The Erasmus Ladder is formed by 2 x 37 rungs positioned between a start box and an end box across which the mice can run back and forth. Each rung on both the left and right side is equipped with a pressure sensor, which is continuously monitored. Based on instantaneous analysis of the activities of these sensors, the walking pattern of the mice can be predicted in the millisecond range, and, if wanted, interrupted by moving each individual rung up or down.

To test if the Erasmus ladder met the abovementioned requirements, and if experiments on the Erasmus Ladder could tell us anything about learning, I measured several (mutant) mice on the Erasmus Ladder with the following protocol: each mouse received 4 motor performance sessions and 4 associative motor learning sessions. During the motor performance sessions a mouse was placed in one of the boxes (shelters). After 10 seconds the shelter light was turned on (run cue 1) followed 3 seconds later by the pressurized air outlet in this shelter (run cue 2). Run cue 2 usually encouraged the mouse to leave the shelter. When the mouse was on the ladder, a second pressurized air outlet was activated, which was directed in the same direction as the travelling path of the mouse. This encouraged the animal to walk over the ladder to the opposite shelter at medium high speed. When the mouse arrived in the opposite shelter, the two pressurized air outlets were switched off. After 10 seconds the protocol as described above was repeated. One trial consists of one run from shelter to shelter. The occasional mouse (< 5%) that did not follow the protocol after one motor performance session was removed from the experiment. One session consisted of 72 trials. Motor performance was assessed by determining the missteps per trial. A misstep is a step on one of the descended rungs.

After the four motor performance sessions I subjected the mice to four associative motor learning sessions in which they were trained to avoid an obstacle using a tone as the conditioned stimulus (CS) and a rising rung in the swing phase of their right paw as the unconditioned stimulus (US). Proper associative conditioning requires precise timing of the CS-US presentation to achieve consistent and appropriate inter-stimulus intervals (ISI). During each trial, step sizes and step times were buffered in real-time and standard deviations (SD) were calculated for every three step combinations using custom written real-time LabView software. The step time is the time needed to transfer the front paw from one rung to the next rung in the travelling path of the mouse. The step size is the distance between these two rungs. Whenever the SD of the step sizes equaled zero and the SD of the accompanying step times was smaller than 150 ms, the stepping pattern was reliable enough to predict when and where the mouse was going to place its right forepaw. With this information, the real-time LabView software calculated an appropriate time and place (i.e. specific half-rung) to present the US perturbation by raising the half-rung by 18 mm to create an obstacle of 12 mm above the stepping surface of the mouse. At a time point 285 ms before this US perturbation was going to take place, the Erasmus Ladder presented a 90 dB, 15 kHz tone (lasting 285 ms) as the CS. The pressurized air outlets provided a background noise of 80dB which prevented auditory startle reactions to the CS. The rung remained in the raised position until the mouse entered the opposing shelter, whereupon it was automatically lowered. The associative motor learning sessions consisted of nine blocks of eight trials; each block consisted of six CS-US paired trials, one US-Only trial, and one CS-Only trial. The key feature of the associative motor learning sessions is that the timing of the US is determined by the stepping pattern of each mouse individually. For each trial I calculated the step time directly

after the CS in order to measure associative motor learning. A decrease in step time directly after the CS over the sessions implies that mice learn to adjust their stepping pattern to the obstacle and is therefore a measure of associative motor learning.

In chapter 2, I present data of Fmr1 knockout mice and expanded CGG mice. The expanded CGG mouse is a model for fragile-X-associated tremor/ataxia syndrome (FXTAS), a progressive neurodegenerative disorder associated with the fragile X premutation. Male patients suffer from cerebellar dysfunction. Expanded CGG mice show a motor performance deficit on the Erasmus Ladder, but not on the accelerating rotarod. Expanded CGG mice show no deficits in the associative motor learning sessions. Fmr1 knockout mice are a model for fragile X syndrome. Fragile X syndrome has been recognized as the most common inherited form of mental retardation. On the Erasmus Ladder the Fmr1 knockout mice have no motor performance deficits, but do have an associative motor learning deficit. From the data of these two mouse models, I conclude that the Erasmus Ladder can distinguish between motor performance deficits and associative motor learning deficits, which to my knowledge cannot be done by any other behavioral task.

In chapter 3, I present data of ßCamKII knockout mice. βCaMKII is highly expressed in the cerebellum and our lab has shown that mice lacking βCaMKII are ataxic and have altered parallel fiber-LTD and parallel fiber-LTP. ßCamKII knockout mouse show a motor performance deficit and an associative motor learning deficit on the Erasmus Ladder.

In chapter 4, I present data of *Lurcher*s and Cx36 knockout mice. Cx36 is essential for the creation of gap junctions in neurons. Cx36 is highly expressed in the olfactory bulb, hippocampus, cerebral cortex, (hypo)thalamus and the inferior olive. A lack of Cx36 generally leads to an absence of electronic coupling and to changes in sub-threshold activities. Cx36 knockout mouse show no motor performance deficits on the Erasmus Ladder, but do show a deficit in the associative motor learning paradigm. The Erasmus Ladder is the first behavioral task which shows a deficit in motor behavior for Cx36 knockout mice. *Lurcher*s are characterized by postnatal degeneration of Purkinje cells and their primary afferents, granule cells and olivary neurons. All *Lurcher*s I measured were of such an age that they no longer had functional Purkinje cells and all mice were visibly ataxic. These mice are the only cerebellum-specific mice that are presented in this thesis. These mice show a motor performance deficit and an associative motor learning deficit on the Erasmus Ladder; thus, the Erasmus Ladder is a cerebellum-specific behavioral task.

The data presented in chapters 2, 3 and 4 show that the Erasmus Ladder meets the above-mentioned requirements. Future planned improvements include the implementation of new sensors, which can measure pressure instead of the current all-or-nothing signal, and a high speed video system, which can follow all the movements of the mice. The Erasmus Ladder will then become an even better behavioral task than it already is.

SAMENVATTING

Welke delen van de hersenen zijn verantwoordelijk voor leren? Hoe en op welke wanneer wordt deze informatie opgeslagen? Dit zijn vragen die neurowetenschappers graag willen beantwoorden. In dit proefschrift probeer ik deze vragen te beantwoorden door bestudering van het cerebellum, een deel van de hersenen dat een belangrijke rol speelt bij het leren van nieuwe bewegingen. Het cerebellum kan onderzocht worden met anatomisch onderzoek, moleculaire biologisch onderzoek, electrophysiologisch onderzoek en het ontwikkelen van modellen die het functioneren van het cerebellum verklaren. De meest directe manier om het functioneren van het cerebellum te onderzoeken is (mutante) muizen te testen in een cerebellaire gedragstaak. Met de huidige transgene technieken is het gebruikelijk cellulaire mechanismes te onderzoeken met behulp van gedragstaken. Muizen zijn de meest geschikte soort om transgeen te maken, en daarom voor gedragstaken, omdat er veel technieken zijn om de eicellen van muizen te manipuleren.

Er zijn veel gedragstaken voor (mutante) muizen ontwikkeld: grid walking, rope climbing, inclined plane kinematic analysis, open-field tasks, gait analysis, measures of ground reaction forces, swimming en accelerating rotarod. De meeste van deze taken zijn gemakkelijk uit te voeren en meten hoe goed muizen bewegingen kunnen uit voeren. Maar geen van deze taken geeft betrouwbare informatie over hoe muizen nieuwe bewegingen leren. Het leren van nieuwe bewegingen bij muizen kan onderzocht worden met twee gedragstaken die ontwikkeld zijn in ons lab: compensatory eye movements en eyeblink conditioning. Het neurale circuit van het cerebellum wordt in beide taken geactiveerd en veranderd en is in detail onderzocht: er zijn directe connecties tussen gedrag en plasticiteit aangetoond. Maar beide taken hebben het probleem dat er een gecompliceerde operatie aan vooraf gaat, er moet opgelet worden tijdens de gedragstaak, de uitval is relatief hoog en de analyse van de gegevens is gecompliceerd.

Hoewel alle bovengenoemde gedragstaken hun waarde hebben bewezen voor cerebellair onderzoek, denk ik dat een nieuwe cerebellaire gedragstaak voor muizen wenselijk is. Daarom heb ik een nieuwe gedragstaak ontwikkeld, de Erasmus Ladder, die aan de volgende esien moest voldoen: (1) de taak moet volledig geautomatiseerd zijn; (2) de taak moet non-invasief zijn; (3) de taak moet meer problemen met het uitvoeren van bewegingen detecteren dan de accelerating rotarod; (4) de leertaak moet afhankelijk zijn van het cerebellum en (5) de taak moet onderscheid kunnen maken tussen problemen met het uitvoeren van bewegingen en leerproblemen.

De Erasmus Ladder bestaat uit 2 x 37 sporten, die twee hokjes met elkaar verbindt, waarover muizen heen en weer kunnen lopen. Elke sport heeft een druksensor, die continu geanalyseerd wordt. Op basis van deze gegevens kan het looppatroon van de muis voorspeld worden en gehinderd worden door het omhoog of omlaag laten bewegen van een sport.

Om te testen of de Erasmus Ladder voldoet aan de bovengenoemde voorwaarden, heb ik verschillende (mutante) muizen gemeten op de Erasmus Ladder met het volgende protocol:

elke muis kreeg 4 motor performance sessies en 4 associative motor learning sessies. Tijdens de motor performance sessies werd de muis in een van de hokjes geplaatst. Na 10 seconden gaat het licht aan in het hokje (aansporing 1), drie seconden later gevolgd door de uitlaat-kleppen voor perslucht (aansporing 2). Aansporing 2 zorgt er meestal voor dat de muis het hokje verlaat. Als de muis op de sporten is wordt een andere uitlaapklep geactiveerd, die de perslucht in dezelfde richting blaast als de muis moet lopen. Dit spoort de muis aan om naar het andere hokje te lopen. Als de muis in het andere hokje is aangekomen worden de uitlaap-kleppen dichtgezet. Na 10 seconden wordt het bovengenoemde protocol herhaald. Een trial is de verplaatsing van het een hokje naar het andere hokje. De incidentele muis (< 5%) die het bovengenoemde protol na de eerste motor performance sessie niet kan uitvoeren, werd uit het experiment verwijderd. Een sessie is 72 trials. Het uitvoeren van bewegingen werd getest door het tellen van de misstappen. Een misstap is een stap op een van de verlaagde sporten.

Na de vier motor performance sessies onderwerp ik de muizen aan vier associative motor learning sessies. Hierin moeten de muizen leren om een obstakel te ontwijken met een toon als conditioned stimulus (CS) en een omhooggaande sport in de baan van hun rechtervoor-poot als unconditioned stumulus (US). Een goede associatieve conditioneringstaak vereist dat de timing van de CS en de US zeer nauwkeurig is. Tijdens elke trial werden de standaard-deviaties (SD) van de stapgrootte en de staptijd continu geanalyseerd. De staptijd is de tijd die het kost om van een sport naar de volgende sport te gaan. De stapgrootte is de afstand tussen deze twee sporten. Als de SD van drie opeenvolgende stapgroottes nul is en de SD van de bijbehorende staptijden minder was dan 150, dan was het stappatroon betrouwbaar genoeg om een voorspelling te maken. Met deze gegevens werd een geschikte tijd en plaats (sport) bepaald om het obstakel (US) op te werpen. Precies 285 ms voordat het obstakel wordt opgeworden, hoort de muis een toon (90 dB, 15 kHZ en 285 ms lang). De perslucht zorgt voor een achtergrondgeluid van 80 dB, waardoor de muizen niet schrikken van de toon. De associative motor learning sessies bestaan uit 9 blokken van 8 trials: elk blok bestaat uit 6 gepaarde CS-US trials, 1 CS-Alleen trial en 1 US-Alleen trial. Het essentiele onderdeel van de associative learning sessies is dat de plaats en timing van het obstakel voor iedere trial van iedere muis uniek is. Een afname van de staptijd, gemeten net na de CS, over de sessies geeft aan dat de muizen hun looppatroon hebben aangepast en is daarom een maat voor leren.

In hoofdstuk 2 laat ik gegevens zien van de Fmr1 knockout muis en de expanded CGG muis. De expanded CGG muis is een model voor fragile-X-associated tremor/ataxia syndrome (FXTAS), een progressieve neurodegeneratieve afwijking geassocieerd met de fragiele X pre-mutatie. Mannelijke FXTAS patienten hebben last van een niet goed functionerend cerebel-lum. Expanded CGG muizen hebben een probleem met het uitvoeren van bewegingen op de Erasmus Ladder maar niet op de accelerating rotarod. Fmr1 knockout muizen zijn een model voor fragiele X. Fragiele X is de meest voorkomende erfelijke vorm van mentale retardatie. Op de Erasmus Ladder hebben deze muizen geen problemen met het uitvoeren van bewegingen

maar ze hebben een leerprobleem. Op basis van de gegevens van deze twee muismodellen concludeer ik dat de Erasmus Ladder een onderscheid kan maken tussen problemen met de uitvoering van bewegingen en leerproblemen.

In hoofdstuk 3 laat ik gegevens zien van ßCamKII knockout muizen. βCaMKII komt hoog tot expressie in het cerebellum en in ons lab hebben we laten zien dat muizen zonder βCaMKII ataxisch zijn en een afwijkende vorm van plasticiteit in de Purkinje cellen hebben. ßCamKII knockout muizen hebben problemen met de uitvoering van bewegingen en leerproblemen.

In hoofdstuk 4 laat ik gegevens zien van *Lurcher* en Cx36 knockout muizen. Cx36 is essentieel voor het maken gap junctions in zenuwcellen. Cx36 knockout muizen hebben geen problemen met het uitvoeren van bewegingen op de Erasmus Ladder maar ze hebben wel leerproblemen. De Erasmus Ladder is de eerste gedragstaak die heeft laten zien dat Cx36 knockout muizen motorische problemen hebben. *Lurchers* zijn gekarakterizeerd door postnatale degeneratie van Purkinje cellen. Al de *Lurchers* die ik gemeten heb waren zo oud dat ze geen functionele Purkinje cellen meer hebben en allen ataxisch zijn. Deze muizen zijn de enige muizen die in dit proefschrift besproken worden die cerebellum-specific mutante muizen zijn. *Lurchers* hebben problemen met het uitvoeren van bewegingen en leerproblemen op de Erasmus Ladder; hiermee is aangetoond dat de Erasmus Ladder een cerebellum-specifieke gedragstaak is.

De gegevens van hoofdstuk 2, 3 en 4 tonen aan dat de Erasmus Ladder voldoet aan de bovengenoemde voorwaarden. Toekomstige verbeteringen, zoals het implementeren van nieuwe sensors die druk kunnen meten in plaats van het huidige alles-of-niets signaal en een video systeem dat alle bewegingen van de muis vastlegt, zullen de Erasmus Ladder een nog beter gedragstaak maken dan die nu al is.

DANKWOORD

Mijn promotieonderzoek op de afdeling neurowetenschappen heeft iets minder dan vijf jaar geduurd. In die tijd was de sfeer op de afdeling altijd goed en heb ik veel lol gehad. Coenen, WP, de Witte Aap, de Consul en andere gelegenheden waar we wetenschap bespraken werden gefrequenteerd; er werden potjes schaak gespeeld; concerten en bioscopen werden bezocht; internetfimpjes werden bekeken; er werden vele avonden squash gespeeld waarna soms pornografische termen werden uitgelegd, soms konijnen achterna werden gezeten en soms werden er genante dingen gezien bij Jan van Nancy; etentjes en feesten werden georganiseerd; er werd overal koffie gedronken; en er werd vooral veel geroddeld over andere collega's.

Daarnaast heb ik hard gewerkt aan mijn promotie, die zonder hulp van anderen echter onmogelijk was geweest. Allereerst wil ik Chris bedanken voor de mogelijkheid om te promeveren, maar vooral voor de vrijheid die jij mij gaf om het project naar eigen inzicht in te vullen. Jouw idee, om de sporten van de Erasmus Ladder omhoog te laten gaan in plaats van naar beneden, was essentieel voor het slagen van dit project.

Bas bedankt voor het meehelpen met het construeren van het prototype en het programmeren van vele LabView programma's die de analyse gemakkelijker maakten. Jouw manier van begeleiden, waarbij jij mij eerst alles zelf liet doen en pas ingreep als het echt mis dreigde te gaan, heeft me zeker beter gemaakt in klussen en programmeren, maar solderen kan ik helaas nog steeds niet.

Ik wil Joop Bos bedanken voor het bouwen van de Erasmus Ladder en Alex Brouwer bedanken voor de het ontwerp; veel figuren in dit proefschrift zijn door jou gemaakt. Vooral het feit dat de Erasmus Ladder Alexanderproof was, getuigt van jullie grote kwaliteit. Verder wil ik ook alle anderen van de afdeling Medische Instrumentatie bedanken die geholpen hebben bij de ontwikkeling van de Erasmus Ladder.

Hans, de snelheid waarmee jij oplossingen verzon voor de vele technische problemen was ongelofelijk.

Niels wil ik bedanken voor het maken van het besturingssysteem. Dit was op zo'n systematisch manier gedaan, dat naarmate de Erasmus Ladder evolueerde, ik met gemak het bestuderingssysteem kon aanpassen.

Meer dan duizend muizen hebben over de Erasmus Ladder gelopen. Dit vereiste samenwerking met veel mensen, die soms ook zelf de experimenten deden. Ik wil Mandy bedanken voor het beheren van de muizendatabase, Martijn voor de interneuron muizen, Ruben voor de Cx36 muizen; Tom voor de injecties in de olijf, Boyan voor de S218L muizen, Geeske voor de ßCamKII muizen, Sander Groffen voor de Doc2B muizen, Ronald van Kesteren voor de Trim3 muizen, Bart voor de *Lurchers*, Elisa voor de Cacna1a muizen, Andrea voor de alcohol experimenten, Giorgia voor de oestrogeen experimenten en Thijs voor de NF1 muizen. Verder wil ik Rob, Ben, Edwin, Judith, Femke, Ingeborg en Ronald bedanken voor alle hulp bij de experimenten met de Fxr, de Fmr1 en de ExpCGG muizen.

CV

Name: Alexander Cupido
Date of Birth: May 7th 1979
Nationality: Dutch
Address: Bergweg 100a, 3036 BE Rotterdam
Phone number: +31 10 26 56190 (home), +31 6 160 128 76 (mobile)
E-mail address: a.cupido@erasmusmc.nl, alexandercupido@hotmail.com

EDUCATION

2004 – 2009 University of Rotterdam / Erasmus MC, The Netherlands: **PhD in Medicine**

Detecting Cerebellar Phenotpyes with the Erasmus Ladder

1997 – 2003 University of Utrecht, The Netherlands: **BSc and MSc in Biology**

Dissertation projects:

A Potential Role for Neuroprotection in Glaucoma Management

An Analysis of Object Localization during Fixation and Smooth Pursuit

The Play Behaviour of Autistic Children

1996 – 2002 University of Oxford, United Kingdom: **Research Assistant**

Measuring intra ocular pressure in NZW rabbits

PORTFOLIO

- Het geven van verscheidene anatomische lessen aan geneeskunde studenten
- Het begeleiden van meerdere MSc studenten en HLO studenten

PUBLICATIONS

· **Cupido A**, Van Der Giessen RS, Koekkoek SK, Van Dorp S, De Gruijl, Khosrovani, Dortland B, Wellershaus K, Degen J, Deuchars J, Fuchs EC, Monyer H, Willecke K, De Jeu MT and De Zeeuw CI (2008). Role of olivary coupling in cerebellar motor learning. Neuron, 58(4):599-612.

· Osborne NN, Wood JP, **Cupido A**, Melena J and Chidlow G (2002). Topical flunarizine reduces IOP and protects the retina against ischemia-excitotoxicity. Invest Ophthalmol Vis Sci, 43(5):1456-64.

· Chidlow G, **Cupido A**, Melena J and Osborne NN (2001). Flesinoxan, a 5-HT1A receptor agonist/alpha 1-adrenoceptor antagonist, lowers intraocular pressure in NZW rabbits. Curr Eye Res, 23(2):144-53.